Electronic Supplementary Material (ESI) for Dalton Transactions.

Carbazole effect on ground- and excited-state properties of rhenium(I) carbonyl complexes with extended terpy-like ligands

Katarzyna Choroba[a], Anna Maroń[a], Anna Świtlicka[a], Agata Szłapa-Kula[a], Mariola Siwy[b], Justyna Grzelak[c], Sebastian Maćkowski[c], Tomasz Pedzinski[d], Ewa Schab-Balcerzak[a,b]* and Barbara Machura[a]*

[a] *Institute of Chemistry, University of Silesia, 9th Szkolna St., 40-006 Katowice, Poland.*
[b] *Centre of Polymer and Carbon Materials, Polish Academy of Sciences, 34th M. Curie-Sklodowska St., 41-819 Zabrze, Poland.*
[c] *Institute of Physics, Faculty of Physics, Astronomy and Informatics, Nicolaus Copernicus University, 5th Grudziadzka St., 87-100 Torun, Poland.*
[d] *Faculty of Chemistry, Adam Mickiewicz University in Poznań, 89b Umultowska, 61-614 Poznań, Poland*

Electronic Supplementary Materials
Table of Contents

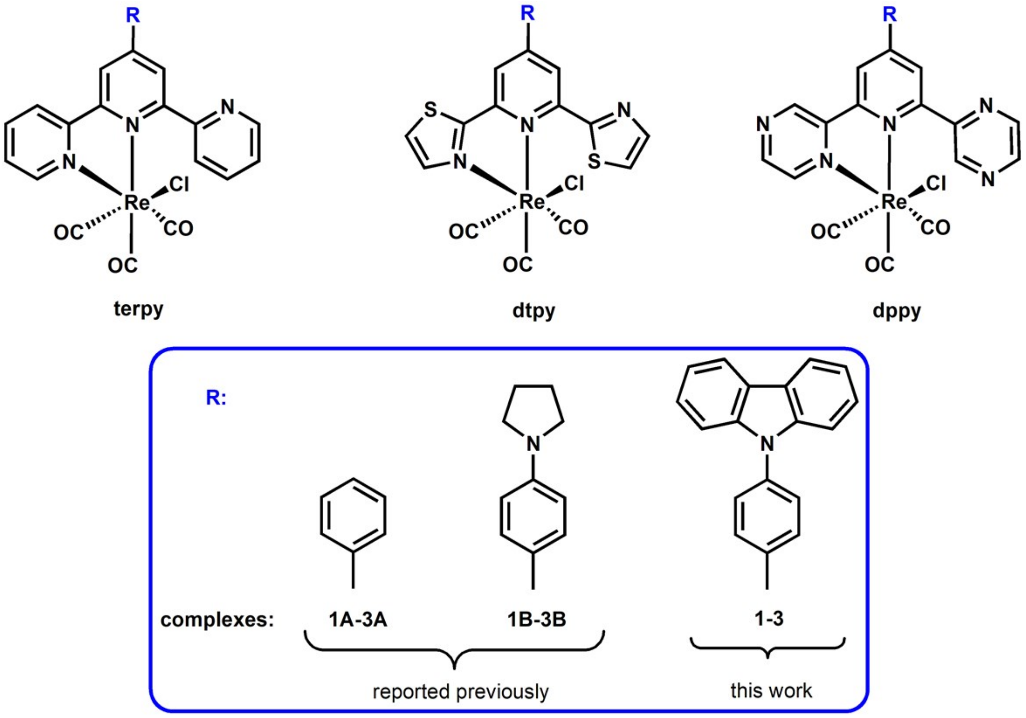
R
R
R
terpy
dtpy
dppy
R:
complexes:
1A-3A
1B-3B
1-3
reported previously
this work

Scheme S1. Formulas of Re(I) carbonyl complexes discussed in the current work. Complexes **1A–3A** and **1B–3B** are reported previously in ref. [1].

Preparation of ligands ($\mathbf{L^1}$-$\mathbf{L^3}$)

Ketone (20 mmol) (2-acetylpyridine, 2-acetylthiazole or 2-acetylpyrazine) was added to the solution of N-(4-formylphenyl)carbazole (10 mmol) in EtOH (75 mL). KOH (1.54 g, 27.5 mmol) and NH_3 (aq) (35 mL) were then added. The solution was stirred at room temperature for 24 h. The solid was collected by filtration and washed with H_2O. Recrystallization from ethanol (**L**^{1}) or toluene (**L**^{2,3}) afforded a crystalline solid.

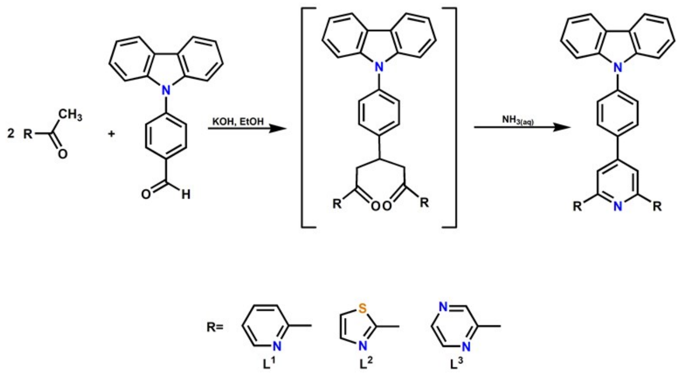

Scheme S2. Synthesis of the ligands **L**^{1}–**L**^{3}.

L^1: Yield: 41%. NMR: **^{1}H NMR (400 MHz, $\mathbf{CDCl_3}$) *δ*** 8.91 (s, 2H, H^{B2}), 8.79 (d, *J* = 4.2 Hz, 2H, $\mathbf{H}^{\mathbf{A1}}$), 8.75 (d, *J* = 7.9 Hz, 2H, $\mathbf{H}^{\mathbf{A4}}$), 8.21 – 8.16 (m, 4H, $\mathbf{H}^{\mathbf{C2,\,D5}}$), 7.96 (t, *J* = 7.4 Hz, 2H, $\mathbf{H}^{\mathbf{A3}}$), 7.75 (d, *J* = 8.2 Hz, 2H, $\mathbf{H}^{\mathbf{C3}}$), 7.52 – 7.40 (m, 6H, $\mathbf{H}^{\mathbf{A2,\,D3,\,D2}}$), 7.35 – 7.30 (m, 2H, $\mathbf{H}^{\mathbf{D4}}$). **^{13}C NMR (100 MHz, $\mathbf{CDCl_3}$) *δ*** 156.1 ($\mathbf{C}^{\mathbf{B1}}$), 149.6 ($\mathbf{C}^{\mathbf{B3}}$), 149.1 ($\mathbf{C}^{\mathbf{B5,\,A1}}$), 140.9 ($\mathbf{C}^{\mathbf{C4}}$), 138.7 ($\mathbf{C}^{\mathbf{C1}}$), 137.6 ($\mathbf{C}^{\mathbf{D1}}$), 137.4 ($\mathbf{C}^{\mathbf{A3}}$), 129.1 ($\mathbf{C}^{\mathbf{C2}}$), 127.6 ($\mathbf{C}^{\mathbf{C3}}$), 126.2 ($\mathbf{C}^{\mathbf{D3}}$), 124.2 ($\mathbf{C}^{\mathbf{A2}}$), 123.7 ($\mathbf{C}^{\mathbf{D6}}$), 121.7 ($\mathbf{C}^{\mathbf{A4}}$), 120.5 ($\mathbf{C}^{\mathbf{D5}}$), 120.3 ($\mathbf{C}^{\mathbf{D4}}$), 119.2 ($\mathbf{C}^{\mathbf{B2}}$), 110.0 ($\mathbf{C}^{\mathbf{D2}}$). Anal. calc. for $N_4C_{33}H_{22}$ (474.55 g mol^{-1}): C 83.52, H 4.67, N 11.81% found: C 83.82; H 4.69; N 12.03%.

L^2: Yield: 46%. NMR: **^{1}H NMR (400 MHz, $\mathbf{CDCl_3}$) *δ*** 8.57 (s, 2H), 8.17 (d, *J* = 7.7 Hz, 2H), 8.09 (d, *J* = 8.5 Hz, 2H), 8.00 (d, *J* = 3.2 Hz, 2H), 7.75 (d, *J* = 8.5 Hz, 2H), 7.53 (d, *J* = 3.2 Hz, 2H), 7.51 – 7.43 (m, 4H), 7.35 – 7.30 (m, 2H). **^{13}C NMR (100 MHz, $\mathbf{CDCl_3}$) *δ*** 168.8, 151.9, 149.9, 144.3, 140.7, 136.2, 128.9, 128.4, 127.6, 126.3, 123.8, 122.1, 120.5, 120.4, 117.9, 109.9. Anal. calc. for $N_4S_2C_{29}H_{18}$ (486.61 g mol^{-1}): C 71.58; H 3.73; N 11.51% found: C 71.19; H 3.73; N 11.21%.

L^3: Yield: 51%. NMR: **^{1}H NMR (400 MHz, $\mathbf{CDCl_3}$) *δ*** 9.92 (s, 2H), 8.84 (s, 2H), 8.70 – 8.69 (m, 4H), 8.17 (d, *J* = 7.7 Hz, 2H), 8.12 (d, *J* = 8.2 Hz, 2H), 7.77 (d, *J* = 8.2 Hz, 2H), 7.52 – 7.43 (m, 4H), 7.33 (t, *J* = 7.3 Hz, 2H). **^{13}C NMR (100 MHz, $\mathbf{CDCl_3}$) *δ*** 154.8, 150.8, 150.0, 145.0, 143.8, 143.8, 140.7, 139.1, 136.9, 128.9, 127.7, 126.2, 123.8, 120.6, 120.4, 119.9, 109.9. Anal. calc. for $N_6C_{31}H_{20}$ (476.53 g mol^{-1}): C 78.13; H 4.23; N 17.64% found: C 78.60; H 4.54; N 18.12%.

IR spectra

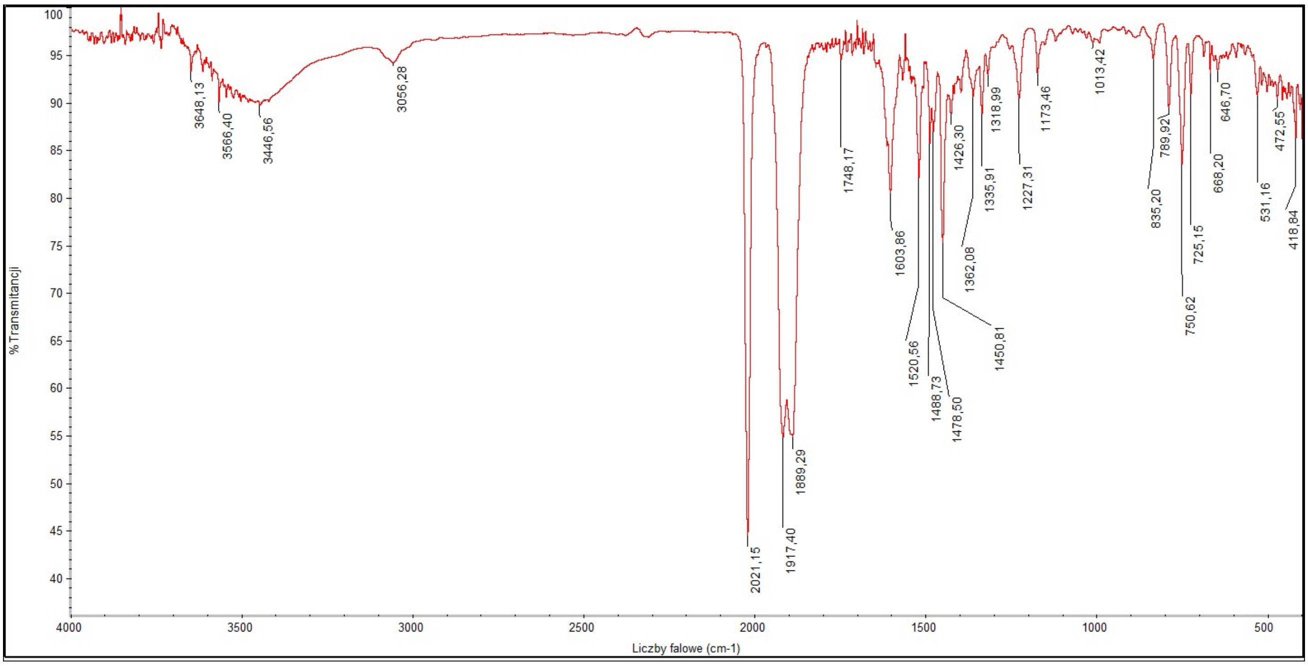

(a)

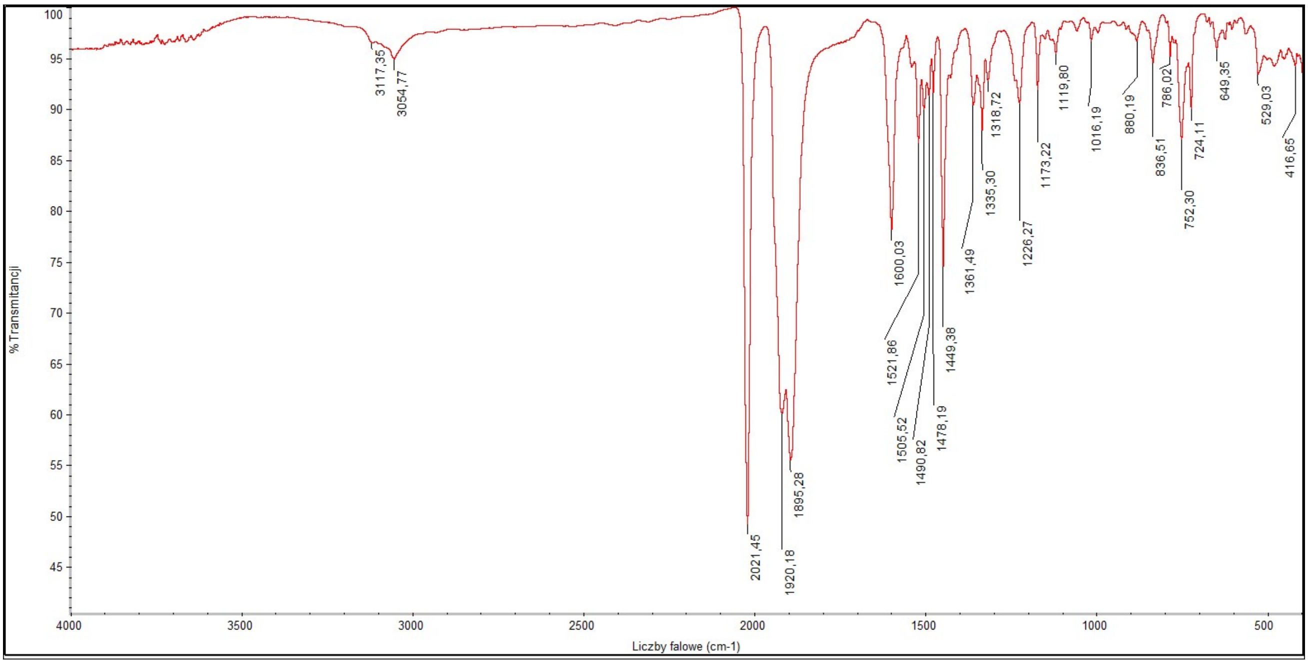

(b)

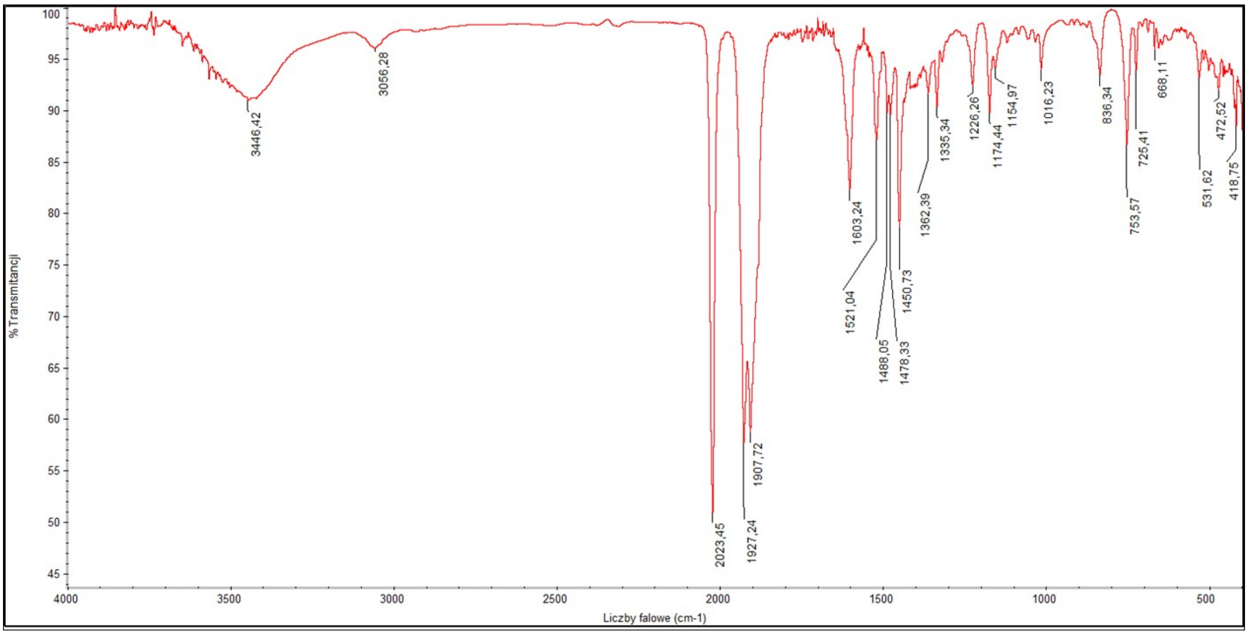

(c)

Figure S1. FT-IR spectra of complexes **1-3** (a-c).

NMR studies

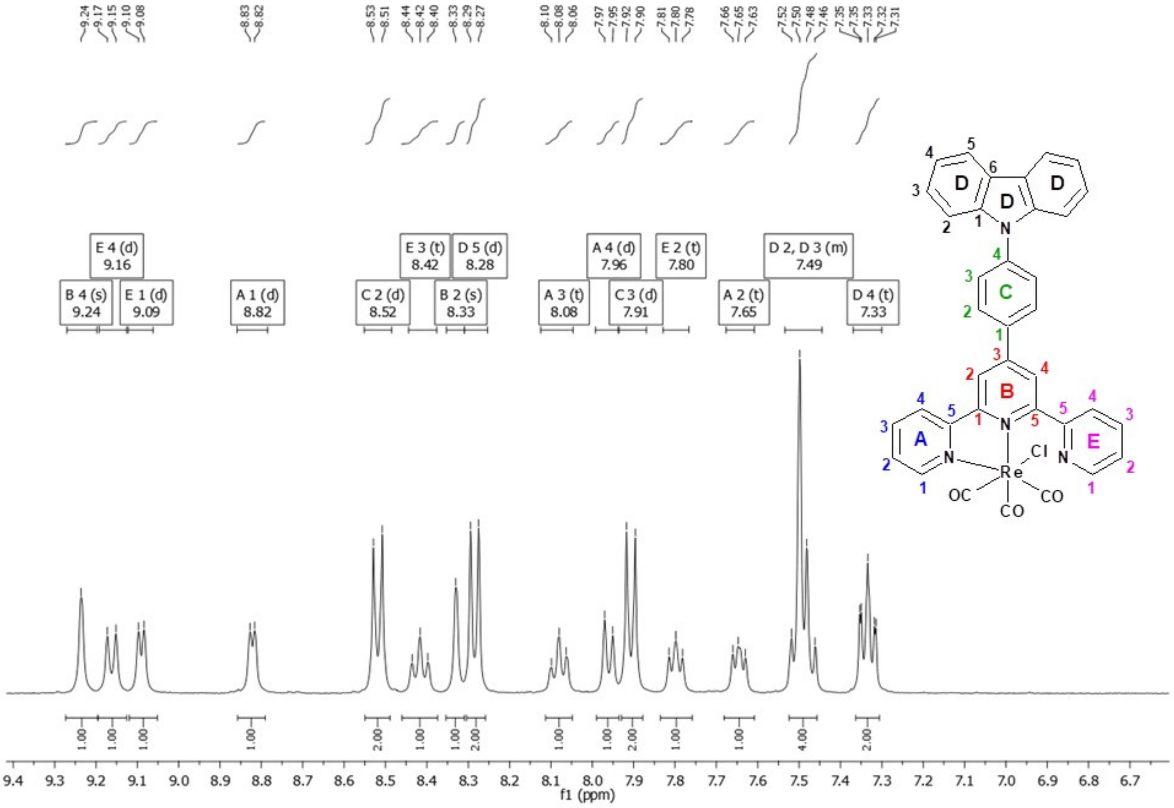

(a)

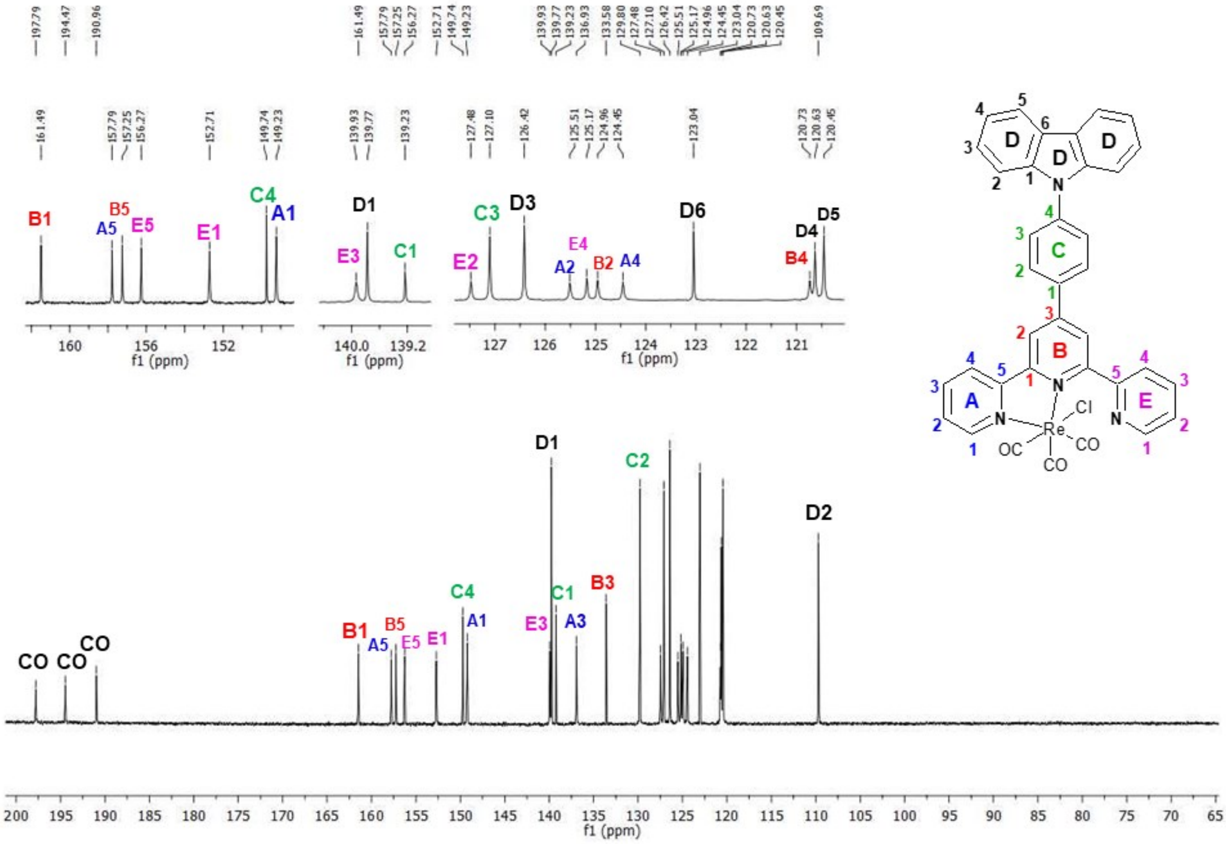

(b)

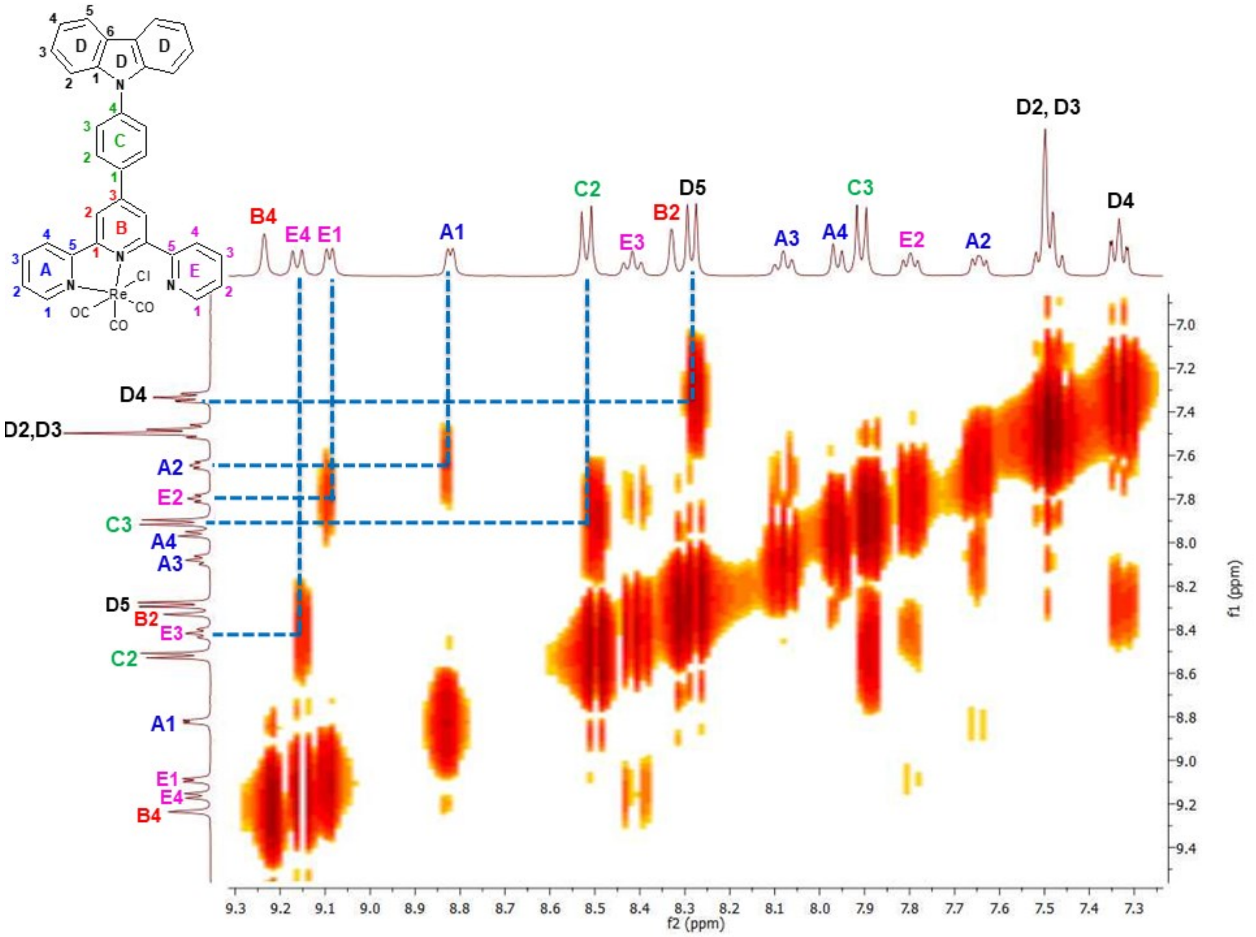
D
D
D
C
A
B
E
Re
Cl
OC
CO
CO
N
B4
E4
E1
A1
C2
E3
B2
D5
A3
A4
C3
E2
A2
D2, D3
D4
D2,D3
D5
B2
E3
C2
A1
E1
E4
B4
f2 (ppm)
f1 (ppm)
9.3
9.2
9.1
9.0
8.9
8.8
8.7
8.6
8.5
8.4
8.3
8.2
8.1
8.0
7.9
7.8
7.7
7.6
7.5
7.4
7.3
7.0
7.2
7.4
7.6
7.8
8.0
8.2
8.4
8.6
8.8
9.0
9.2
9.4

(c)

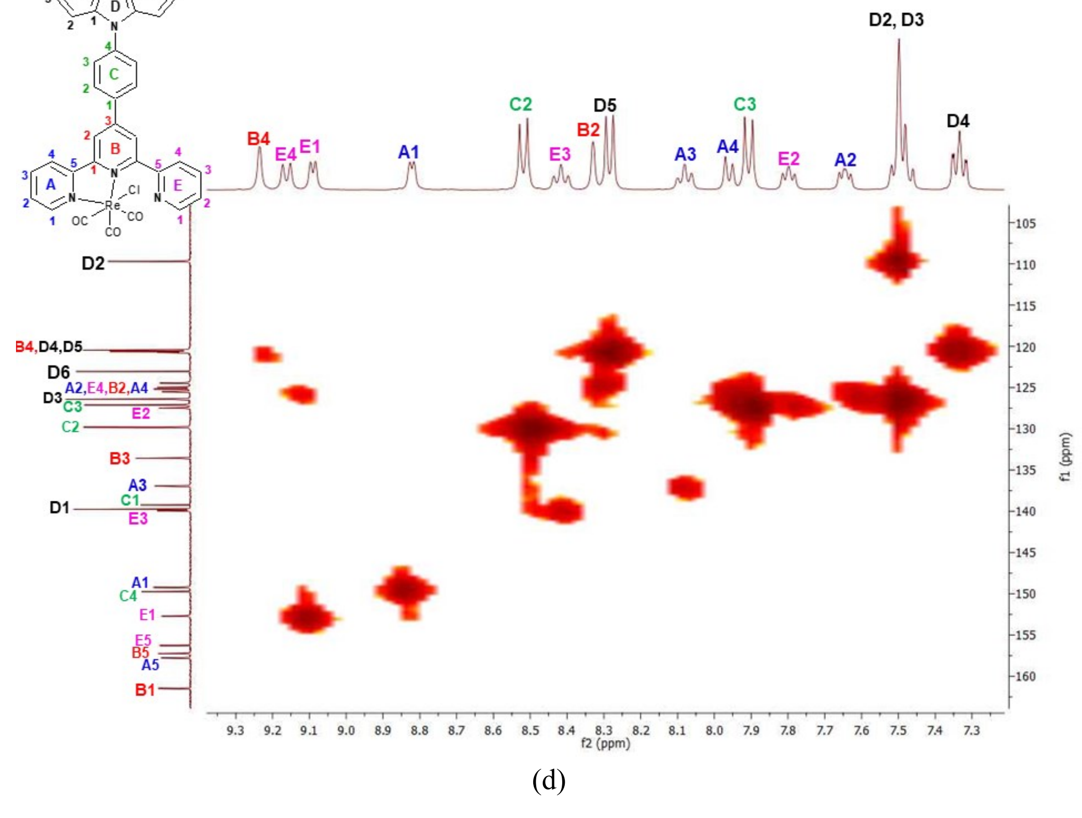
D
D
D
C
A
B
E
Re
Cl
OC
CO
CO
N
B4
E4
E1
A1
C2
E3
B2
D5
A3
A4
C3
E2
A2
D2, D3
D4
D2
B4,D4,D5
D6
D3
A2,E4,B2,A4
C3
E2
C2
B3
A3
C1
D1
E3
A1
C4
E1
E5
B5
A5
B1
f2 (ppm)
f1 (ppm)
9.3
9.2
9.1
9.0
8.9
8.8
8.7
8.6
8.5
8.4
8.3
8.2
8.1
8.0
7.9
7.8
7.7
7.6
7.5
7.4
7.3
105
110
115
120
125
130
135
140
145
150
155
160

(d)

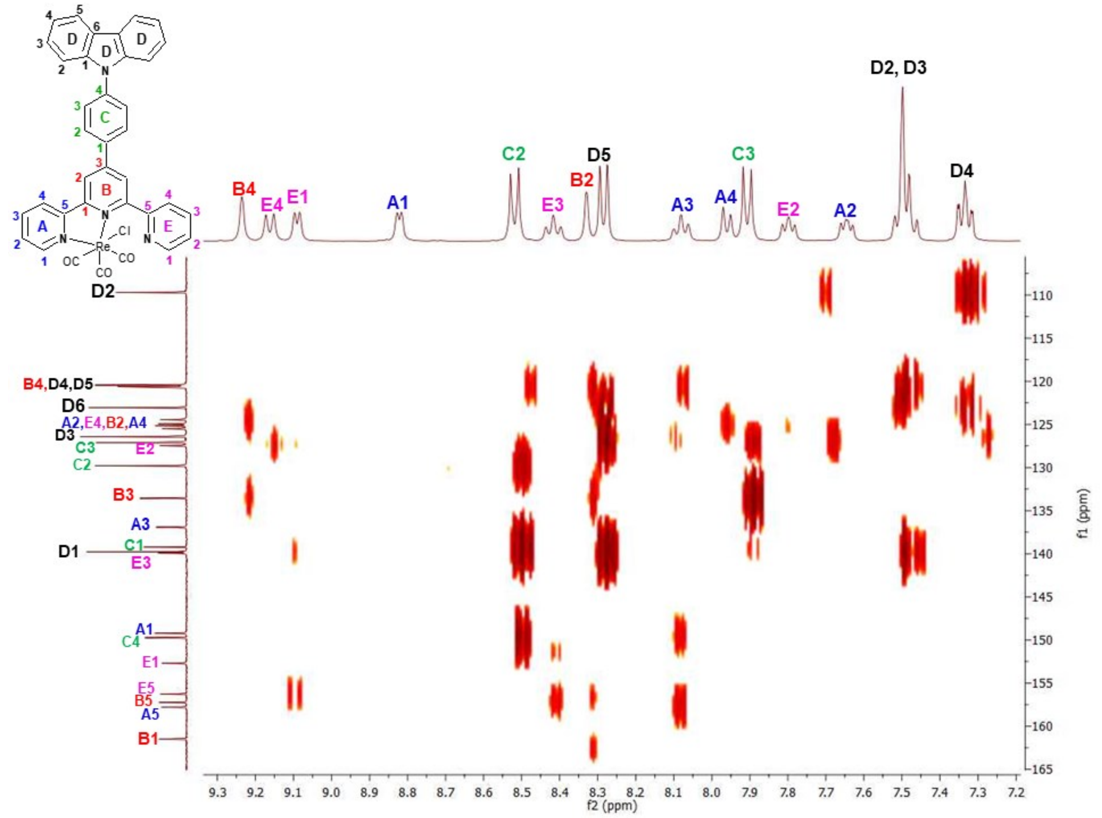

(e)

Figure S2. NMR spectra of complex **1** in DMSO-d^{6}. ^{1}H (a), ^{13}C (b), ^{1}H–^{1}H COSY (c), ^{1}H–^{13}C HMQC (d), ^{1}H–^{13}C HMBC (e).

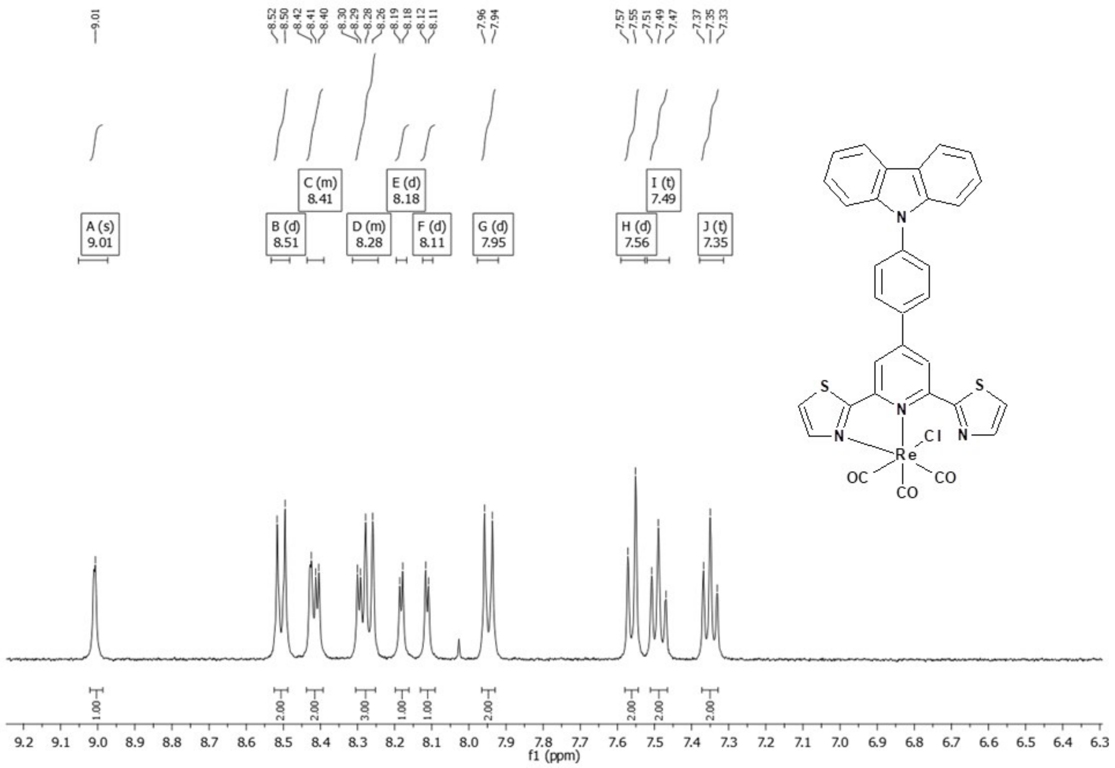

Figure S3. NMR spectra of complex **2** in acetone-d^{6} ^{1}H

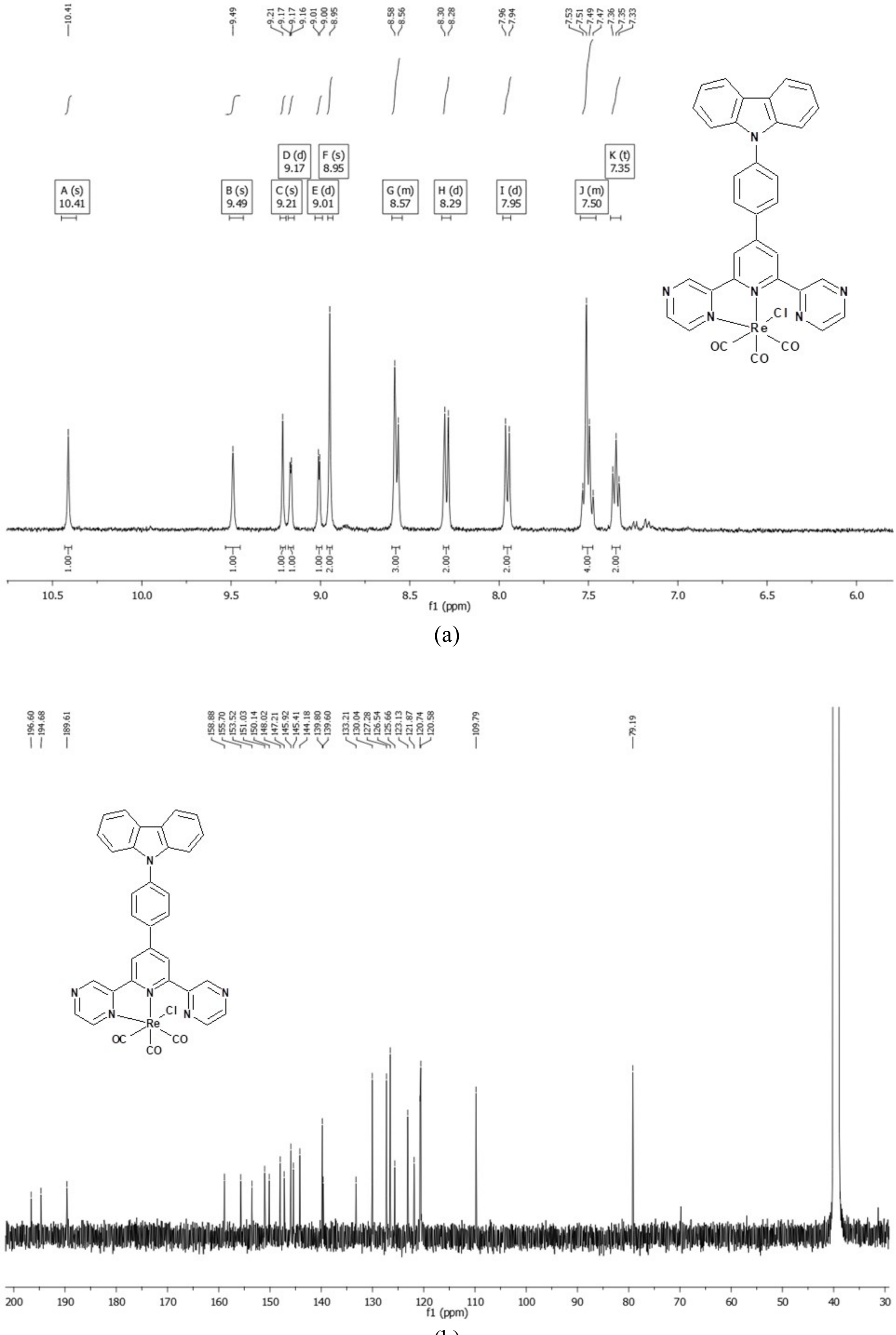

(a)

(b)

Figure S4. NMR spectra of complex **3** in DMSO-d^6. ^{1}H (a), ^{13}C (b).

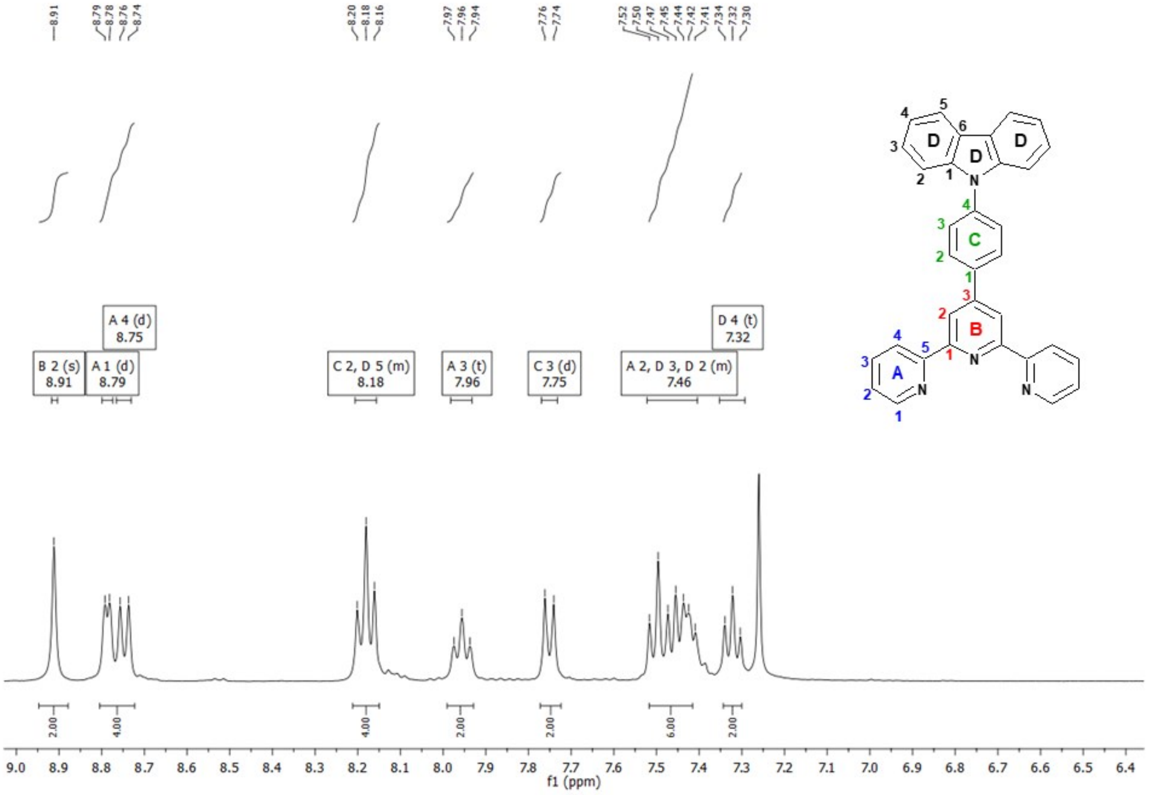
8.91
8.79
8.78
8.76
8.74
8.20
8.18
8.16
7.97
7.96
7.94
7.76
7.74
7.52
7.50
7.47
7.45
7.44
7.42
7.41
7.34
7.32
7.30
B 2 (s) 8.91
A 1 (d) 8.79
A 4 (d) 8.75
C 2, D 5 (m) 8.18
A 3 (t) 7.96
C 3 (d) 7.75
A 2, D 3, D 2 (m) 7.46
D 4 (t) 7.32
2.00
4.00
4.00
2.00
2.00
6.00
2.00
9.0
8.9
8.8
8.7
8.6
8.5
8.4
8.3
8.2
8.1
8.0
7.9
7.8
7.7
7.6
7.5
7.4
7.3
7.2
7.1
7.0
6.9
6.8
6.7
6.6
6.5
6.4
f1 (ppm)
A
B
C
D
N

(a)

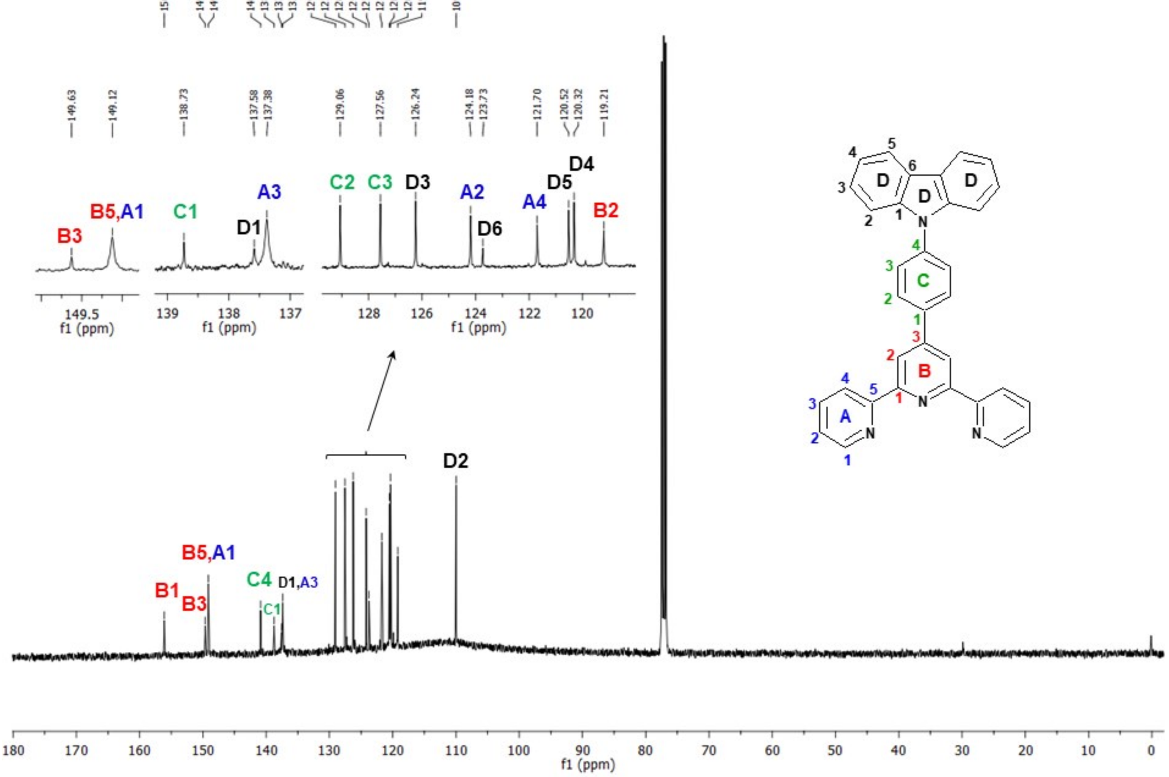
156.09
149.63
149.12
140.87
138.73
137.58
137.38
129.06
127.56
126.24
124.18
123.73
121.70
120.52
120.32
119.21
109.98
B3
B5,A1
C1
D1
A3
C2
C3
D3
A2
D6
A4
D5
D4
B2
149.5
139
138
137
128
126
124
122
120
f1 (ppm)
B1
C4
D1,A3
D2
180
170
160
150
140
130
120
110
100
90
80
70
60
50
40
30
20
10
0
f1 (ppm)
A
B
C
D
N

(b)

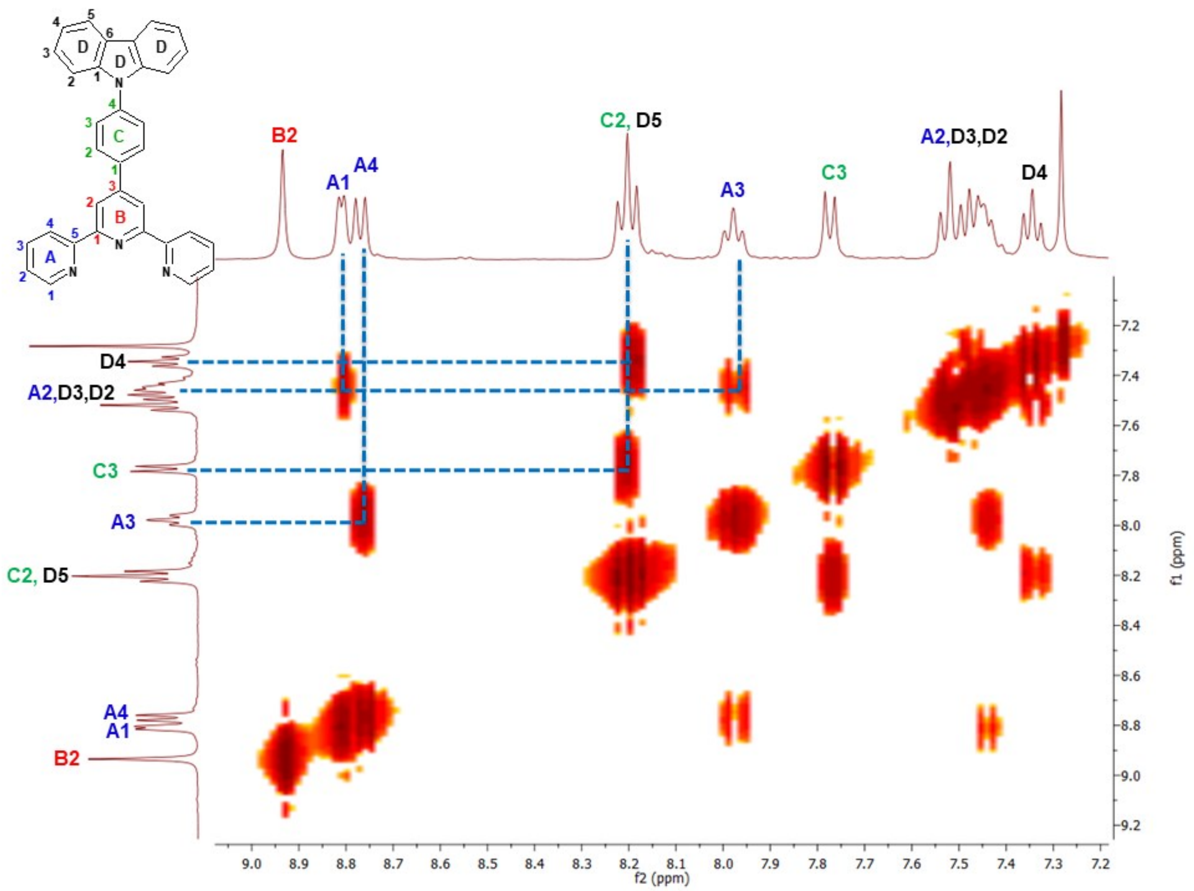
B2
A1
A4
C2, D5
A3
C3
A2,D3,D2
D4
A2,D3,D2
C3
A3
C2, D5
A4
A1
B2
f2 (ppm)
f1 (ppm)
9.0
8.9
8.8
8.7
8.6
8.5
8.4
8.3
8.2
8.1
8.0
7.9
7.8
7.7
7.6
7.5
7.4
7.3
7.2
9.2

(c)

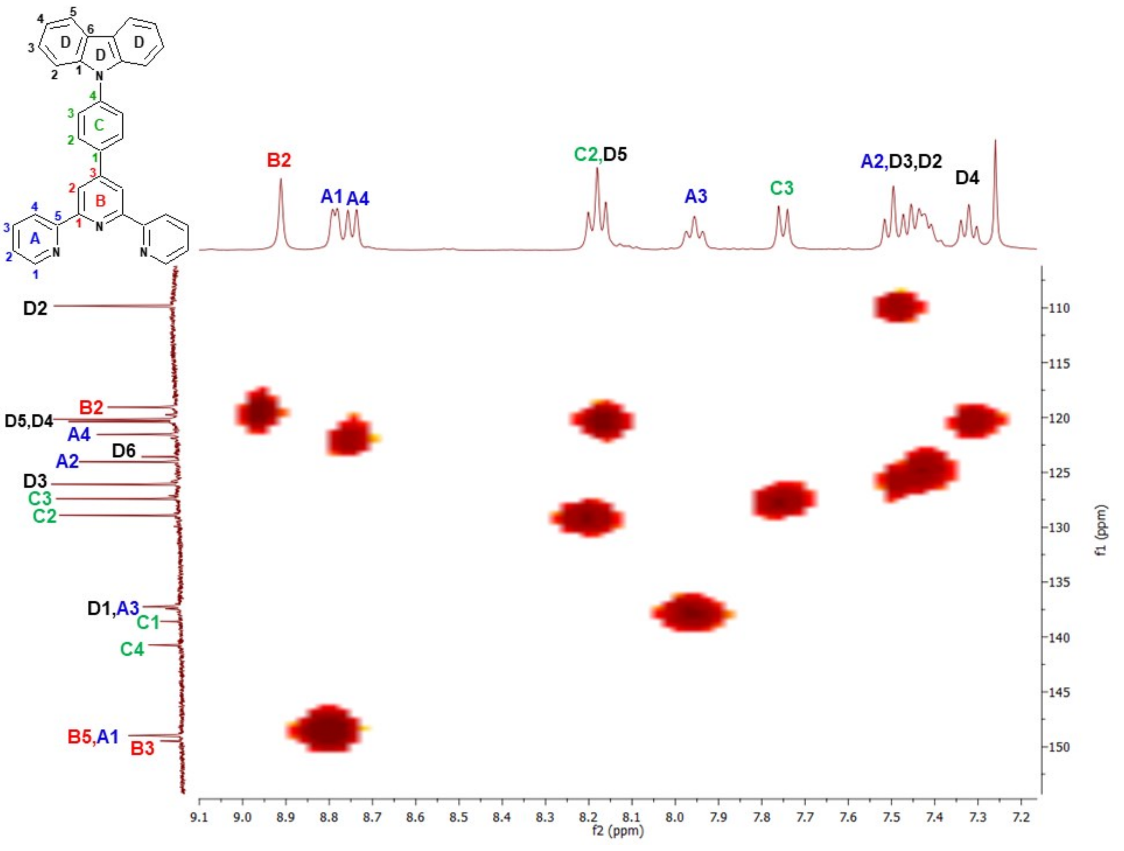
B2
A1
A4
C2,D5
A3
C3
A2,D3,D2
D4
D2
B2
D5,D4
A4
D6
A2
D3
C3
C2
D1,A3
C1
C4
B5,A1
B3
f2 (ppm)
f1 (ppm)
110
115
120
125
130
135
140
145
150

(d)

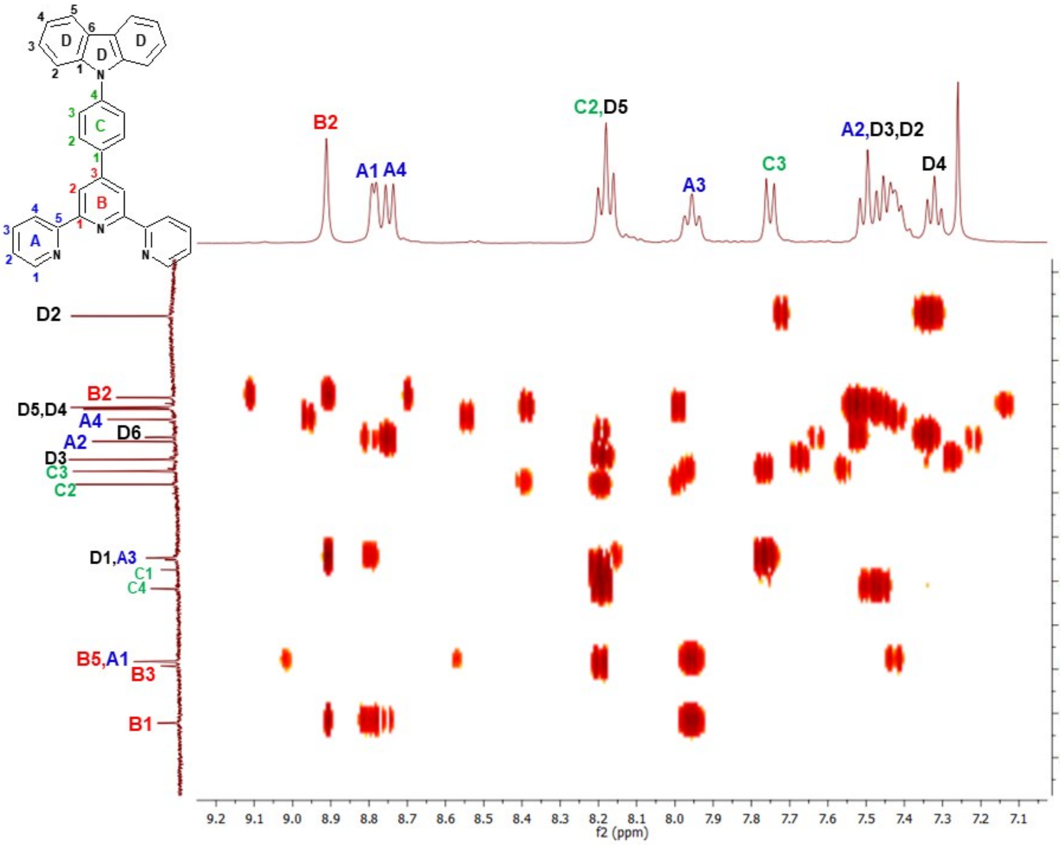

(e)

Figure S5. NMR spectra of ligand **L^1** in CDCl$_3$. ^{1}H (a), ^{13}C (b), ^{1}H–^{1}H COSY (c), ^{1}H–^{13}C HMQC (d), ^{1}H–^{13}C HMBC (e).

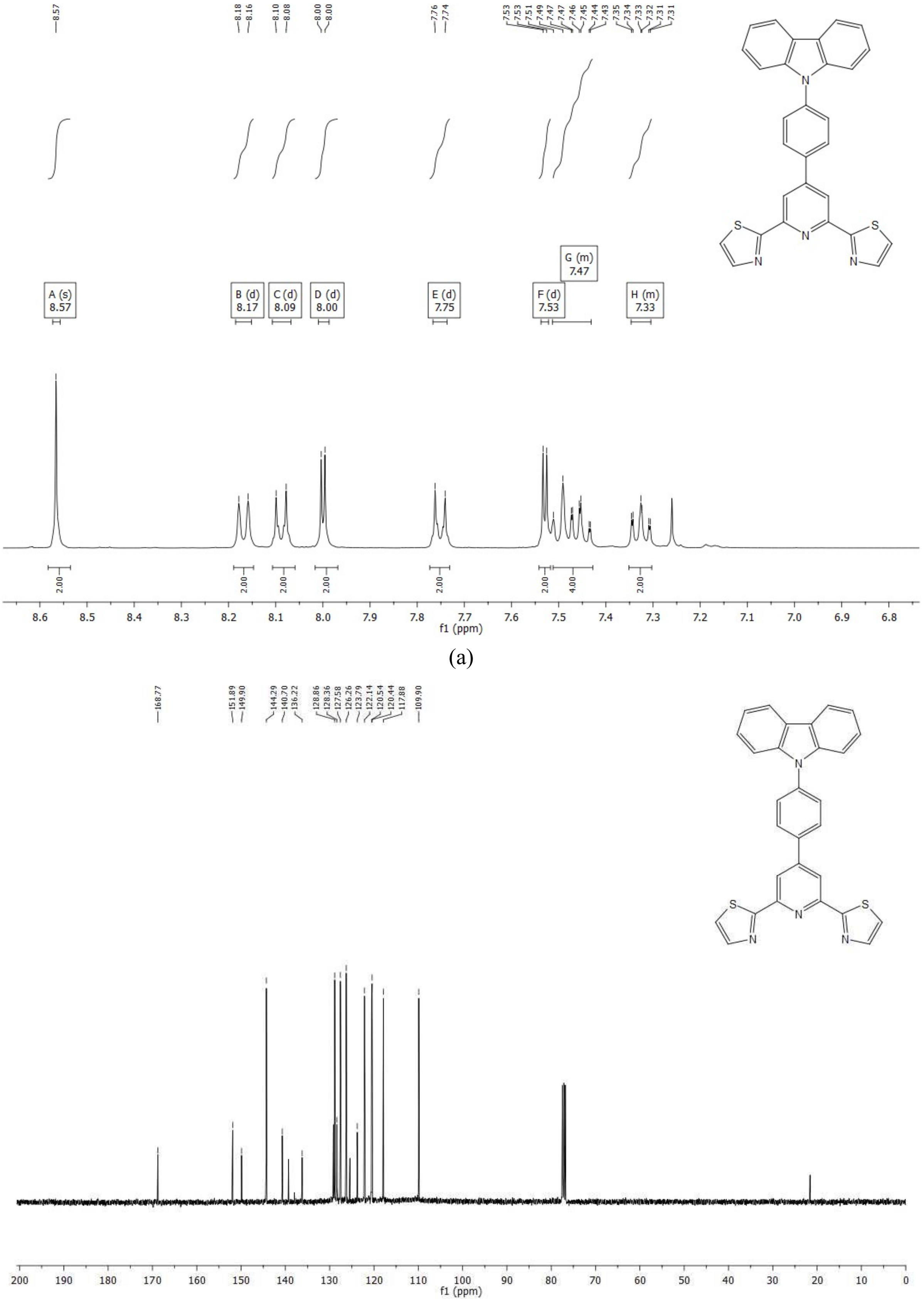

(a)

(b)

Figure S6. NMR spectra of ligand $\mathbf{L^2}$ in $CDCl_3$. ^1H (a), ^{13}C (b).

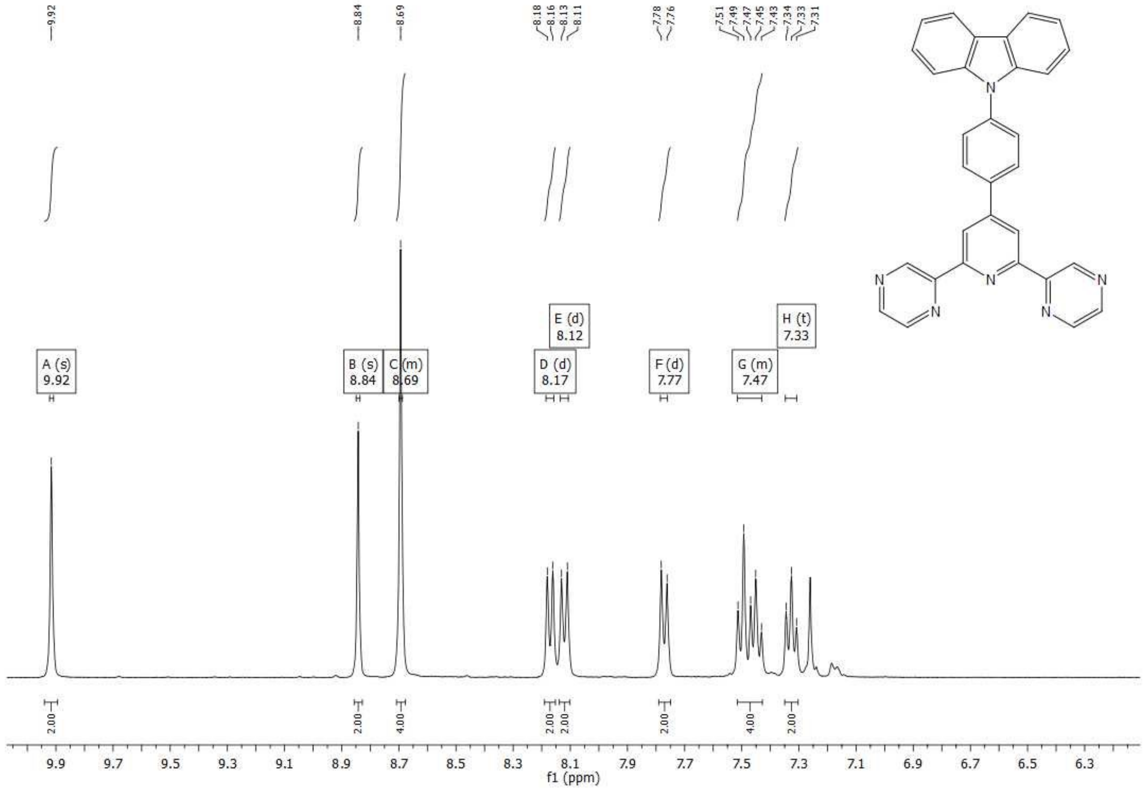

(a)

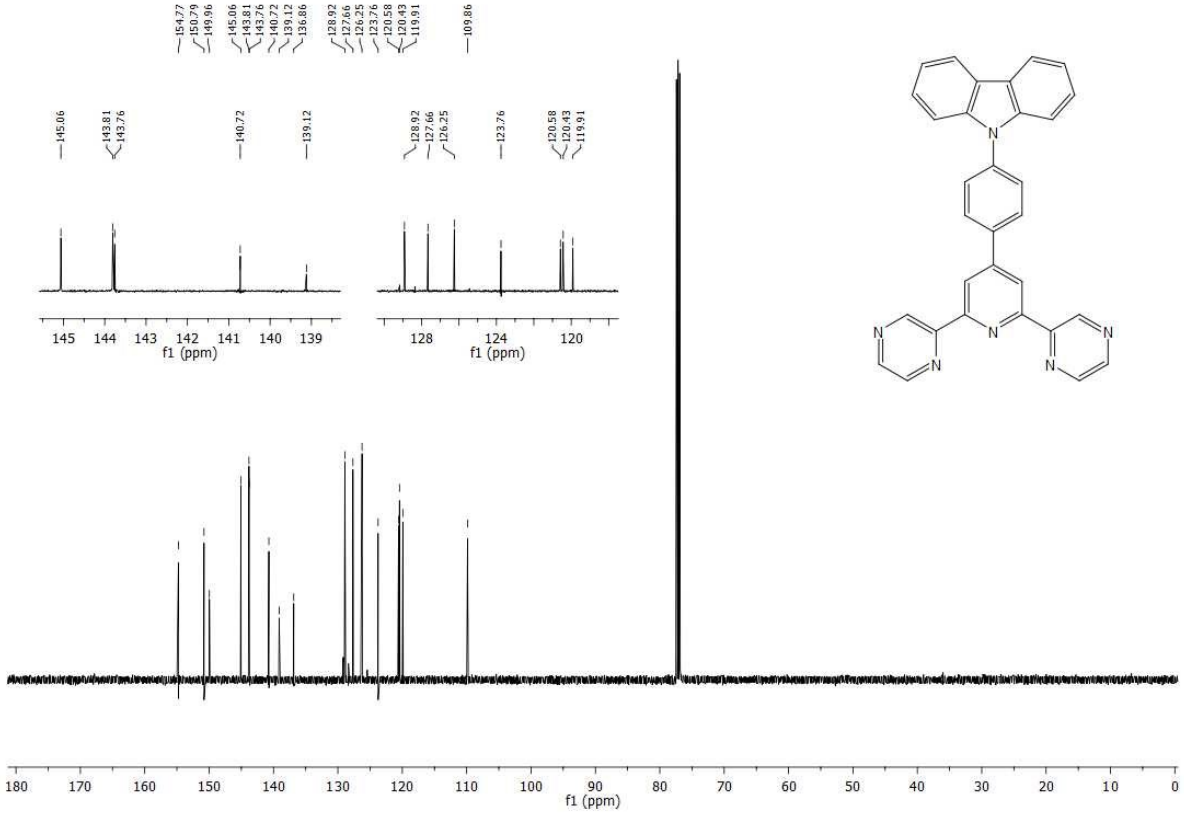

(b)

Figure S7. NMR spectra of ligand $\mathbf{L^3}$ in $CDCl_3$. ^1H (a), ^{13}C (b).

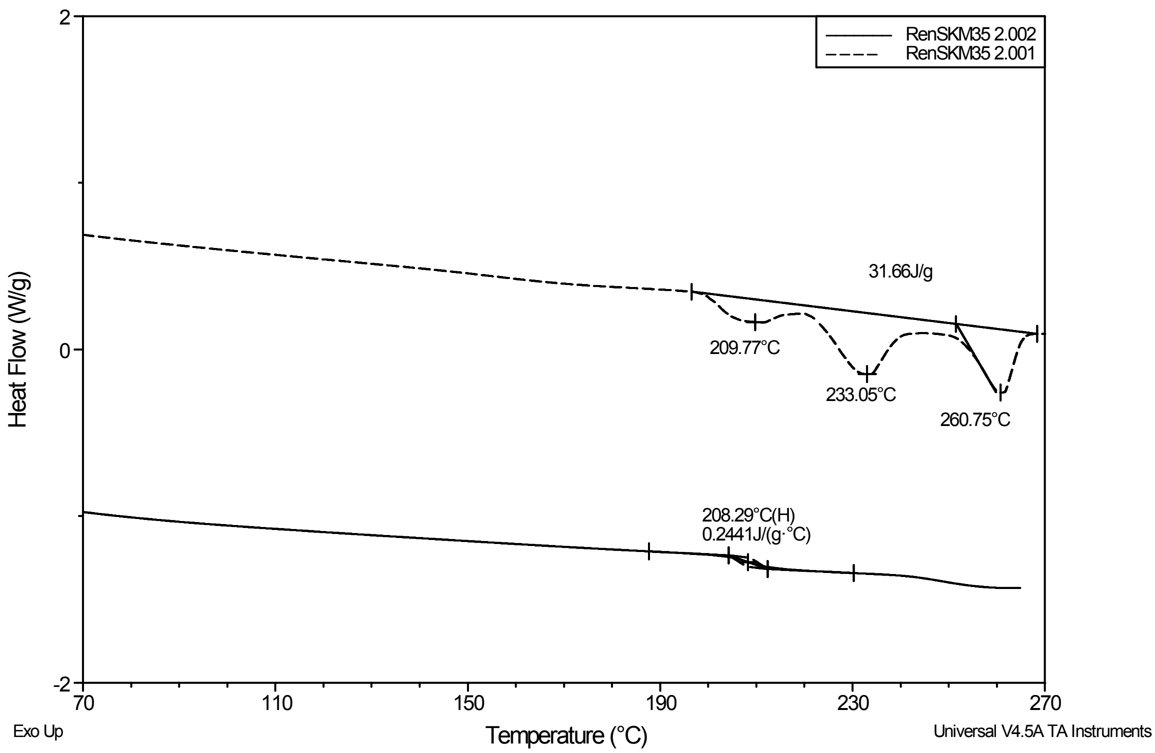

Figure S8. DSC thermograms of complex **1** registered during I and II heating scan

X-Ray analysis

Table S1. Experimental and theoretical bond lengths [Å] and angles [°] for **2**, along with calculated lengths [Å] and angles [°] for **1** and **3**.

Bond lengths				
	1	**2**		**3**
	theoretical	**experimental**	**theoretical**	**theoretical**
Re(1)–C(1)	1.923	1.916(4)	1.922	1.925
Re(1)–C(2)	1.906	1.906(4)	1.904	1.909
Re(1)–C(3)	1.901	1.916(4)	1.904	1.905
Re(1)–N(1)	2.179	2.153(3)	2.169	2.172
Re(1)–N(2)	2.239	2.243(3)	2.265	2.240
Re(1)–Cl(1)	2.499	2.4836(10)	2.496	2.492
C(1)–O(1)	1.149	1.153(4)	1.149	1.148
C(2)–O(2)	1.152	1.143(5)	1.151	1.150
C(3)–O(3)	1.155	1.116(5)	1.154	1.154

Bond angles				
	1	**2**		**3**
	theoretical	**experimental**	**theoretical**	**theoretical**
C(1)–Re(1)–N(1)	175.02	173.48(13)	174.28	174.95
C(1)–Re(1)–N(2)	102.13	99.76(13)	101.90	102.08
C(2)–Re(1)–N(1)	97.32	96.85(14)	96.81	97.17
C(2)–Re(1)–N(2)	170.11	169.67(13)	170.01	170.10
C(3)–Re(1)–N(1)	93.96	92.26(14)	94.22	93.82
C(3)–Re(1)–N(2)	97.22	98.38(13)	96.86	97.11
C(1)–Re(1)–C(2)	85.87	88.70(16)	86.60	86.03
C(2)–Re(1)–C(3)	88.52	87.24(16)	88.22	88.45
C(1)–Re(1)–C(3)	89.94	91.43(16)	90.47	90.16
N(1)–Re(1)–N(2)	74.32	74.37(11)	74.30	74.36
C(1)–Re(1)–Cl(1)	91.81	90.83(12)	91.10	91.80
C(2)–Re(1)–Cl(1)	92.19	92.47(12)	92.85	92.30
C(3)–Re(1)–Cl(1)	178.15	177.72(12)	178.15	177.94
N(1)–Re(1)–Cl(1)	84.26	85.53(8)	84.16	84.18
N(2)–Re(1)–Cl(1)	81.84	81.57(8)	81.86	81.88

Table S2. Comparative structural analysis for discussed compounds. Data for complexes **1A–3A** and **1B–3B** are taken from ref. [1]

compound	**2**	**2A**	**2B**	**1A**	**1B**	**3A**	**3B**
Ligand core	**dtpy**			**terpy**		**dppy**	
substituent R	**carbazole**	**phenyl**	**pyrrolidine**	**phenyl**	**pyrrolidine**	**phenyl**	**pyrrolidine**
Re(1)–N(1) [Å]	2.153(3)	2.157(5)	2.151(4)	2.178(5)	2.171(3)	2.160(4)	2.159(4)
Re(1)–N(2) [Å]	2.243(3)	2.243(7)	2.236(4)	2.223(4)	2.204(4)	2.199(4)	2.213(4)
Re(1)–C(1) [Å]	1.916(4)	1.913(9)	1.916(6)	1.942(8)	1.915(5)	1.934(6)	1.917(6)
Re(1)–C(2) [Å]	1.906(4)	1.912(9)	1.890(5)	1.887(6)	1.895(8)	1.896(6)	1.897(8)
Re(1)–C(3) [Å]	1.916(4)	1.911(8)	1.903(6)	1.883(7)	1.889(4)	1.888(5)	1.896(4)
Re(1)–Cl(1) [Å]	2.4836(10)	2.480(2)	2.487(1)	2.486(2)	2.490(1)	2.499(1)	2.482(1)
N(1)–Re(1)–N(2) [°]	74.37(11)	74.9(2)	74.1(1)	74.6(2)	74.2(1)	74.4(2)	74.2(1)
N(2)–Re(1)–C(1) [°]	99.76(13)	102.2(3)	100.4(2)	101.8(2)	102.7(2)	100.3(2)	103.3(2)
dihedral angle pyridine–coordinated peripheral ring [°]	15.83(14)	2.41	15.15	13.43	8.79	11.36	10.59
dihedral angle pyridine–uncoordinated peripheral ring [°]	50.90(12)	59.34	33.12	50.25	63.93	48.22	61.46
dihedral angle pyridine–phenyl [°]	34.67(19)	6.68	17.69	10.84	13.89	17.77	13.99
dihedral angle phenyl–substituent [°]	48.61(14)	–	17.35	–	3.94	–	12.78

Table S3. Weak interactions and hydrogen bonds detected in the structure of **2**.

Short intra- and intermolecular hydrogen bonds

D–H•••A	D–H [Å]	H•••A [Å]	D–A [Å]	D–H•••A [°]
C(8)–H(8)•••S(1)	0.93	2.85	3.206(4)	104.00
C(30)–H(30)•••O(3)[a]	0.93	2.57	3.204(8)	126.00

Short π•••π interactions

Cg(I)•••Cg(J)	Cg(I)•••Cg(J) [Å]	α [°]	β [°]	γ [°]	Cg(I)-Perp [Å]	Cg(J)-Perp [Å]
Cg(1)•••Cg(2)[b]	3.714(3)	12.9(2)	14.1	26.8	3.3136(18)	3.603(2)

X—Y•••Cg(J)(π-ring) interactions

X—Y•••Cg(J)	X(I)•••Cg(J) [Å]	X-Perp [Å]	γ′ [°]	Y-X(I)•••Cg(J) [°]
C(1)-O(1)•••Cg(3)	3.230(4)	-3.216	5.24	84.0(3)

α = dihedral angle between *Cg*(I) and *Cg*(J); β = angle *Cg*(I)→*Cg*(J) vector and normal to ring I; γ = angle *Cg*(I) →*Cg*(J) vector and normal to plane J; *Cg*(I)-Perp = Perpendicular distance of *Cg*(I) on ring J; *Cg*(J)-Perp = perpendicular distance of *Cg*(J) on ring I; γ′ = angle X(I)→Cg(J) vector and normal to plane J.

Cg(1) is the centroid of atoms = N2/C7/C8/C9/C10/C11; Cg(2) is the centroid of atoms = C21/C22/C23/C24/C25/C26; Cg(3) is the centroid of atoms = S2/C12/N3/C13/C14.

Symmetry codes: *a* = 2-*x*,-1/2+*y*,3/2-*z*; *b* = 2-*x*,1-*y*,1-*z*.

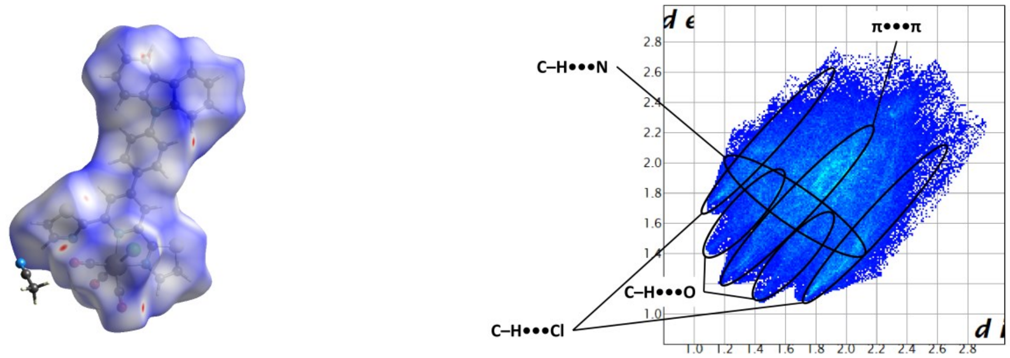

(a) (b)

Figure S9. Hirshfeld surface mapped with d_{norm} (a), and 2D fingerprint plot (b) for **2**.

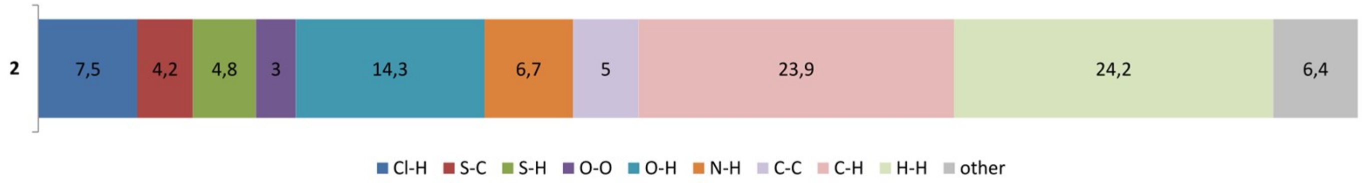

Figure S10. The relative contributions (%) of various intermolecular interactions to the Hirshfeld surface of **2**.

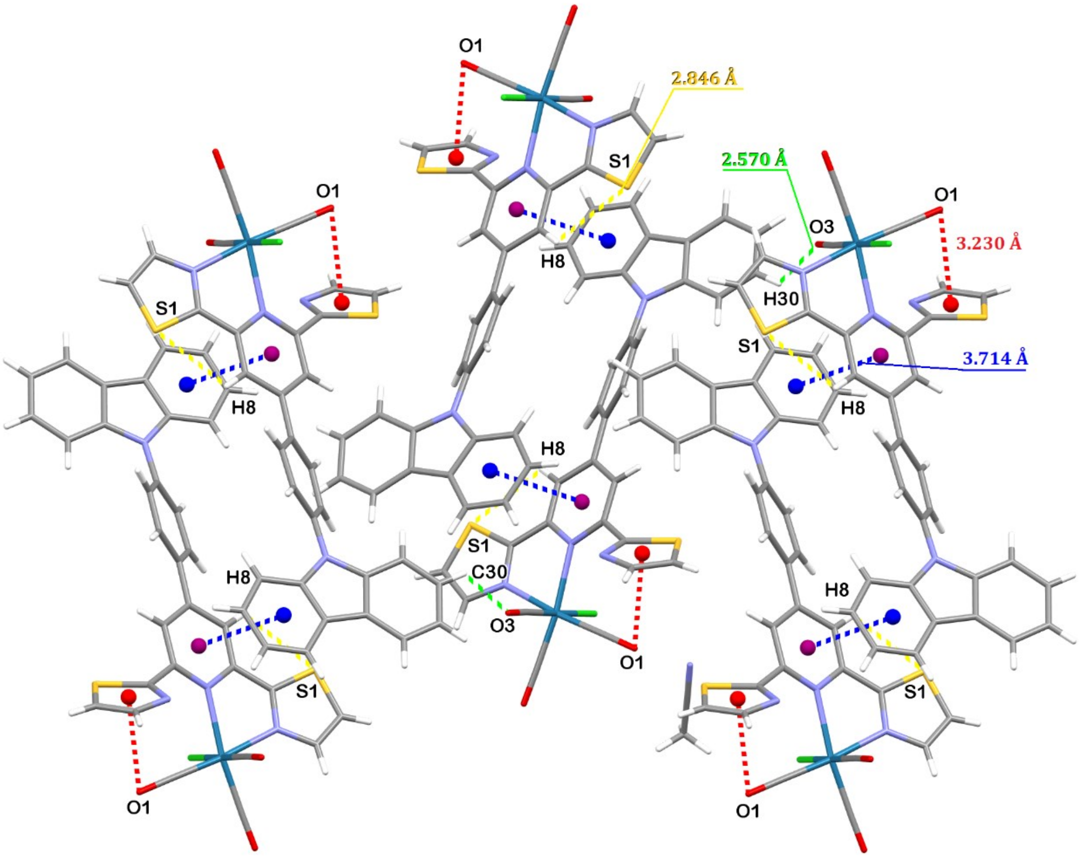

Figure S11. Weak interactions detected in the crystal lattice of **2**.

Frontier molecular orbital analysis

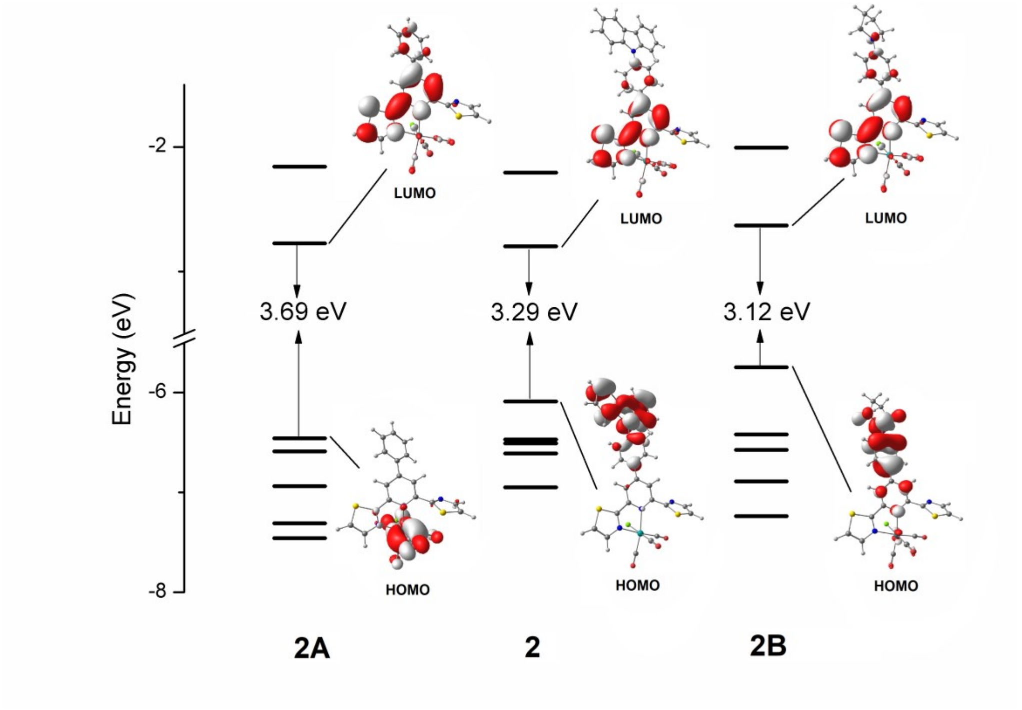

(a)

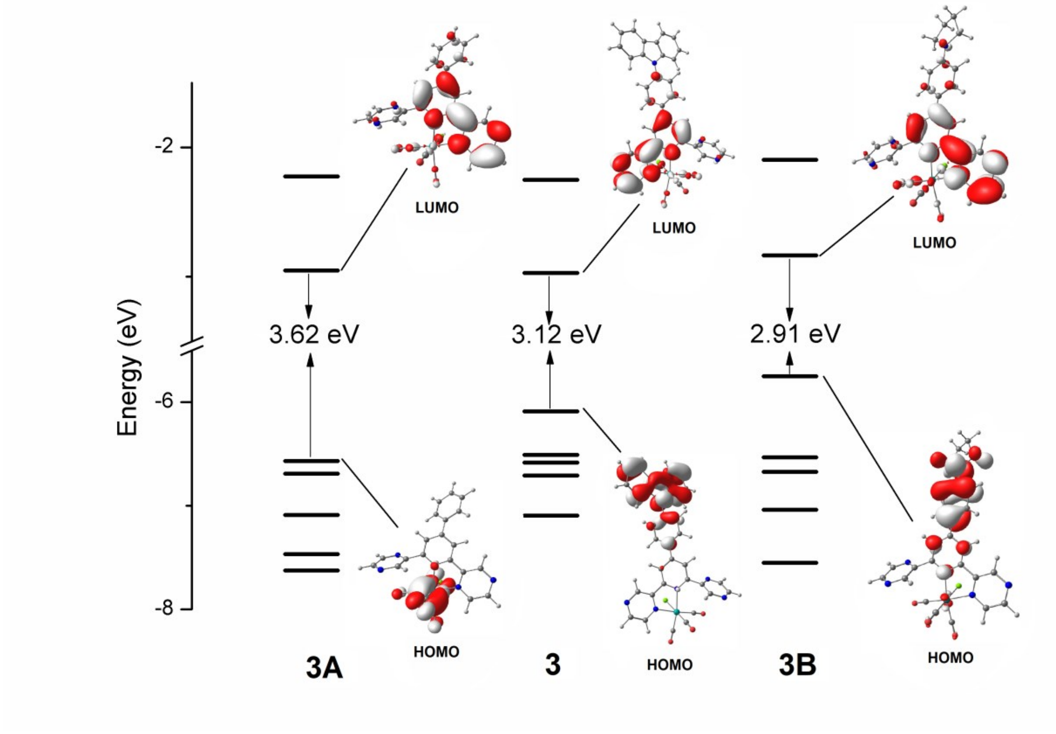

(b)

Figure S12. Partial molecular orbital energy levels of **2–3** (a-b) in comparison to the parent complexes [ReCl(CO)$_3$(L^n-κ^{2}N)] without any group attached to the phenyl ring (**2A/3A**) and that bearing pyrrolidine instead of carbazole (**2B/3B**), computed at TD-DFT/PBE1PBE/def2-TZVPD/def2-TZVP level with the use of the PCM model at polarities corresponding to MeCN. Data for complexes **2A–3A** and **2B–3B** are taken from ref. [1]

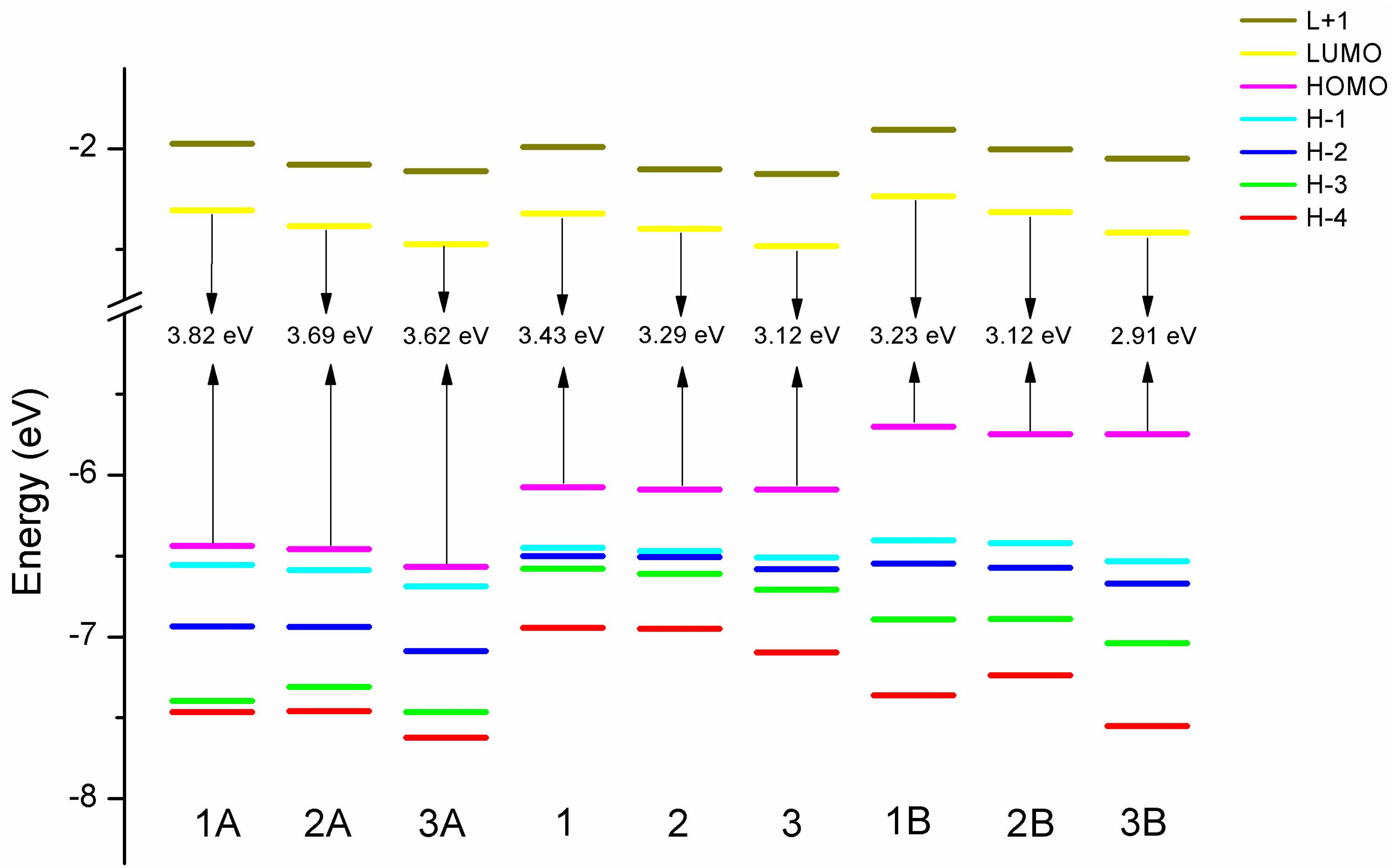

Figure S13. Energy diagram for complexes **1A–3A, 1–3, 1B–3B**. Data for complexes **1A–3A** and **1B–3B** are taken from ref. [1]

orbital compound		H-4	H-3	H-2	H-1	H	L	L+1
1A	terpy	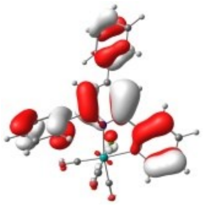	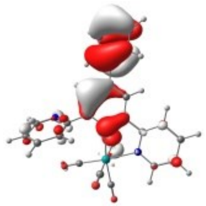	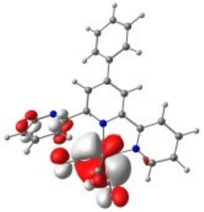	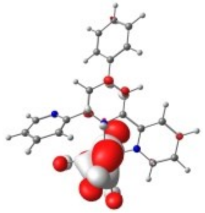	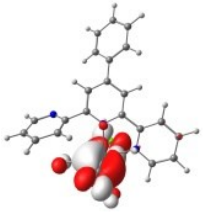	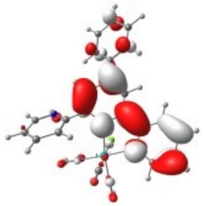	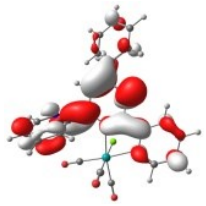
1		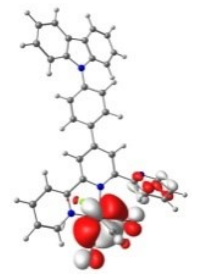	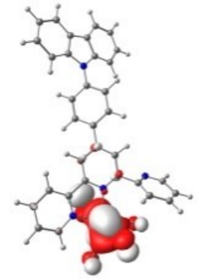	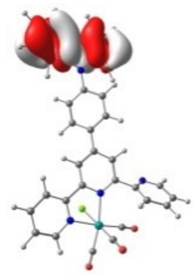	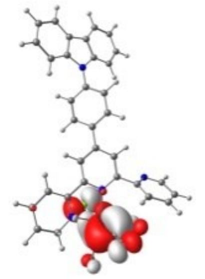	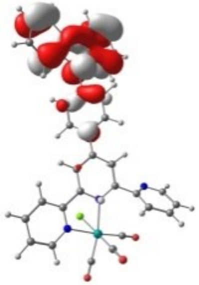	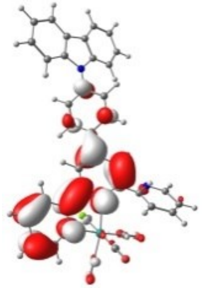	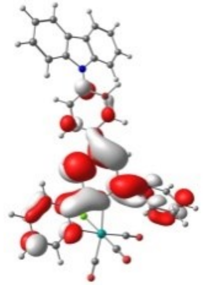
1B		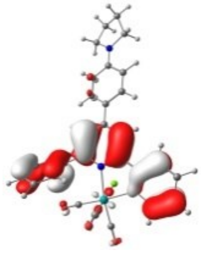	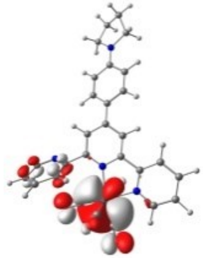	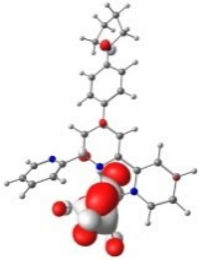	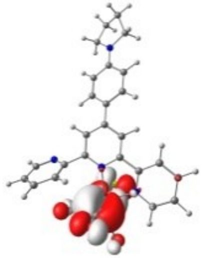	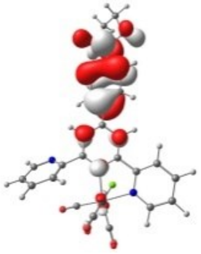	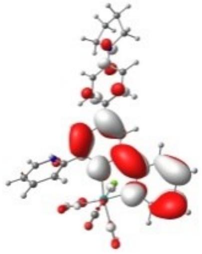	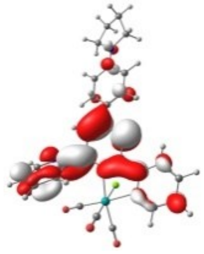

orbital compound		H-4	H-3	H-2	H-1	H	L	L+1
2A	dtpy	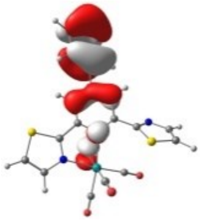	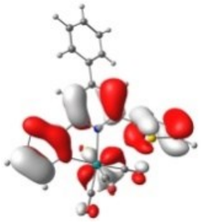	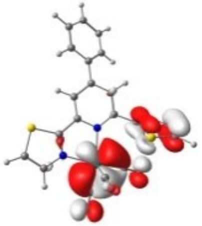	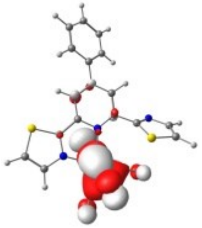	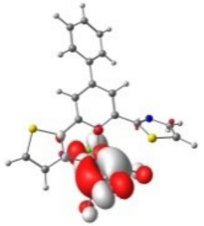	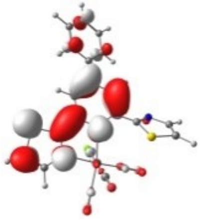	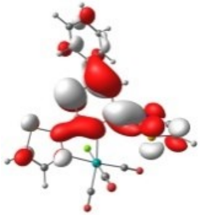
2		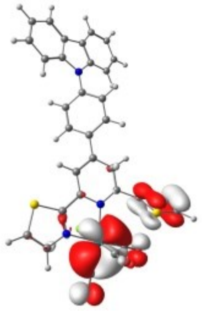	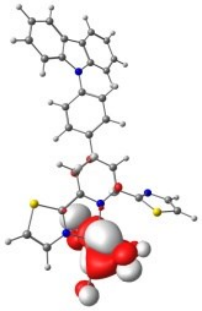	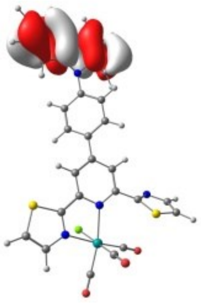	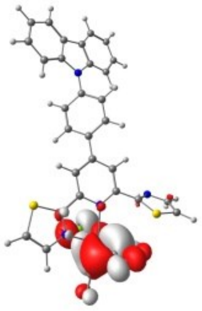	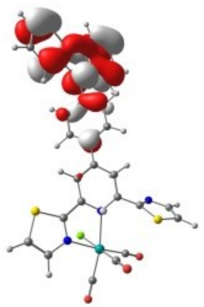	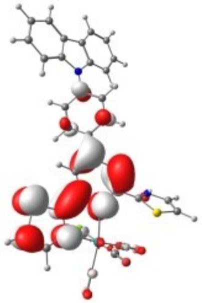	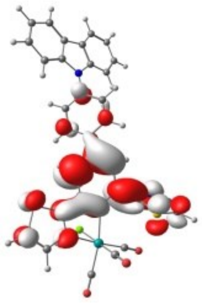
2B		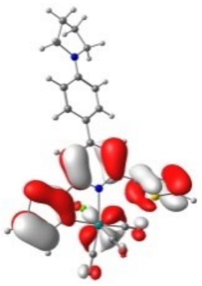	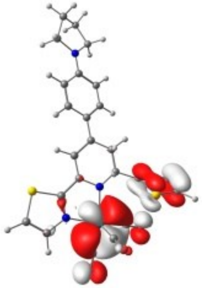	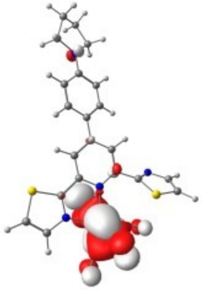	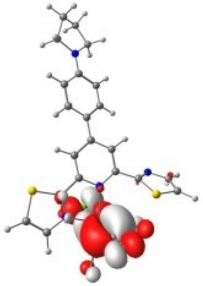	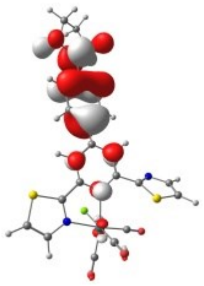	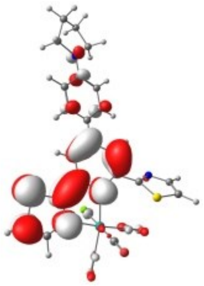	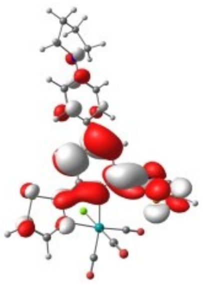

orbital compound		H-4	H-3	H-2	H-1	H	L	L+1
3A	dppy	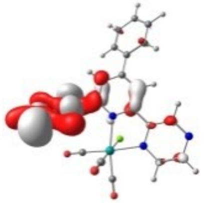	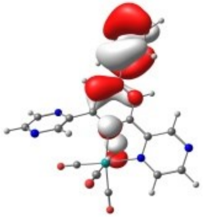	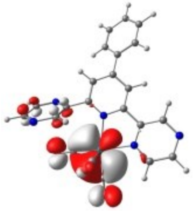	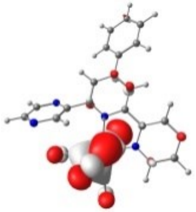	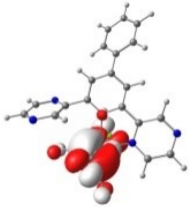	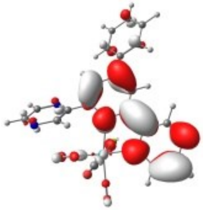	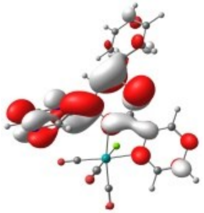
3		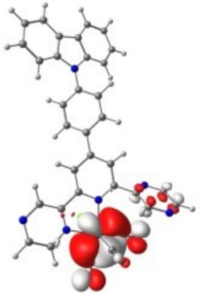	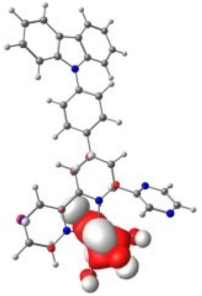	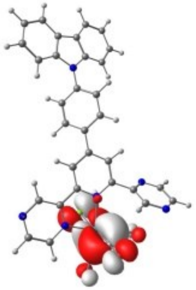	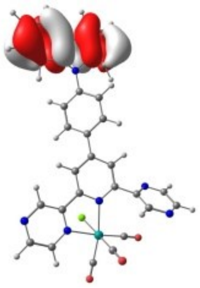	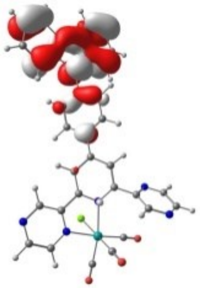	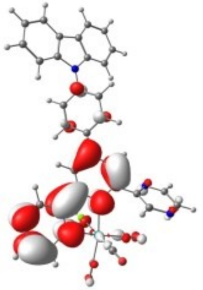	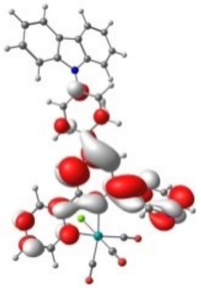
3B		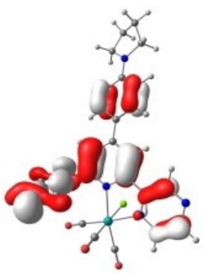	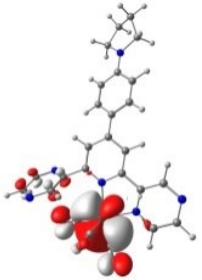	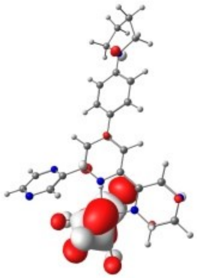	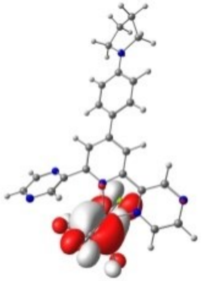	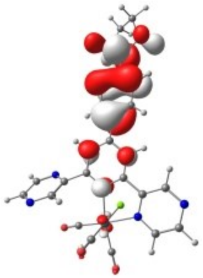	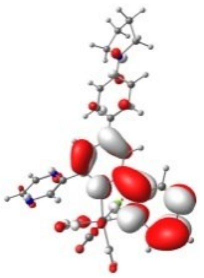	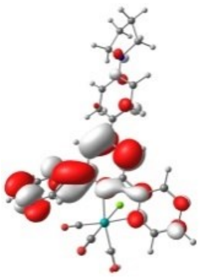

Figure S14. Selected molecular orbitals of complexes 1-3 in comparison to those for 1A-3A and 1B-3B. Data for complexes 1A–3A and 1B–3B are taken from ref. [1].

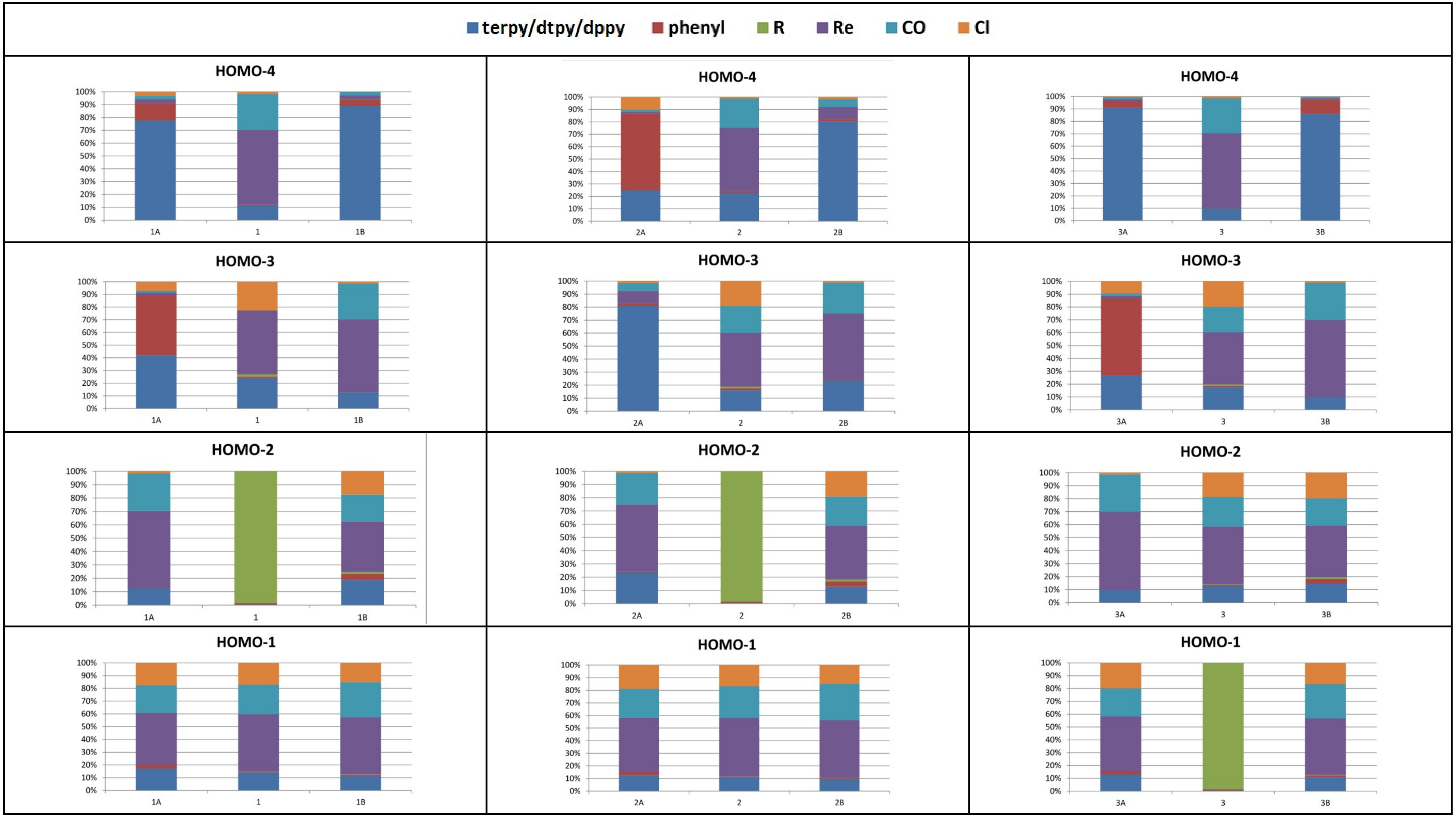
■ terpy/dtpy/dppy
■ phenyl
■ R
■ Re
■ CO
■ Cl
HOMO-4
HOMO-4
HOMO-4
100%
90%
80%
70%
60%
50%
40%
30%
20%
10%
0%
1A
1
1B
2A
2
2B
3A
3
3B
HOMO-3
HOMO-3
HOMO-3
1A
1
1B
2A
2
2B
3A
3
3B
HOMO-2
HOMO-2
HOMO-2
1A
1
1B
2A
2
2B
3A
3
3B
HOMO-1
HOMO-1
HOMO-1
1A
1
1B
2A
2
2B
3A
3
3B

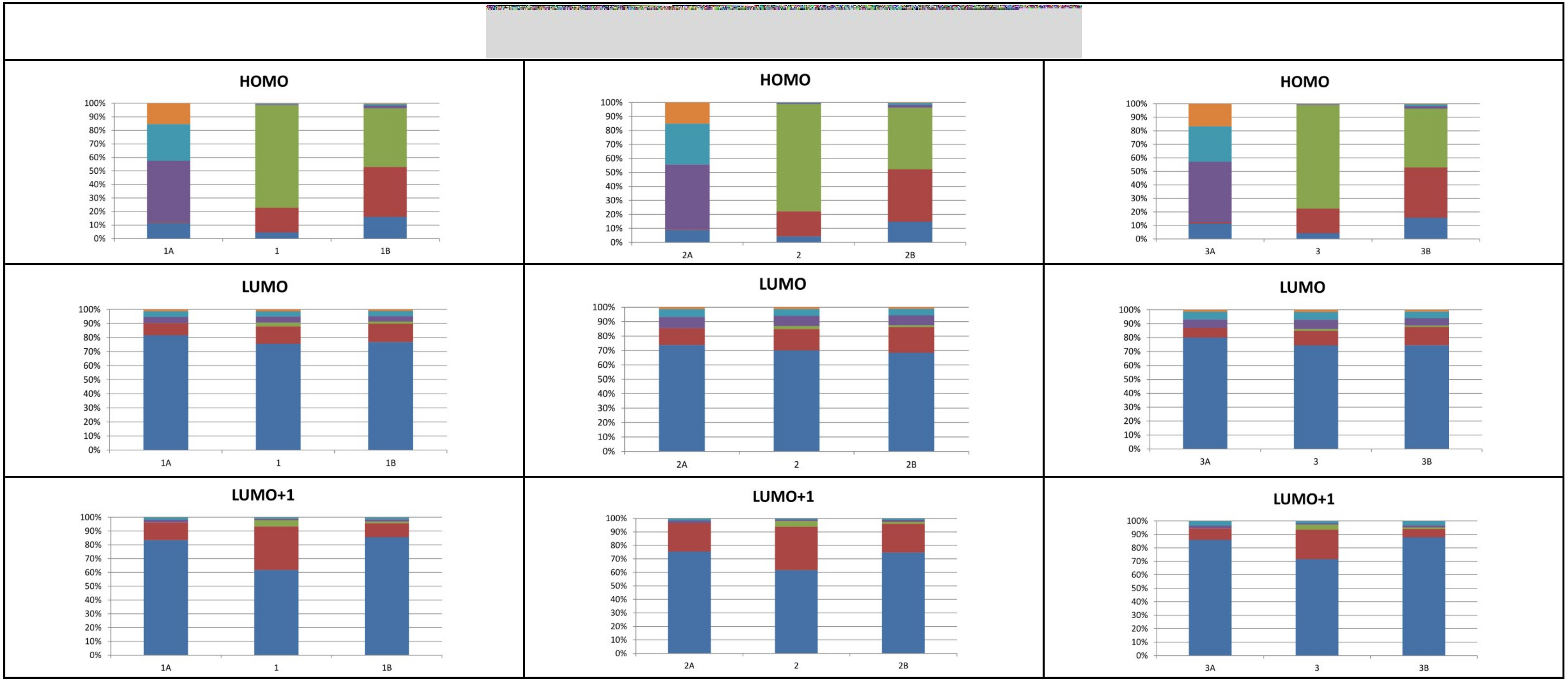

Figure S15. Percentage composition of selected molecular orbitals of complexes **1-3, 1A-3A** and **1B-3B**. Data for complexes **1A–3A** and **1B–3B** are taken from ref. [1]

Table S4. Calculated ionization potentials and electron affinities (vertical and adiabatic), energy gap, as well as hole and electrons reorganization energies and extraction potentials (DFT/PBE1PBE/def2-TZVPD/def2-TZVP) for **1–3** in comparison with **1A-3A** and **1B-3B**. Data for complexes **1A–3A** and **1B–3B** are taken from ref. [1]

Complex	IP(v) [eV]	IP(a) [eV]	EA(v) [eV]	EA(a) [eV]	λ_{hole} [eV]	$\lambda_{electron}$ [eV]	HEP [eV]	EEP [eV]	energy gap(a) [eV]
1A	6.16	5.83	2.89	3.05	0.71	0.33	5.45	3.21	2.78
1	5.78	5.73	2.92	3.08	0.10	0.38	5.68	3.30	2.65
1B	5.38	5.32	2.76	2.93	0.11	0.34	5.26	3.10	2.39
2A	6.18	5.85	3.06	3.22	0.70	0.32	5.48	3.38	2.63
2	5.80	5.75	3.08	3.24	0.10	0.38	5.70	3.46	2.51
2B	5.42	5.36	2.92	3.10	0.12	0.35	5.30	3.27	2.27
3A	6.29	5.97	3.22	3.38	0.69	0.31	5.60	3.54	2.59
3	5.80	5.75	3.24	3.40	0.10	0.38	5.70	3.62	2.35
3B	5.42	5.36	3.11	3.27	0.12	0.33	5.30	3.44	2.09

The ionization potentials (IPs), electronic affinities (EAs) and reorganization energies (λ_{hole} and $\lambda_{electron}$) were calculated and compared with those for **1A**–**3A** and **1B**–**3B** in order to estimate the impact of 9-carbazole unit on the energy barriers for injection and transport rates of the holes and electrons of the designed complexes [ReCl(CO)$_3$(L^n-κ^{2}N)]. The more efficient charge-transfer rate is predicted for systems showing higher EA(v) and lower IP(v) values, and thus lower reorganization energies reflecting the geometric relaxation associated with going from the neutral to the ionized state, and vice versa.

The EAs and EEPs values increase in the order [ReCl(CO)$_3$(R-*terpy*-κ^{2}N)] (**1**) < [ReCl(CO)$_3$(R-*dtpy*-κ^{2}N)] (**2**) < ReCl(CO)$_3$(R-*dppy*-κ^{2}N)] (**3**), which correlates well with increasing stabilization of LUMO energy level in this sequence. On the contrary, IPs of the designed complexes **1**–**3** have comparable values, falling in the narrow range 5.78–5.80 eV for IP(v) and 5.73–5.75 eV for IP(a). With respect to the corresponding parent complexes **1A**–**3A**, the IP values of **1**–**3** are lower, while EAs remain almost the same (Table S4). On the contrary, the replacement of the 9-carbazole unit by pyrrolidine leads to decreasing of both IP and EA values. Importantly, functionalization of the imine ligand with 9-carbazole and pyrrolidine results in effective reduction of the values λ_{hole} relative to the parent complexes (**1A**–**3A**), which may support their better hole transporting performance. On the other hand, there is no significant difference in $\lambda_{electron}$ between **1**–**3** and comparative compounds (**1A**–**3A** and **1B**–**3B**). Consequently, opposite trends are observed in $\lambda_{electron}$ and λ_{hole} values for the parent complexes **1A**–**3A** and [ReCl(CO)$_3$(L^n-κ^{2}N)] complexes bearing 9-carbazole- and pyrrolidine-substituted triimine ligands. For the latter $\lambda_{electron}$ values are higher than λ_{hole} ones.

Electrochemistry

Compound	DPV	CV
1	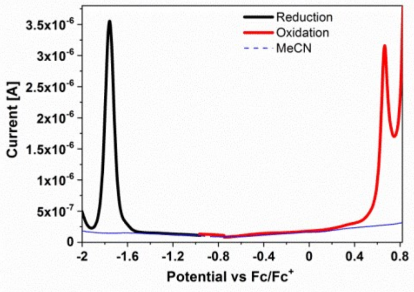	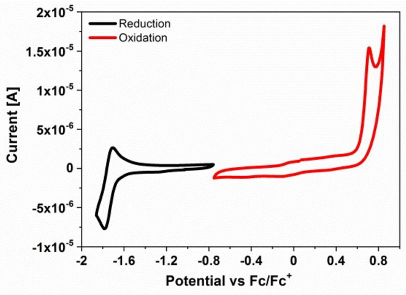
2	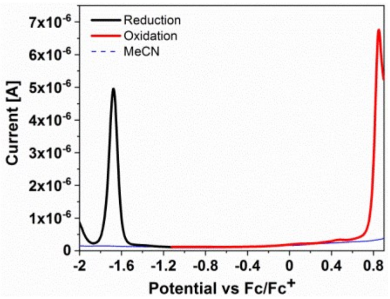	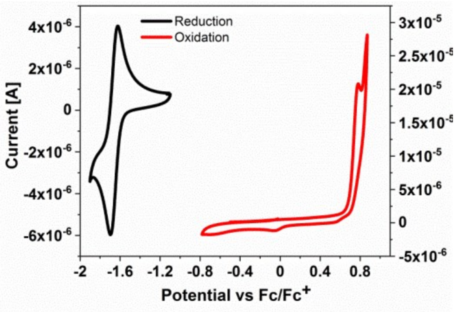
3	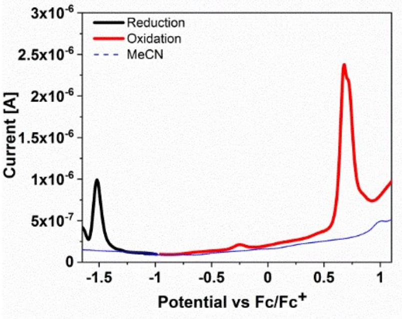	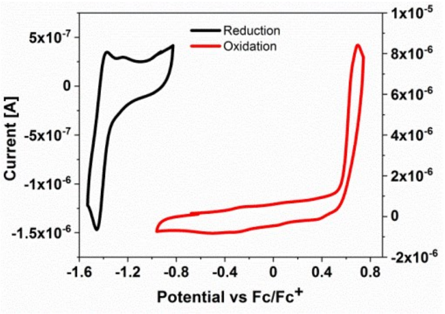

Figure S16. Cyclic voltammetry (CV, right side) and differential pulse voltammetry (DPV, left side) curves of **1–3**.

Table S5. Comparison of electrochemical properties of **1–3** with those for **1A–3A** and **1B–3B.** Data for complexes **1A–3A** and **1B–3B** are taken from ref. [1].

compound	E_{red1} [V] *(E_{pc}-E_{pa} [V])*	E_{red2} [V]	E_{red3} [V]	$E_{red1onset}$ [V]	EA [eV]^a	E_{ox1} [V] *(E_{pc}-E_{pa} [V])*	E_{ox2} [V]	E_{ox3} [V]	$E_{ox1onset}$ [V]	IP [eV] ^{a}	E_g [eV]	E_g^{opt} [eV] ^{c}
1A	-1.73 *(0.095)*	-2.04	–	-1.61	-3.49	0.78	0.91	1.07	0.68	-5.78	2.29	1.86
1	-1.78	-2.04	–	-1.65	-3.45	0.71	0.86	–	0.59	-5.69	2.24	1.91
1B	-1.84 *(0.091)*	-2.07	-2.23	-1.67	-3.43	0.58	0.81	–	0.46	-5.56	2.13	1.78
2A	-1.60 *(0.101)*	-2.00	–	-1.47	-3.63	0.93	–	–	0.79	-5.89	2.26	1.69
2	-1.69	-2.07	–	-1.59	-3.51	0.78	0.85	–	0.66	-5.76	2.25	1.69
2B	-1.71 *(0.083)*	-2.10	-2.21	-1.59	-3.51	0.56 *(0.090)*	0.88	–	0.44	-5.54	2.03	1.66
3A	-1.34 *(0.111)*	-1.83	–	-1.25	-3.85	0.83	1.10	–	0.57	-5.67	1.82	1.69
3	-1.46	-1.68	–	-1.32	-3.78	0.69	–	–	0.55	-5.65	1.87	1.69
3B	-1.50 *(0.098)*	-1.76	-1.99	-1.38	-3.72	0.59 *(0.089)*	1.05	–	0.46	-5.56	1.84	1.70

^{a}EA = -5,1 – $E_{red1onset}$, IP = -5,1 – $E_{ox1\ onset}$, $^c E_g^{opt}$ = 1241/λ_{em}

Absorption Spectral Behavior and Time-Dependent DFT calculations

Table S6. The absorption maxima and molar extinction coefficient values for **1–3, 1A–3A** and **1B–3B**. Data for complexes **1A–3A** and **1B–3B** are taken from ref. [1].

compound	medium	absorbance /nm ($\varepsilon \cdot 10^4$ /$M^{-1}cm^{-1}$)
1A	acetonitrile	374.4 (0.46), 324.1 (1.34), 293.1 (2.54), 260.3 (2.84), 218.0 (2.94)
	chloroform	396.9 (0.28), 297.4 (1.60), 263.8 (1.82)
1	acetonitrile	378 (1.24), 313 (1.72), 286 (2.19), 251 (3.56), 235 (5.06)
	chloroform	393 (0.99), 337 (0.99), 309 (1.79), 285 (2.55), 245 (4.01)
1B	acetonitrile	414.1 (2.51), 308.2 (2.40), 247.7 (3.05), 191.1 (8.68)
	chloroform	420.9 (2.42), 306.9 (2.83), 246.9 (3.38)
2A	acetonitrile	388.6 (0.53), 328.8 (1.70), 294.6 (2.57), 278.0 (2.48)
	chloroform	417.4 (0.44), 325.2 (1.69), 296.4 (2.24), 278.9 (2.28)
2	acetonitrile	385 (1.37), 334 (2.14), 286 (2.86), 235 (5.24)
	chloroform	412 (2.12), 335 (3.65), 329 (3.59), 287 (5.60), 244 (7.60)
2B	acetonitrile	446.1 (2.62), 380.2 (1.34), 330.7 (1.78), 318.1 (1.85), 259.6 (2.26), 195.0 (6.13)
	chloroform	456.8 (3.21), 389.2 (1.87), 332.9 (2.16), 321.4 (2.38), 262.1 (2.93)
3A	acetonitrile	405.0 (0.42), 334.2 (1.35), 303.7 (2.24), 277.2 (2.41), 242.4 (2.05)
	chloroform	431.4 (0.42), 314.8 (2.46), 274.2 (2.44), 247.7 (2.17)
3	acetonitrile	396 (2.11), 335 (3.67), 317 (4.38), 279 (6.81), 236 (9.91)
	chloroform	424 (0.41), 319 (0.99), 277 (1.76), 258 (1.89), 245 (2.08)
3B	acetonitrile	454.2 (0.45), 369.8 (0.41), 318.7 (0.57), 248.5 (0.62), 192.6 (1.41)
	chloroform	470.1 (1.13), 374.3 (1.23), 315.3 (1.76), 247.7 (1.89)

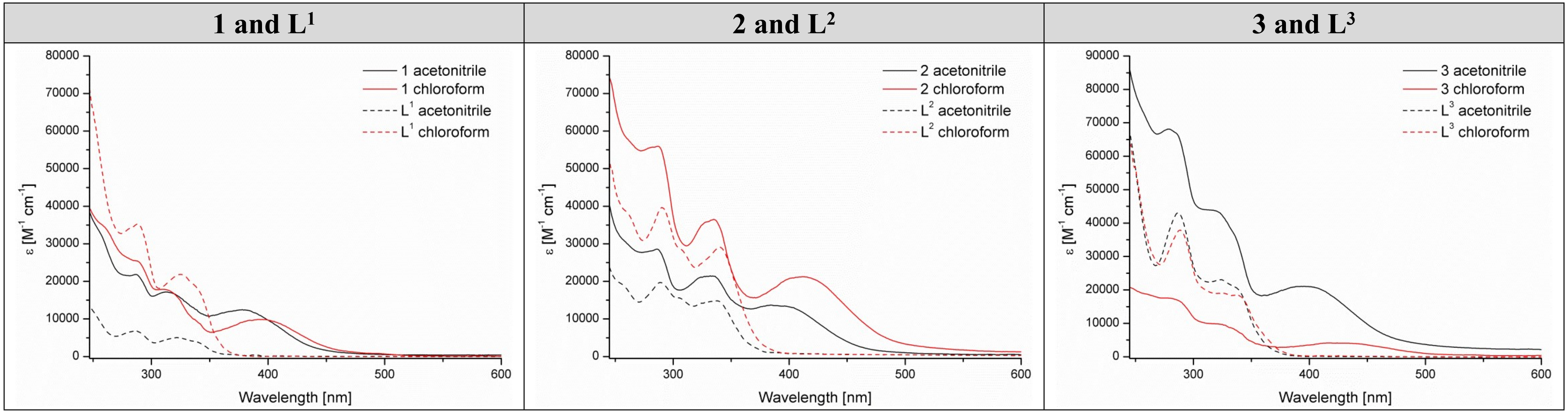

1 and L^1

2 and L^2

3 and L^3

Figure S17. UV-Vis spectroscopic properties of 1–3 in comparison to the free ligands **L^1–L^3**

	1 in comparison to 1A and 1B	**2 in comparison to 2A and 2B**	**3 in comparison to 3A and 3B**
	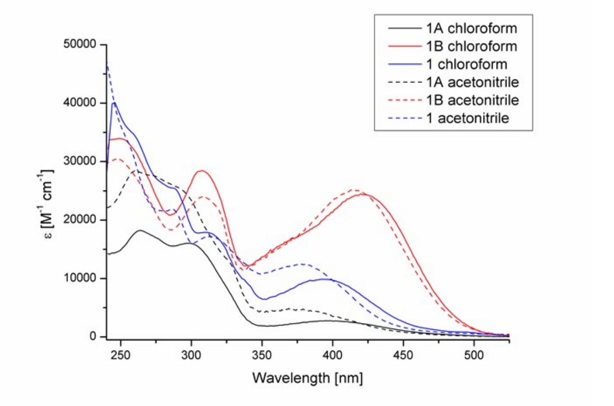	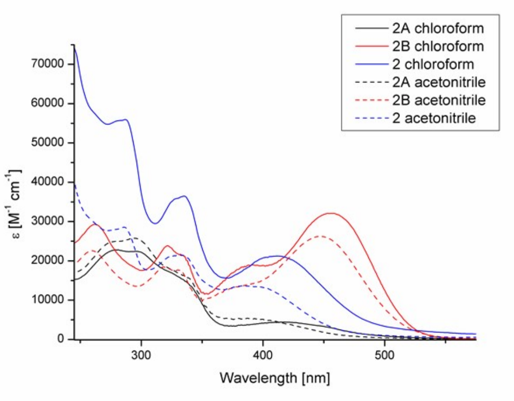	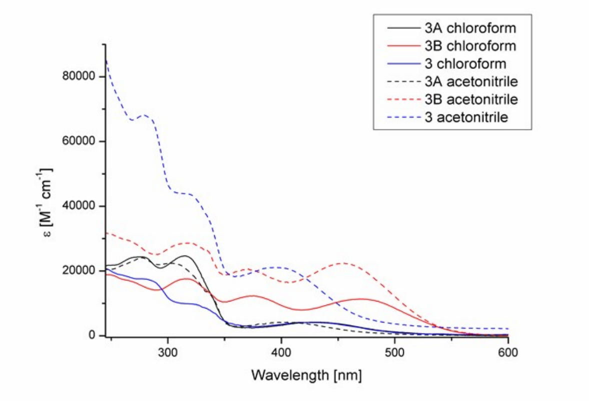
acetonitrile	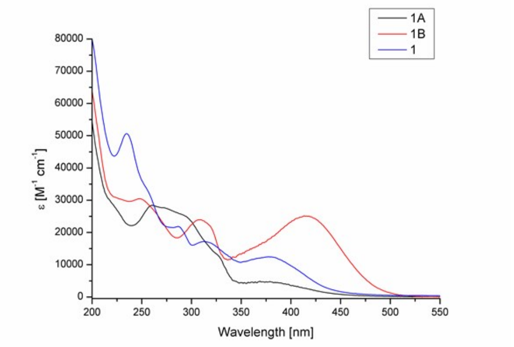	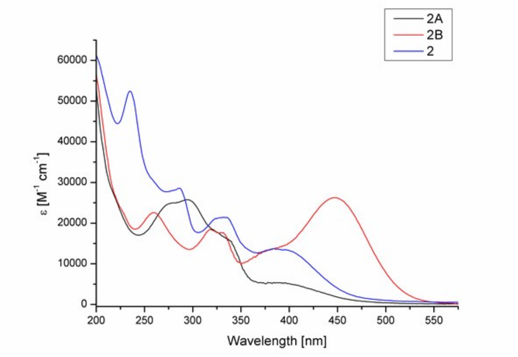	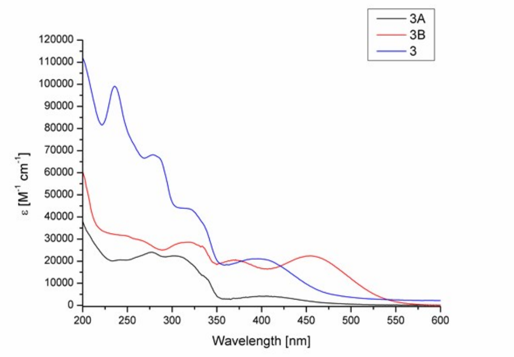
chloroform	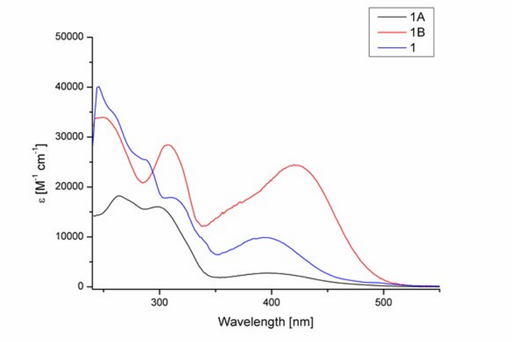	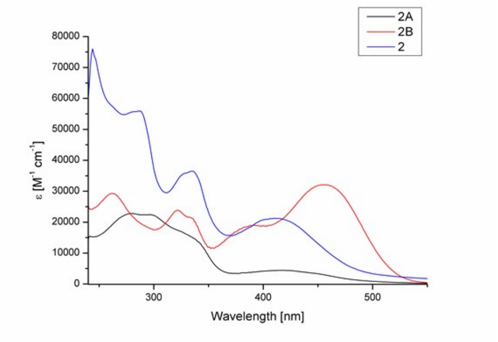	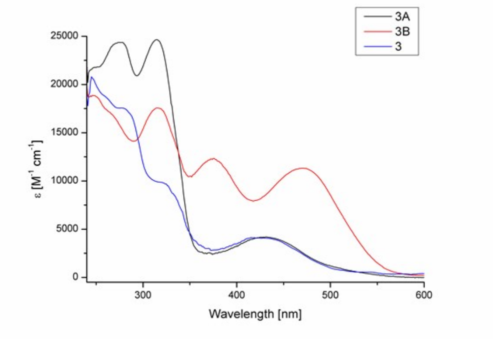

Figure S18. UV-Vis spectroscopic properties of **1–3** in comparison to the spectral profiles of **1A–3A** and **1B–3B**. Data for complexes **1A–3A** and **1B–3B** are taken from ref. [1].

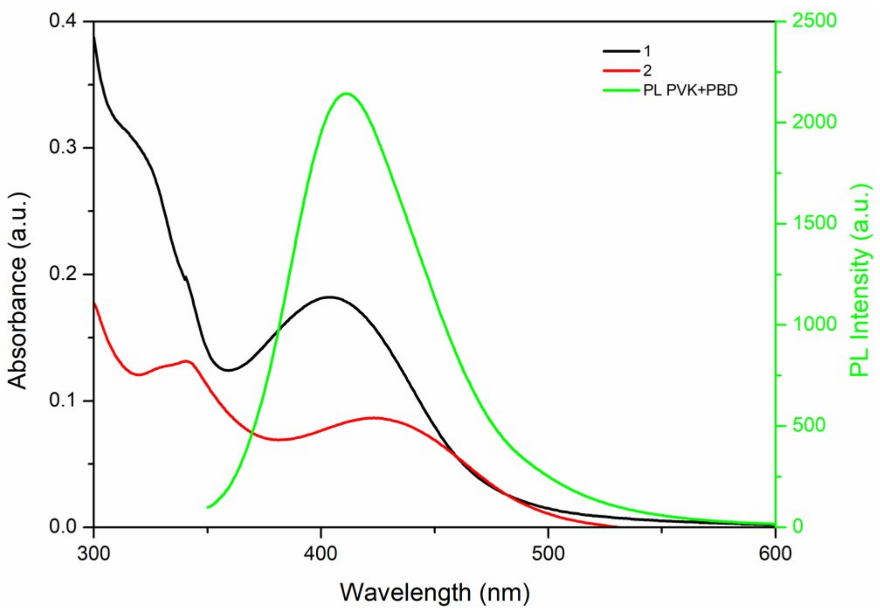

Figure S19. UV-vis spectra of **1** and **2** as thin films on glass substrate and photoluminescence spectrum of PVK:PBD. Green spectra are scaled to the right Y axis.

	1A	**1**	**1B**
acetonitrile	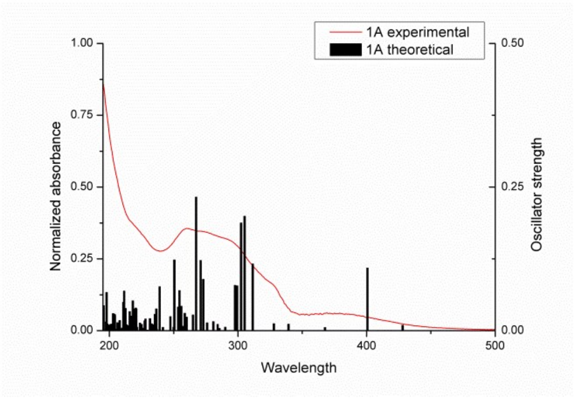	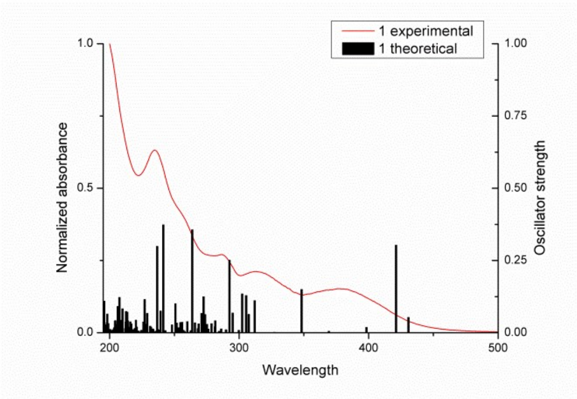	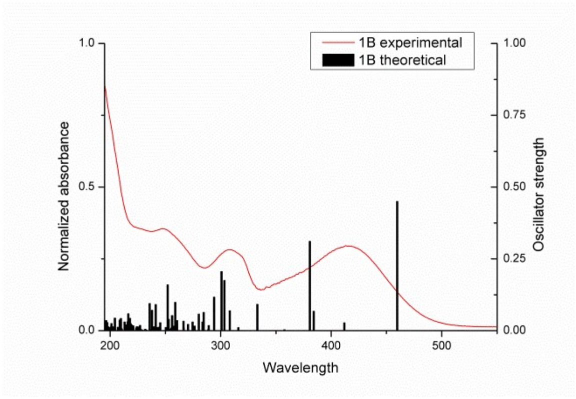
chloroform	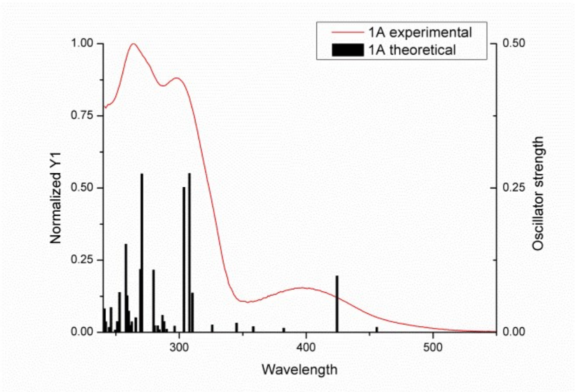	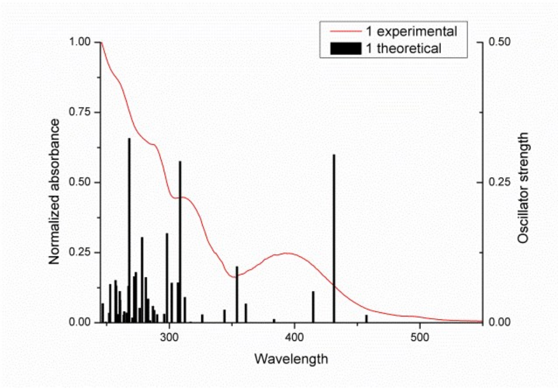	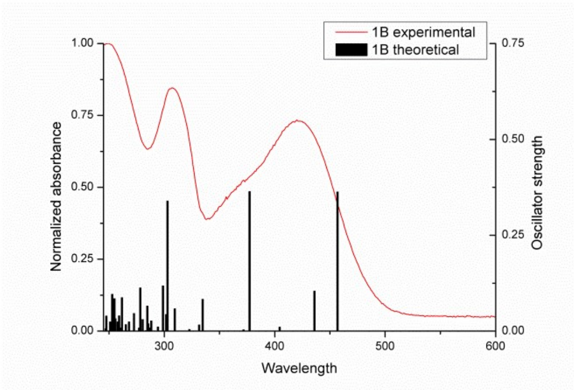
	2A	**2**	**2B**
acetonitrile	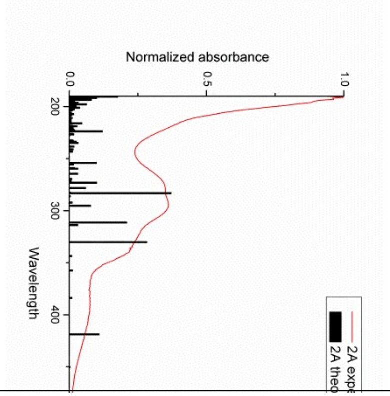	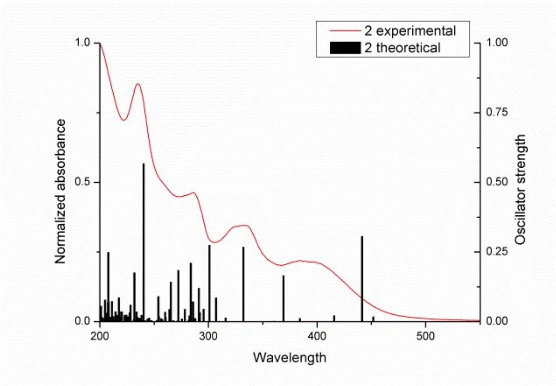	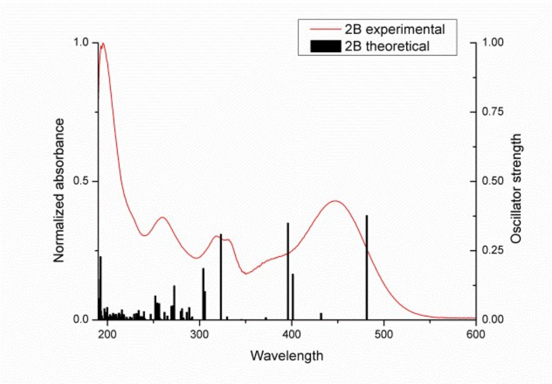

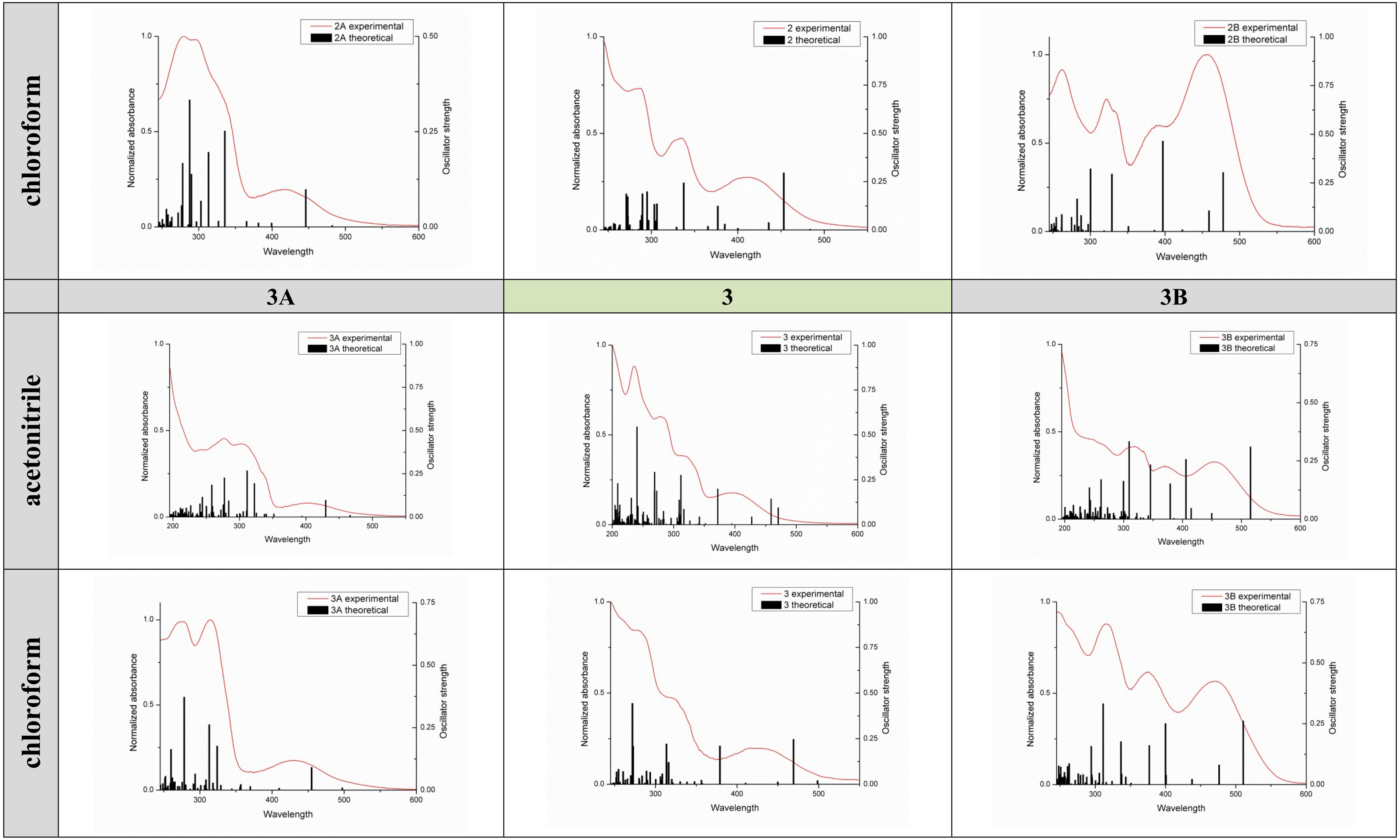

Figure S20. Experimental (red line) absorption spectra and calculated transitions (black) of for **1–3**, **1A–3A** and **1B–3B**. The transitions were computed at TD-DFT/PBE1PBE/def2-TZVPD/def2-TZVP level with the use of the PCM model at polarities corresponding to MeCN and $CHCl_3$, respectively. Data for complexes **1A–3A** and **1B–3B** are taken from ref. [1].

Table S7. The energies and characters of spin-allowed electronic transitions assigned to the lowest wavelength absorption bands of complexes **1–3, 1A–3A** and **1B–3B**. The transitions were computed at TD-DFT/PBE1PBE/def2-TZVPD/def2-TZVP level with the use of the PCM model at polarities corresponding to MeCN. Data for complexes **1A–3A** and **1B–3B** are taken from ref. [1].

Compound (medium)	**Experimental absorption λ; nm (10^4 ε; $M^{-1}cm^{-1}$)**	**Calculated transitions**				
		Major contribution (%)	**Character**	**E [eV]**	**λ [nm]**	**Oscillator strength**
1A	374.4 (0.46)	H → L (99%)	MLLCT	2.90	428.06	*0.0098* S_1
		H-1 → L (98%)	MLLCT	3.09	400.71	*0.1093* S_2
		H-2 → L (98%)	MLLCT	3.37	367.72	*0.0057* S_3
1	378 (1.24)	H-1 → L (83%) H → L (14%)	MLCT ILCT	2.88	430.78	*0.0536* S_1
		H → L (76%) H-1 → L (16%)	ILCT MLCT	2.94	421.20	*0.3034*S_2
		H-3 → L (90%)	MLCT	3.11	398.38	*0.0187*S_3
		H-4 → L (98%)	MLCT	3.36	369.26	*0.0054* S_4
		H-2 → L (98%)	ILCT	3.45	359.45	*0.0001* S_5
		H → L+1 (90%)	ILCT	3.56	348.22	*0.1498* S_6
1B	414.1 (2.51)	H → L (97%)	ILCT	2.70	459.61	*0.4501* S_1
		H-1 → L (98%)	MLLCT	3.01	411.82	*0.0274* S_2
		H-2 → L (90%)	MLLCT	3.23	384.16	*0.0681* S_3
		H → L+1 (90%)	ILCT	3.26	380.67	*0.3118* S_4
2A	388.6 (0.53)	H → L (98%)	MLLCT	2.75	450.24	*0.0034* S_1
		H-1 → L (97%)	MLLCT	2.96	418.75	*0.1094* S_2
		H-2 → L (96%)	MLLCT	3.23	383.78	*0.0106* S_3
2	385 (1.37)	H-1 → L (89%)	MLCT	2.74	451.77	*0.0176* S_1
		H → L (83%) H-1 → L (10%)	ILCT MLCT	2.81	441.38	*0.3066* S_2
		H-3 → L (90%)	MLCT	2.98	415.72	*0.0216* S_3
		H-4 → L (95%)	MLCT	3.22	384.14	*0.0120* S_4
		H → L+1 (92%)	ILCT	3.36	369.02	*0.1652* S_6
		H-1 → L+1 (95%)	MLCT	3.44	360.15	*0.0021* S_7
2B	446.1 (2.62)	H → L (96%)	ILCT	2.58	481.41	*0.3772* S_1
		H-1 → L (98%)	MLLCT	2.87	431.85	*0.0247* S_2
		H-2 → L (79%)	MLLCT	3.09	401.18	*0.1661* S_3
	380.2 (1.34)	H → L+1 (78%)	ILCT	3.13	395.88	*0.3501* S_4
3A	405.0 (0.42)	H → L (99%)	MLLCT	2.66	466.40	*0.0104* S_1
		H-1 → L (98%)	MLLCT	2.89	429.65	*0.0979* S_2
		H-2 → L (98%)	MLLCT	3.15	394.03	*0.0056* S_3
3	396 (2.11)	H-2→ L (60%) H → L (37%)	MLCT ILCT	2.63	470.58	*0.0952* S_1
		H → L (58%) H-2 → L (39%)	ILCT MLCT	2.70	458.94	*0.1441* S_2
		H-3 → L (94%)	MLCT	2.90	427.38	*0.0443* S_3
		H-4 → L (98%)	MLCT	3.14	394.75	*0.0055* S_4
		H → L+1 (94%)	ILCT	3.33	371.98	*0.1993* S_6
		H-2 → L+2 (96%)	MLCT	3.52	351.87	*0.0064* S_7
3B	454.2 (0.45)	H → L (97%)	ILCT	2.40	515.39	*0.3106* S_1
		H-1 → L (97%)	MLLCT	2.76	449.51	*0.0255* S_2
		H-2 → L (96%)	MLLCT	2.99	414.63	*0.0472* S_3
		H → L+1 (93%)	ILCT	3.05	405.93	*0.2571* S_4
	369.8 (0.41)	H-3 → L (98%)	MLLCT	3.22	385.19	*0.0036* S_5
		H → L+2 (94%)	ILCT	3.27	379.16	*0.1525* S_6
		H → L+3 (94%)	ILCT	3.59	345.52	*0.2343* S_7

Emission properties

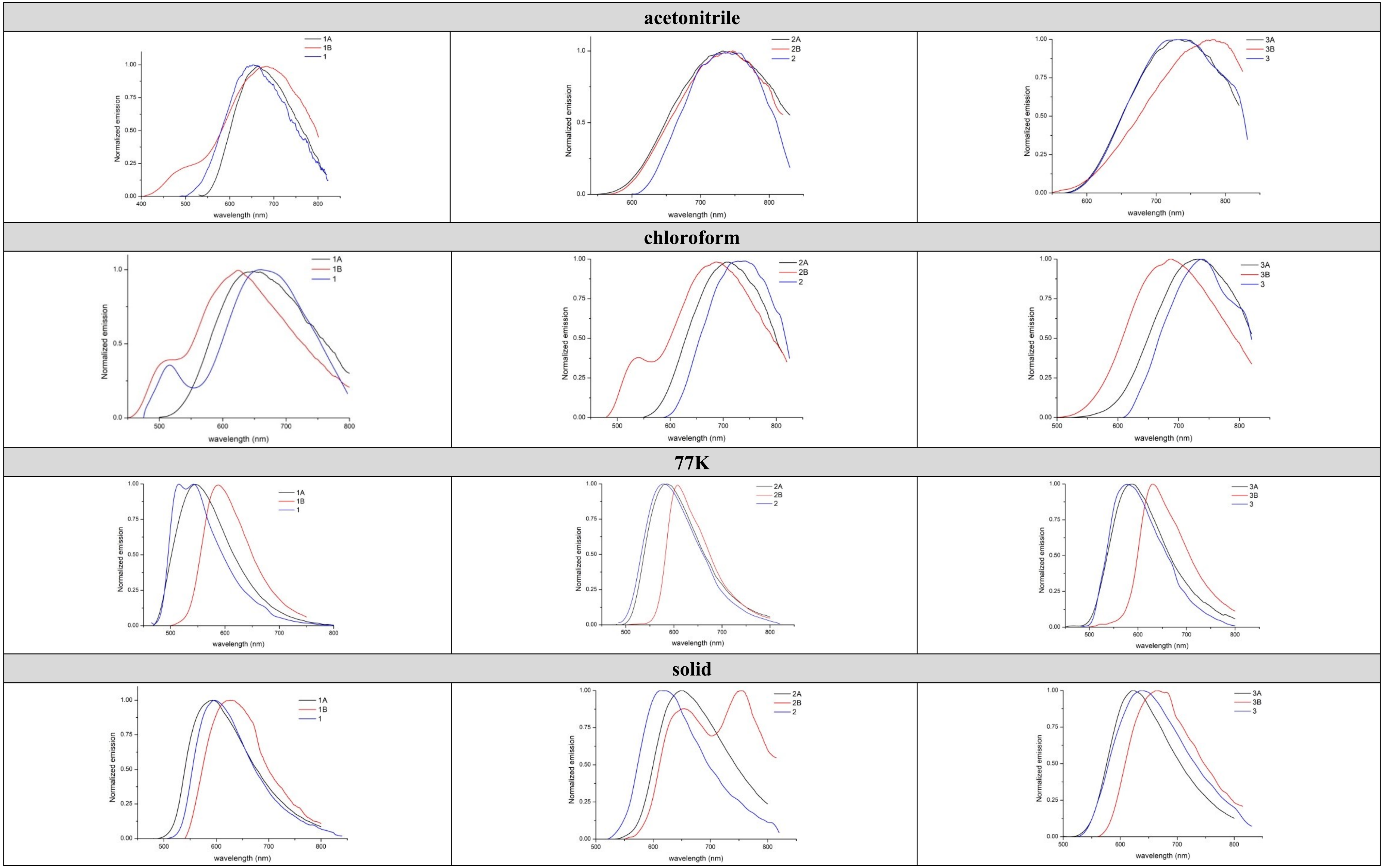

Figure S21. Comparison of emission spectra of **1-3** with their analogues (**1A-3A** and **1B-3B**) in different media. Data for complexes **1A–3A** and **1B–3B** are taken from ref. [1].

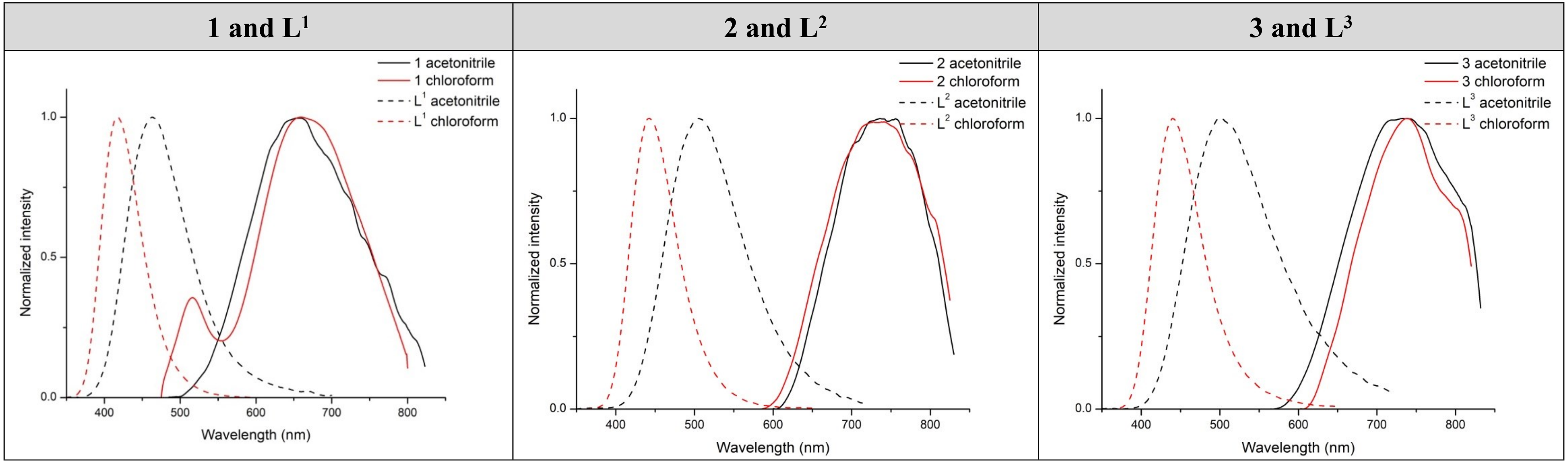

Figure S22. Emission spectra of **L^1–L^3** in comparison to **1–3**.

Table S8. Summary of photoluminescence properties of **1–3** in comparison with photoluminescence data for **1A–3A** and **1B–3B**. Data for complexes **1A–3A** and **1B–3B** are taken from ref. [1].

compound	medium	excitation	emission	Lifetime [ns]	χ^2	φ [%]
1A	MeCN	380, 321, 300, 251	666	2.18 (71.42%), 16.01 (28.58%)	0.971	0.21
	$CHCl_3$	400, 300, 266	667	3.27 (71.01%), 28.45 (28.99%)	1.052	0.43
	77K	384, 366, 333, 305	543	2 282 (22.41%), 5 878 (77.59%)	1.013	-
	solid	442, 369, 302, 261	592	30.04 (65.78%), 94.89 (34.22%)	1.184	1.28
1B	MeCN	458, 365, 315, 257	702	0.079	1.426	0.36
	$CHCl_3$	404, 329, 289	507	3.74	1.073	0.14
		432, 369, 303, 265	617	3.04 (20.60%) 49.78 (79.40%)	1.103	
	77K	429, 319	588	93 460 (20.55%), 279 070 (79.45%)	1.022	-
	solid	522, 351, 302	625	696.33 (44.36%), 3 541 (55.65%)	1.131	1.29
1	MeCN	370, 326, 282, 254	651	0.58 (13.33%), 2.60 (86.67%)	0.955	0.58
	$CHCl_3$	385, 316, 287, 261	506	7.74 (76.77%), 2.90 (23.23%)	1.044	1.39
			657	3.17 (73.15%), 7.66 (26.85%)	1.052	
	77K	400, 322, 289, 278, 240	513, 540	9 874 (41.66%), 38 355 (58.34%)	1.080	-
	solid	486	596	332.71	0.958	15.42
	film	404	580	-	-	-
	blend with 1wt.%	340	404,552	-	-	-
	blend with 2 wt.%	340	392,551	-	-	-
	blend with 15wt. %	340	376,565	-	-	-
2A	MeCN	392, 331, 304, 261	735	4.44	1.035	0.36
	$CHCl_3$	419, 327, 300, 267	727	6.38	1.092	0.28
	77K	392, 343, 331, 310	585	1 822.8 (85.47%), 9 198.9 (14.53%)	1.061	-
	solid	502, 393, 310, 265	650	68.51 (54.28%), 205.69 (45.72%)	0.924	2.54
2B	MeCN	450, 365, 331, 290	741	0.08 (84.69%), 6.98 (15.31%)	1.232	0.25
	$CHCl_3$	427, 348, 306	536	2.06 (48.61%), 4.03 (51.39%)	0.986	1.53
		463, 328, 267	686	15.07	1.212	
	77K	457, 336	607	69 340 (23.27%), 212 650 (76.73%)	1.117	-
	solid	551, 513, 382, 307	652	114.52 (20.80%), 613.27 (79.20%)	1.130	1.53
		563, 386, 306	752	280.52 (45.77%), 1 163 (54.23%)	1.073	
2	MeCN	386, 334, 304, 253	733	3.98	0.961	0.92
	$CHCl_3$	410, 334, 265	734	5.78	1.086	0.77
	77K	402, 327, 287, 239	578	2 635 (56.68%), 9 826 (43.32%)	1.131	-
	solid	494	618	46.67 (38.05%); 300.57 (61.95%)	1.076	7.55
	film	423	610	-	-	-
	blend with 1wt.%	340	383	-	-	-
	blend with 2 wt.%	340	411	-	-	-
	blend with 15wt. %	340	417, 604	-	-	-
3A	MeCN	403, 325, 303, 260	736	3.39	1.129	0.34
	$CHCl_3$	430, 329, 300, 263	732	4.77	1.172	0.38
	77K	410, 386, 369, 344, 329, 309	587	2 691 (73.41%), 10 914 (26.59%)	1.077	-
	solid	486, 396, 305, 263	623	76.15 (20.11%), 214.07 (79.89%)	1.071	0.19
3B	MeCN	480, 400, 341	781	0.06 (23.73%), 3.55 (49.78%), 23.72 (26.49%)	1.200	0.14
	$CHCl_3$	462, 382, 323, 268	690	10.06 (27.75%), 41.36 (72.25%)	0.980	0.93
	77K	466, 390, 334	632	30 630 (23.51%), 86 330 (76.49%)	1.139	-
	solid	536, 413, 302	661	26.60 (8.93%), 164.58 (42.21%), 614.49 (48.86%)	0.968	2.27
3	MeCN	400, 322, 288	734	3.35	0.996	0.51
	$CHCl_3$	411, 326, 287, 259	738	3.95 (53.05%), 9.26 (46.95%)	1.016	0.99
	77K	421, 331, 288	578	29 376 (52.62%), 156 554 (47.38%)	1.126	-
	solid	512	638	30.44 (21.47%); 114.69 (78.53%)	1.000	8.60
	film	449	576	-	-	-
	blend with 1wt.%	340	391	-	-	-
	blend with 2 wt.%	340	392	-	-	-
	blend with 15wt. %	340	391, 592	-	-	-

Table S9. Summary of photoluminescence properties of **1–3.**

<table>
<tr><th colspan="3">1</th></tr>
<tr><td>MeCN</td><td>
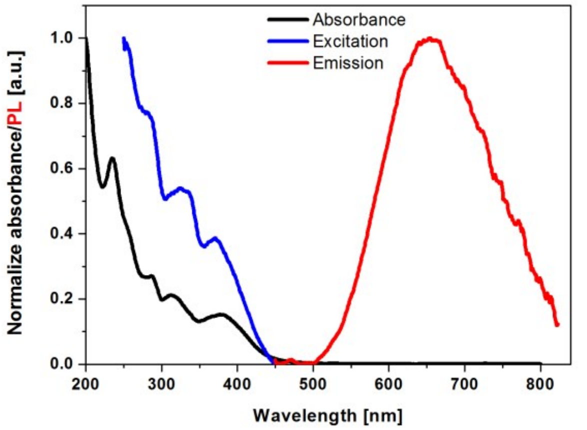

</td><td>
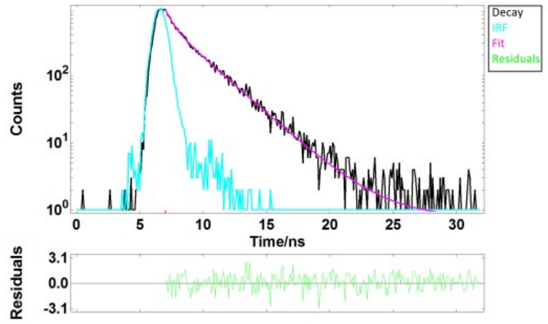

</td></tr>
<tr><td>CHCl₃</td><td>
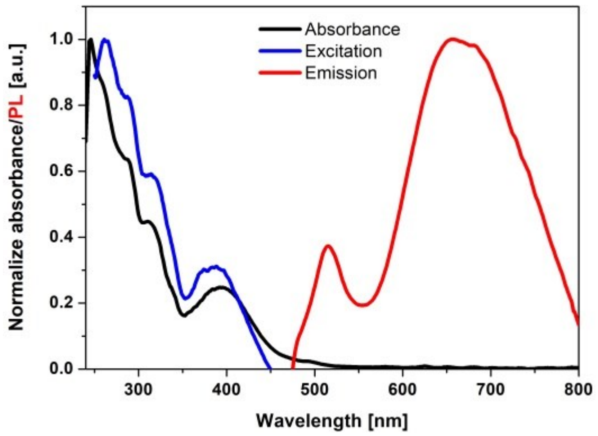

</td><td>
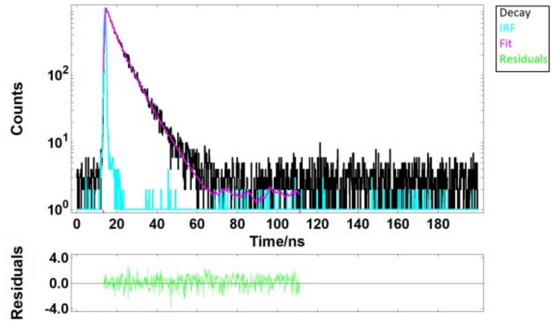

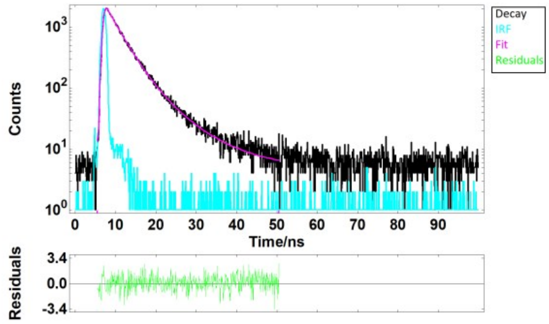

</td></tr>
<tr><td>Solid</td><td>
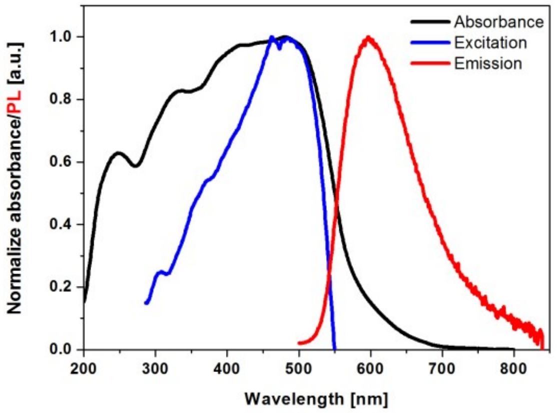

</td><td>
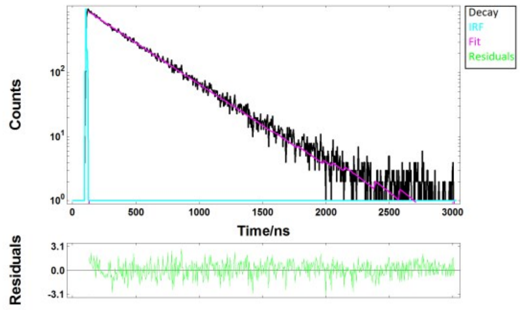

</td></tr>
</table>

<table>
<tr>
<td>EtOH:MeOH
(77K)</td>
<td>
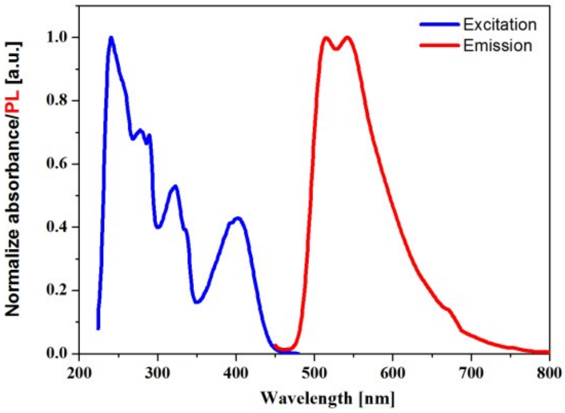

</td>
<td>
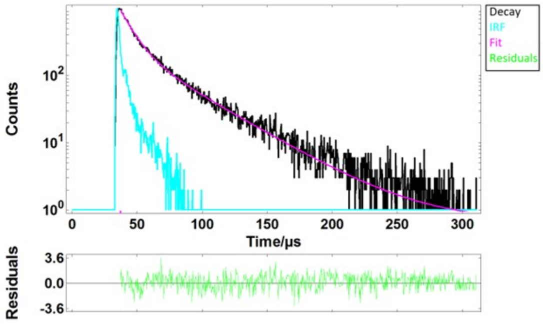

</td>
</tr>
<tr>
<td colspan="3">2</td>
</tr>
<tr>
<td>MeCN</td>
<td>
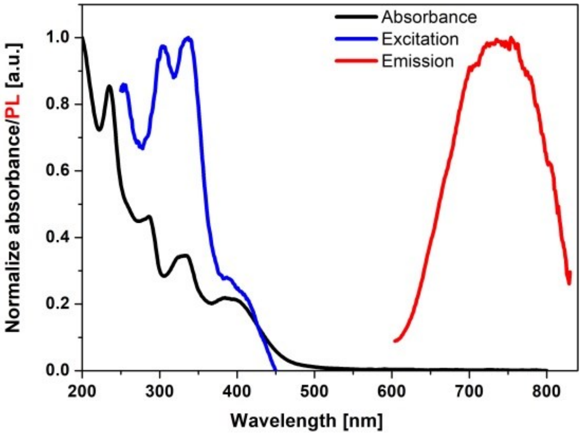

</td>
<td>
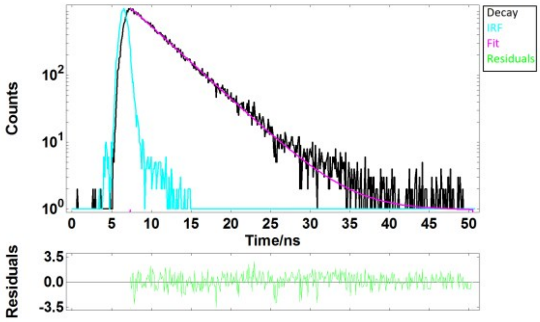

</td>
</tr>
<tr>
<td>$CHCl_3$</td>
<td>
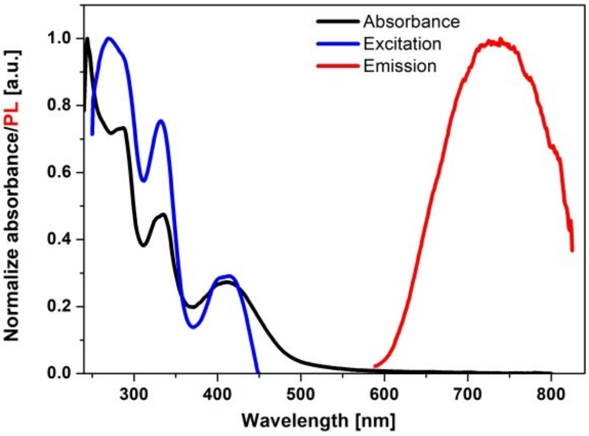

</td>
<td>
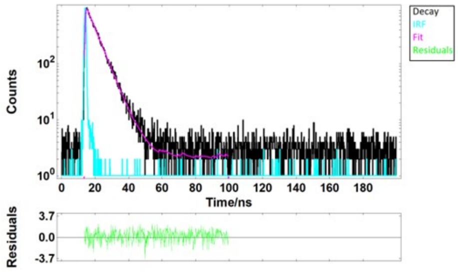

</td>
</tr>
<tr>
<td>Solid</td>
<td>
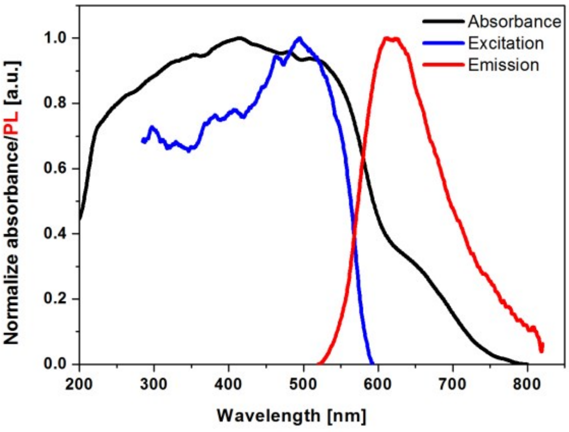

</td>
<td>
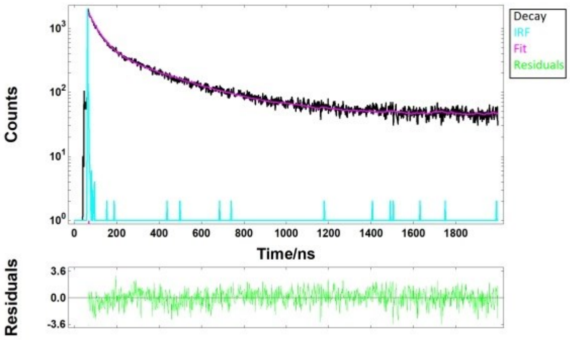

</td>
</tr>
</table>

EtOH:MeOH (77K)	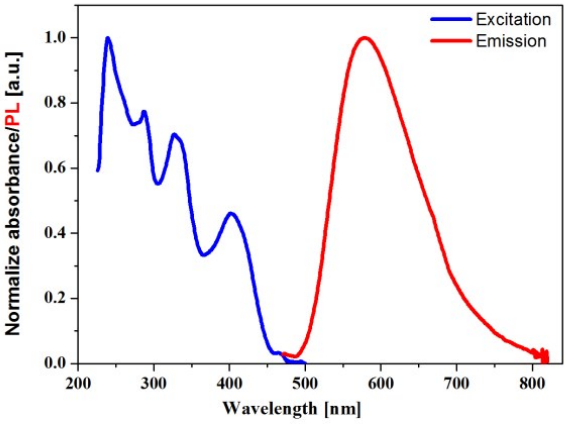	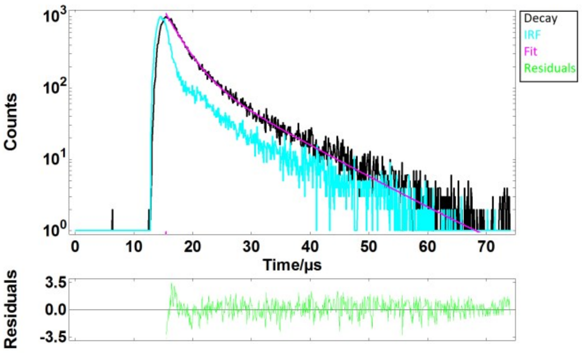
3		
MeCN	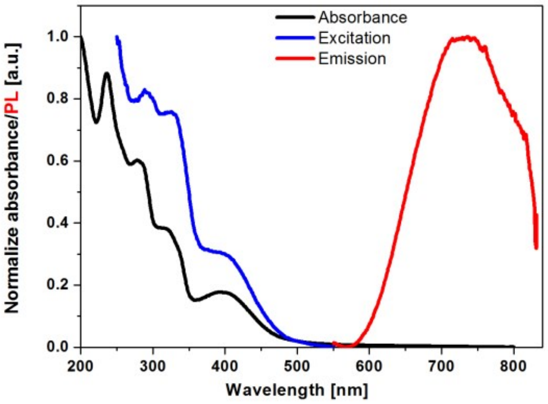	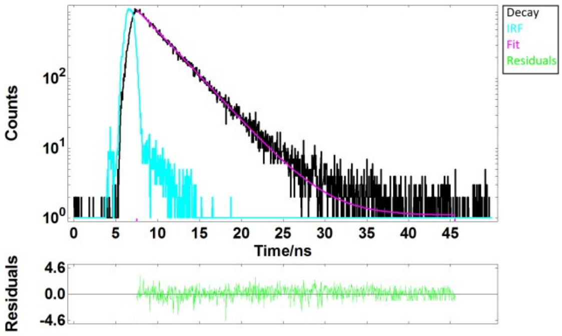
$CHCl_3$	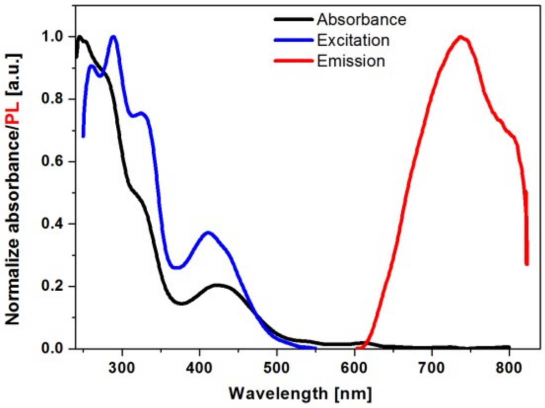	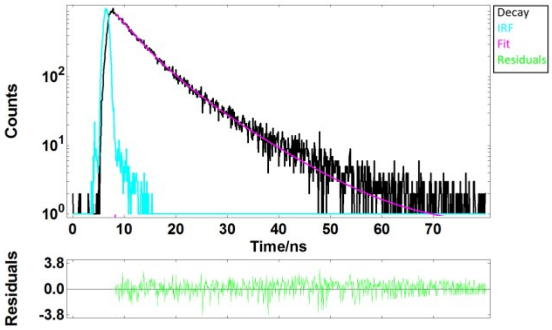
Solid	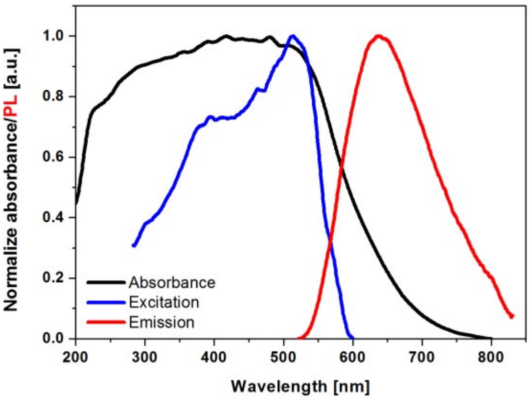	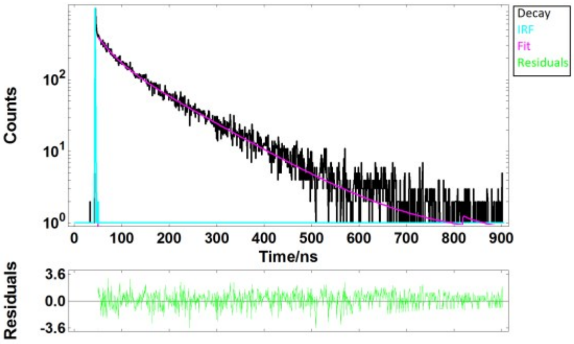

EtOH:MeOH (77K)	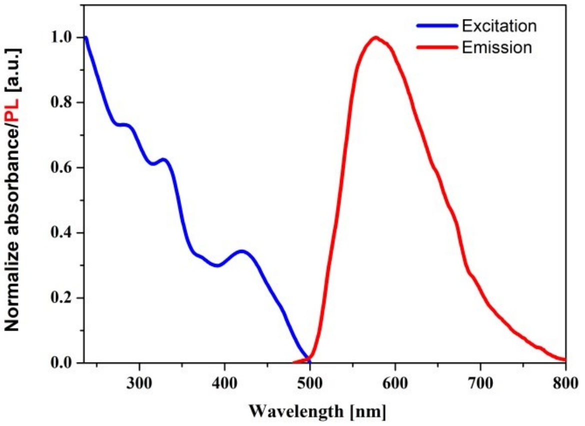	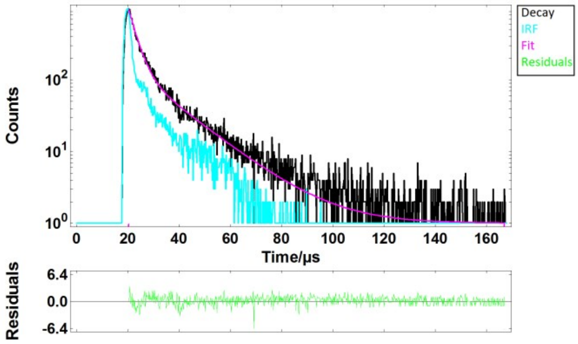

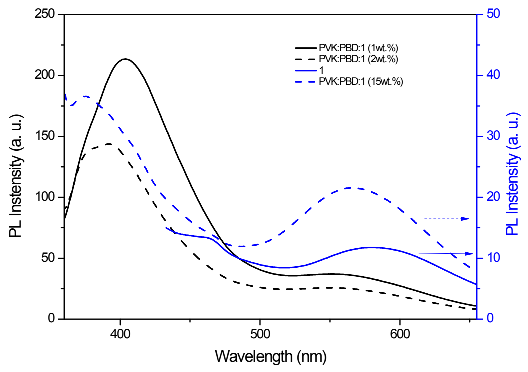

1

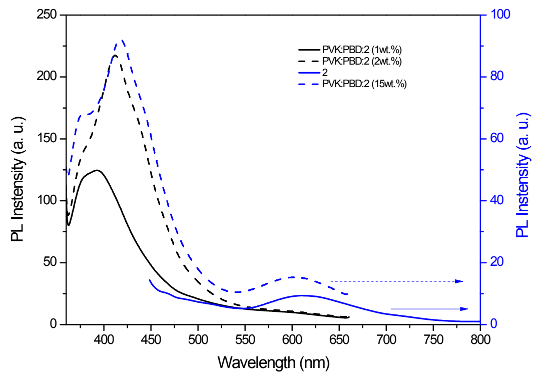

2

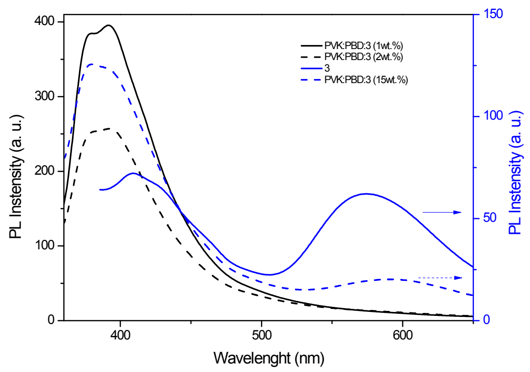

3

Figure S23. PL spectra of investigated compounds in thin film and in blend with PVK:PBD deposited on glass. Blue spectra are scaled to the right Y axis, while black spectra are scaled to the left Y axis.

1

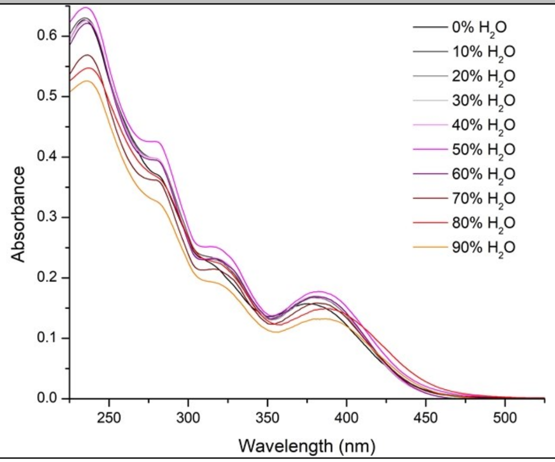

2

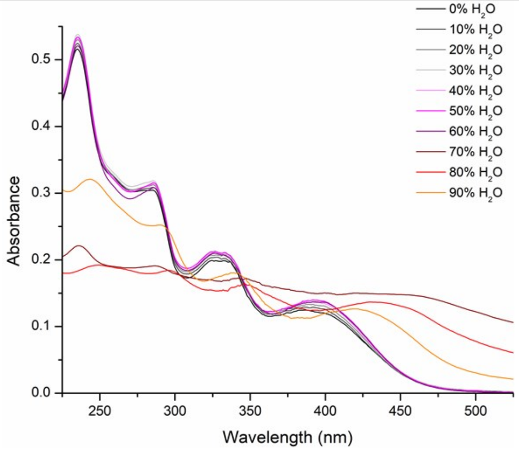

3

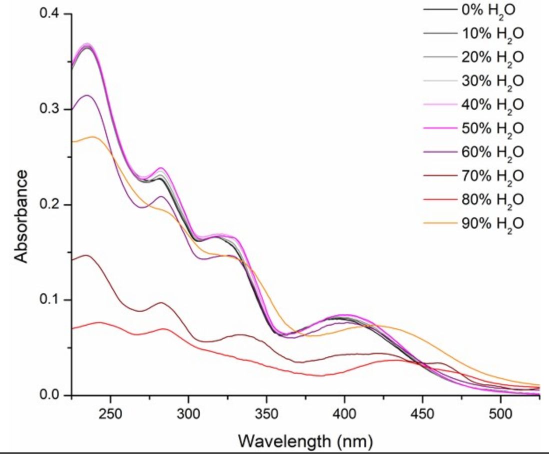

(a)

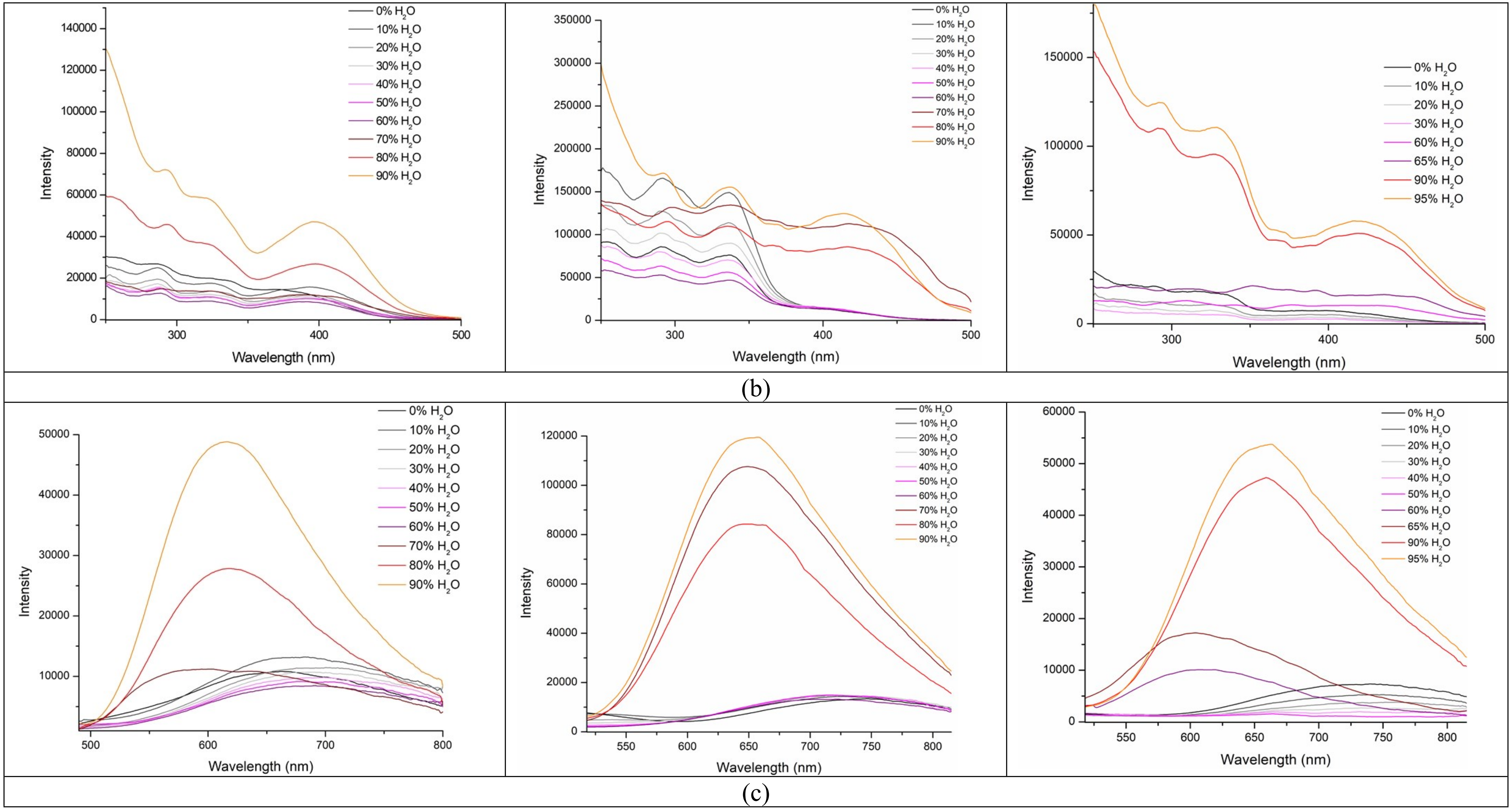

(b)

(c)

Figure S24. Absorption (a), excitation (b) and emission (c) spectra of **1-3** in CH_3CN/H_2O mixture with different water fraction (f_w).

Electroluminescence

Table S10. Data obtained from EL spectra of diodes based on Re(I) complexes: position of λ_{EL} under external voltage (V) and its maximal reached EL intensity

Re(I) complex	Active layer structure							
	Neat complex		**PVK:PBD:complex 1 wt.%**		**PVK:PBD:complex 2 wt.%**		**PVK:PBD:complex 15 wt.%**	
	λ_{EL} [nm] (V)	Intensity [a.u.]	λ_{EL} [nm] (V)	Intensity [a.u.]	λ_{EL} [nm] (V)	Intensity [a.u.]	λ_{EL} [nm] (V)	Intensity [a.u.]
1	625 (15)	598	600 (22)	6624	600 (25)	36041	600 (30)	159790
2	–	–	615 (23)	2861	630 (27)	8799	630 (30)	24618
3	–	–	615 (22)	23826	610 (23)	9518	620 (22)	1425

The EL spectra were registered as a function of applied voltage. For diodes with structure ITO/PEDOT:PSS/complex/Al, it was found that only the device based on the Re(I) complex with *terpy* core (**1**) showed weak EL with maximum of the emission band (λ_{EL}) at 625 nm (Table S10 and Figure 9). Additionally, due to partial overlap between the absorption spectrum of the complexes with the emission spectrum of the applied matrix PVK:PBD (Figure S19), devices with guest-host configuration were prepared (ITO/PEDOT:PSS/PVK:PBD:complex/Al). However, taking into account the PL spectra of the blends, that is, the Re(I) complexes dispersed molecularly in a PVK:PBD, only in the case of complex bearing *terpy* core (**1**), for all its content in matrix, a band originating from the emission of **1** is seen (Figure S23). In all PL spectra of blends the emission of the matrix observed at shorter wavelengths dominates, which confirms incomplete quenching of the PVK:PBD photoluminescence due to incomplete energy transfer from the matrix to the luminophore. All guest-host diodes emitted red light with varied intensity. It can be noticed that the maximal EL intensity was reached under high external voltage. It was found that dispersion of complex in a matrix results in a significant increase in light emission intensity. The most favorable complex content in blend, which provides intense EL is 15 and 1 wt.% for diode with **1**, **2** and **3**, respectively (Table S10). The EL spectra of devices based on **1**, **2** and **3** recorded under the same external voltage were compared to determine the impact of complexes chemical structure on emission of light (Figure 9).

In examination of the effect of the complex structure in a diode architecture with its 1 wt. % content in a matrix under 22 or 23 V, it can be noticed that the most intense EL emission was observed for the device containing compound with *dppy* core (**3**). On the other hand, the increase of complex content in blend to 2 and 15 wt.% caused that the diode with molecule bearing *terpy* unit (**1**) exhibited the highest emission.

Finally, the most intense light emission under voltage was observed for diode with active layer bearing 15 wt.% of complex **1**. It can be concluded that the presence of *terpy* (**1**) unit compared to *dtpy* (**2**) and *dppy* (**3**) structure provides better ability for light emission induced by both radiation and voltage. Considering the previously reported systems – without any groups attached to the phenyl ring and bearing pyrrolidine instead of carbazole (Scheme S1)[1] - the effect of these substituents in complex with *terpy* (**1A**, **1B** and **1**), *dtpy* (**2A**, **2B** and **2**) and *dppy* (**3A**, **3B** and **3**) core on voltage induced emission can be analyzed. The slight impact of complex structure on energy of emitted light was seen and all diodes with architecture ITO/PEDOT:PSS/complex/Al exhibited red EL. However, significant differences in emitted light intensity were observed. In the examination of such type of diodes, it can be noticed that device based on compound with *terpy* and unsubstituted phenyl ring (**1A**) was non emissive contrary to diodes with *terpy* substituted with pyrrolidine (**1B**) and carbazole (**1**) unit. The diodes without carbazole unit and *dtpy* (**2A** and **2B**) and *dppy* (**3A** and **3B**) core showed EL. The more intense EL showed diode with pyrrolidine and *dtpy* core (**2B**). When evaluating guest-host devices (with 2 wt.% complex content in a matrix), substitution of phenyl ring in complex increases the EL intensity. The replacement of carbazole (**1**–**3**) with pyrrolidone (**1B**–**3B**) unit enhances the EL intensity.

Nano- and femtosecond transient absorption

<table>
<tr><th>1</th><th>1A</th></tr>
<tr><td>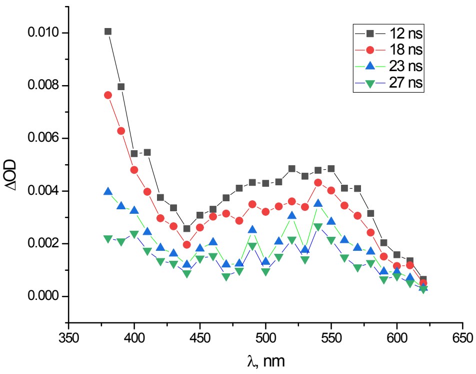
</td><td>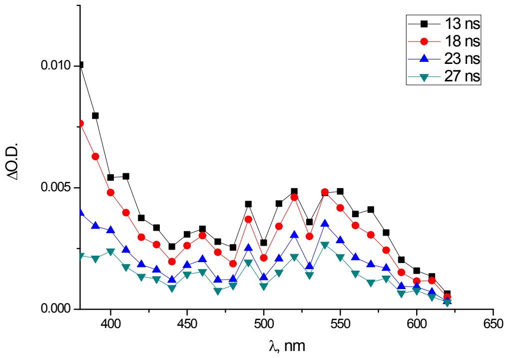
</td></tr>
</table>

(a)

<table>
<tr><th colspan="2">1B</th></tr>
<tr><th>CH₃CN</th><th>CHCl₃</th></tr>
<tr><td>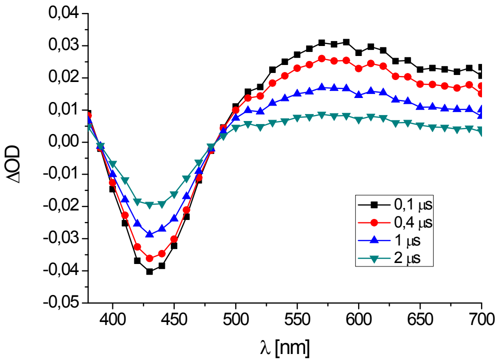
</td><td>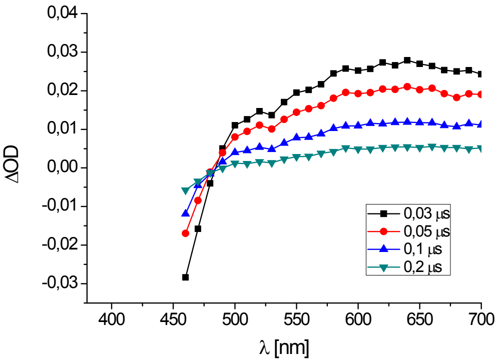
</td></tr>
<tr><th colspan="2">L1B</th></tr>
<tr><th>CH₃CN</th><th>CHCl₃</th></tr>
<tr><td>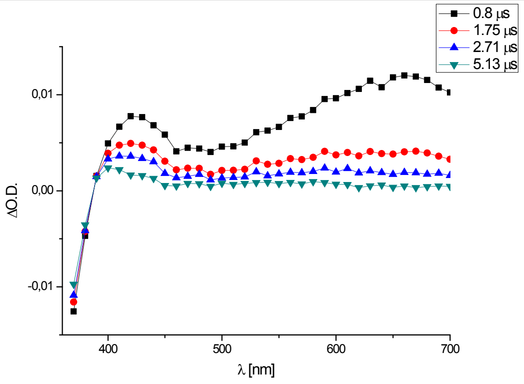
</td><td>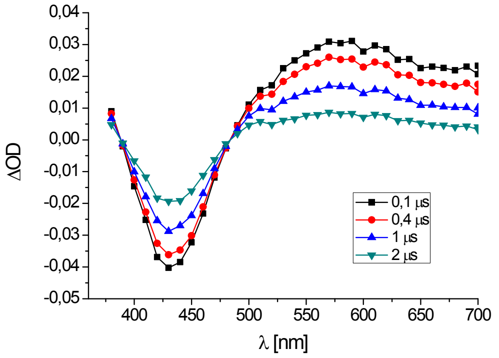
</td></tr>
</table>

(b)

Figure S25. Nanosecond transient absorption spectra of complexes **1** and **1A** in CH$_3$CN (argon bubbling) (a). Nanosecond transient absorption spectra of complex **1B** and ligand **L^{1B}** in CH$_3$CN or CHCl$_3$ (argon bubbling) (b). Data for complex **1B** taken from ref. [1].

<table>
<tr><th>1</th><th>1A</th><th>1B</th></tr>
<tr><td colspan="3">Pump 420 VIS</td></tr>
<tr>
<td>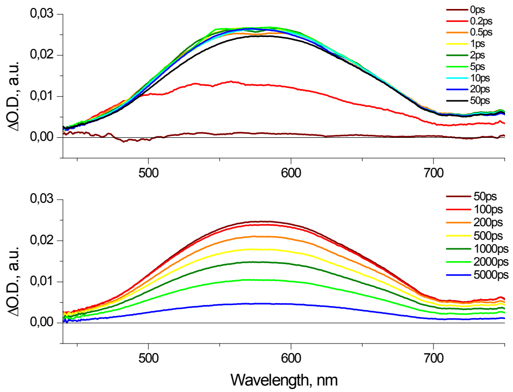
</td>
<td>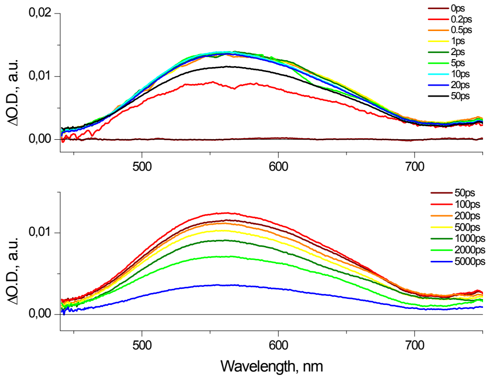
</td>
<td>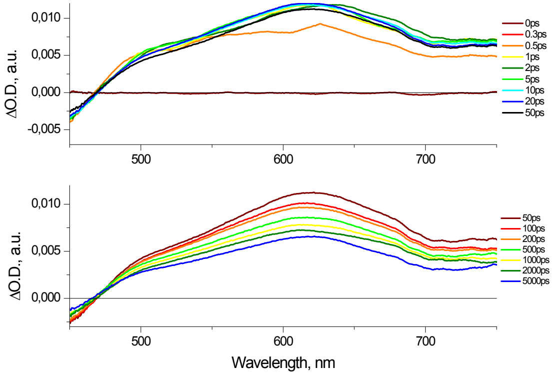
</td>
</tr>
<tr><td colspan="3">Pump 355 UV</td></tr>
<tr>
<td>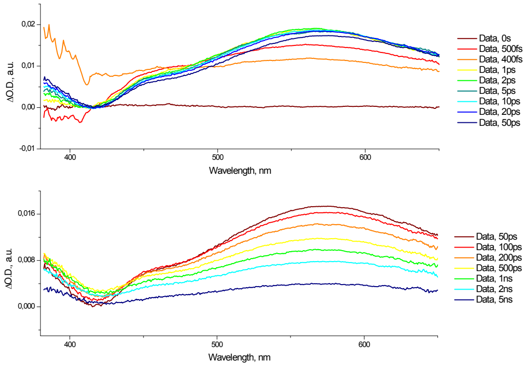
</td>
<td>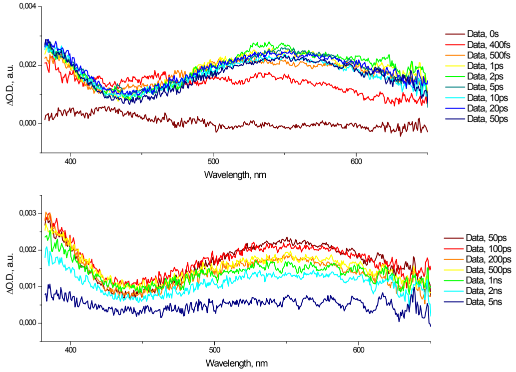
</td>
<td>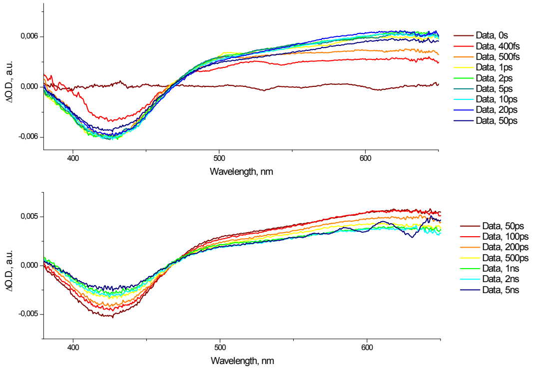
</td>
</tr>
</table>

1	**1A**	**1B**
Pump 420 UV		
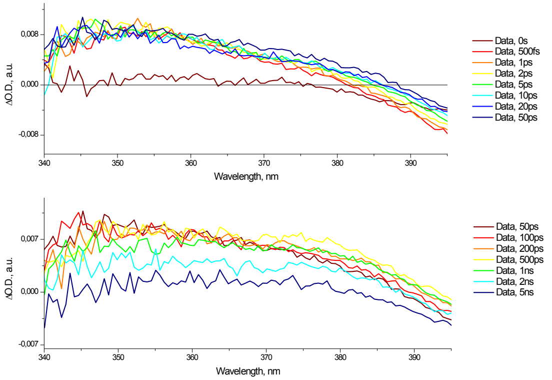	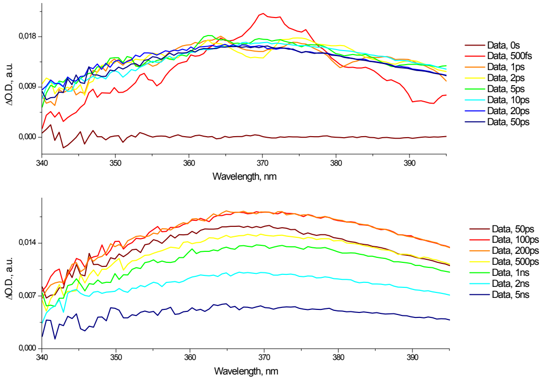	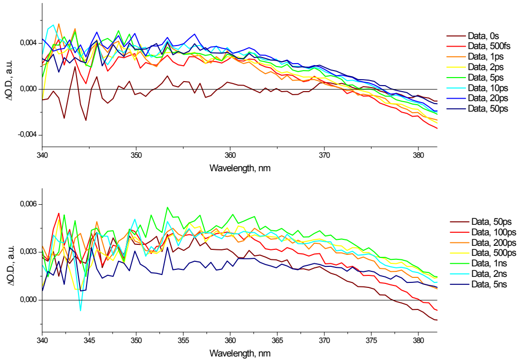

Figure S26. Femtosecond transient absorption spectra of **1, 1A** and **1B** (visible region with pump 420 nm and 355 nm and near UV region with pump 420 nm).

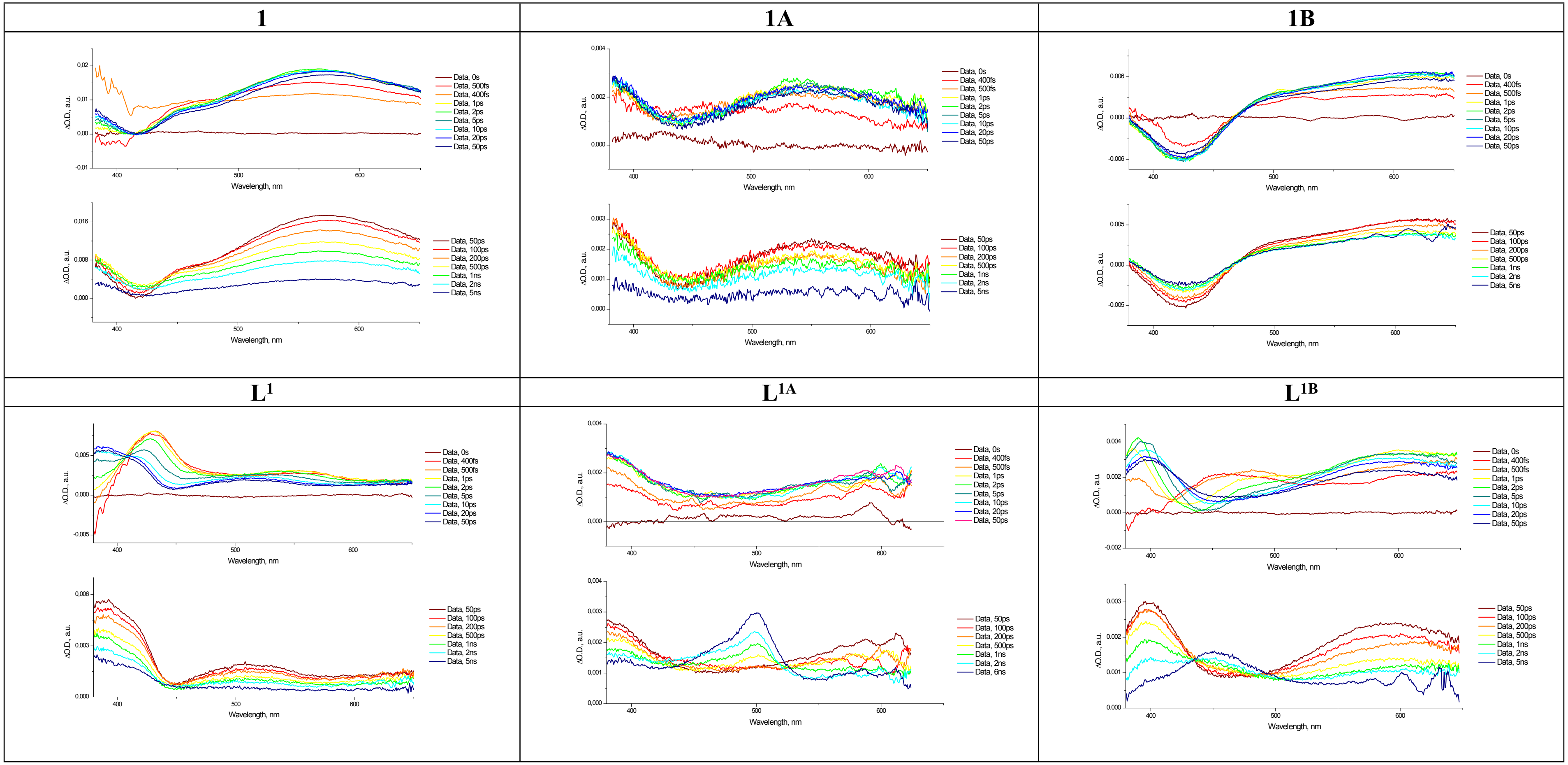

Figure S27. Comparison of fs-TA spectra of complexes **1, 1A, 1B** and the corresponding ligands.

Table S11. Fit of kinetic of selected wavelengths of complex **1**.

The value of the first time component was obtained from the analysis of cropped delay time range (20 ps) and then fixed. This ultrafast component is related to the decay of ESA band at 472 nm and growing of ESA band at 580 nm. The decay kinetics of two visible ESA bands were fitted for samples pumped at 420 nm and 355 nm. The shapes of decay curves at both pumping wavelengths are similar and the obtained time constrains are within error bars. The greater differences are visible for ESA band at 472 nm (t2 = 15.7 ± 5.68 ps for 420nm pump and t2 = 36.9 ± 4.97 ps for 355 nm pump).

Complex 1				
Pump 420nm				
	Fit of kinetic (472 nm)		**Fit of Kinetic (580nm)**	
	t, ps	Normalized amplitude	t, ps	Normalized amplitude
t_1	0.272 (fixed)	0.171	0.251 (fixed)	-0.146
t_2	15.7 ± 5.68	0.103	178 ± 22.7	0.223
t_3	2950 ± 291	0.678	3210 ± 376	0.614
t_4	Inf	0.047	Inf	0.017
	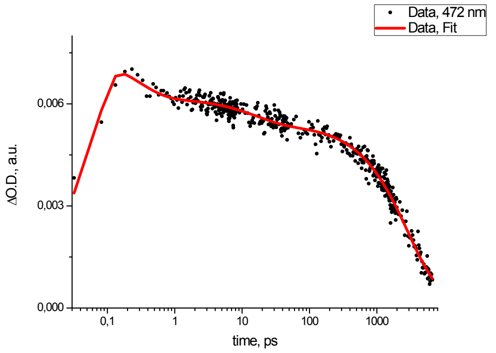		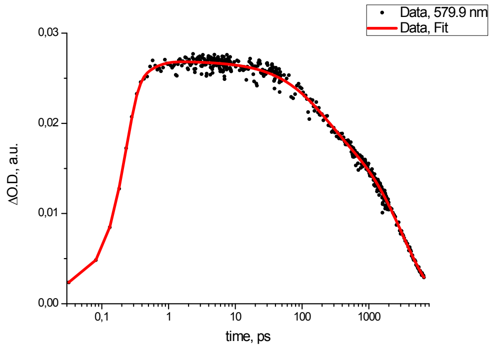	
Pump 355nm				
	Fit of kinetic (472 nm)		**Fit of Kinetic (580nm)**	
	t, ps	Normalized amplitude	t, ps	Normalized amplitude
t_1	0.272 (fixed)	0.197	0.251 (fixed)	0.264
t_2	36.9 ± 4.97	0.159	194 ± 12.1	0.246
t_3	2690 ± 198	0.554	3470 ± 344	0.434
t_4	Inf	0.090	Inf	0.055
	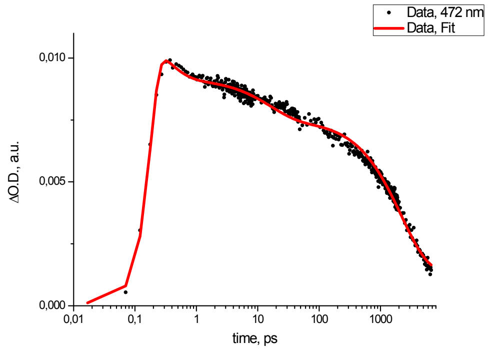		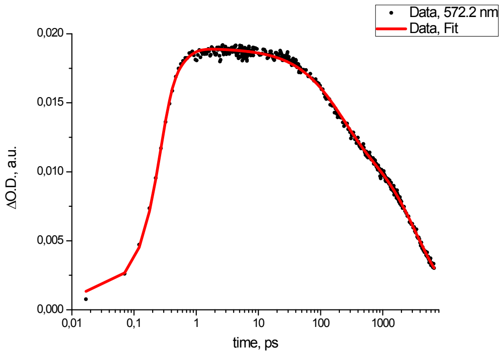	

Table S12. Fit of kinetic of selected wavelength of complex **1A**.

The value of the first time component was obtained from the analysis of cropped delay time range (20 ps) and then fixed. This ultrafast component is related to the growing of ESA band at 563 nm. The decay kinetic of visible ESA band was fitted for samples pumped at 420 nm and 355 nm. The shapes of decay curves at both pumping wavelengths are similar and the obtained time constrains are within error bars.

Complex 1A		
Pump 420 nm		
	Fit of kinetic (563 nm)	
	t, ps	Normalized amplitude
t_1	0.186 (fixed)	-0.158
t_2	94.5 ± 18.2	0.140
t_3	3880 ± 428	0.676
t_4	Inf	0.026
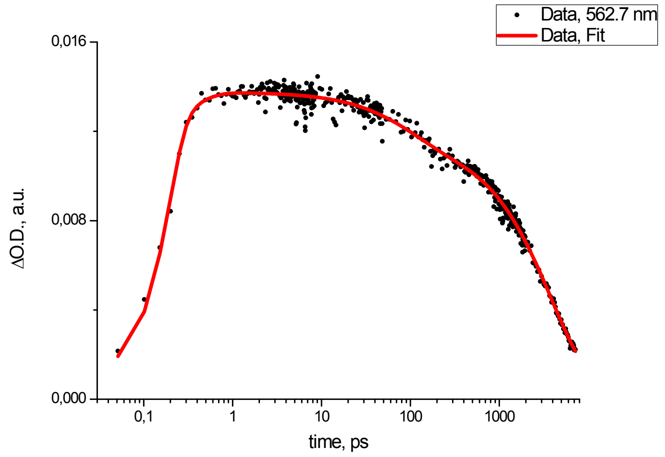		
Pump 355 nm		
	Fit of kinetic (563 nm)	
	t, ps	Normalized amplitude
t_1	0.186 (fixed)	-0.0801
t_2	96.8 ± 23	0.238
t_3	3560 ± 938	0.549
t_4	Inf	0.133
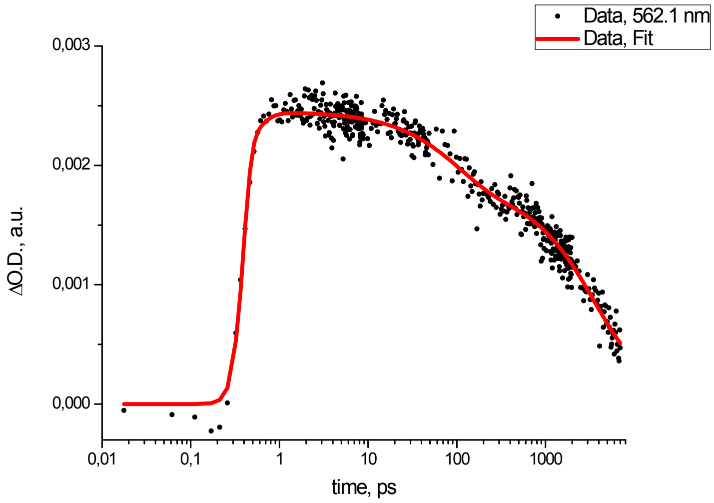		

Table S13. Fit of kinetic of selected wavelengths of complex **1B**.

The value of the first time component was obtained from the analysis of cropped delay time range (20 ps) and then used as an initial value or fixed. The ultrafast component is related to the decaying of ESA band at 509 nm and the growing of ESA band at 618 nm. The additional growing time constrain is visible for ESA at 618 nm. The decay kinetics of two visible ESA bands were fitted for samples pumped at 420 nm and 355 nm. The shapes of decay curves at both pumping wavelengths are similar and the obtained time constrains are within error bars.

<table>
<tr><th colspan="5">Complex 1B</th></tr>
<tr><th colspan="5">Pump 420 nm</th></tr>
<tr><th></th><th colspan="2">Fit of kinetic (509 nm)</th><th colspan="2">Fit of Kinetic (618nm)</th></tr>
<tr><th></th><th>t, ps</th><th>Normalized amplitude</th><th>t, ps</th><th>Normalized amplitude</th></tr>
<tr><td>t_1</td><td>0.173 ± 0.805</td><td>0.146</td><td>0.248 ± 0.197</td><td>-0.282</td></tr>
<tr><td>t_2</td><td>135 ± 16.7</td><td>0.271</td><td>7.1 ± 3.69</td><td>-0.062</td></tr>
<tr><td>t_3</td><td>19200 ± 2240</td><td>0.584</td><td>163 ± 21.4</td><td>0.235</td></tr>
<tr><td>t_4</td><td></td><td></td><td>20000 ± 2280</td><td>0.421</td></tr>
<tr><td colspan="3">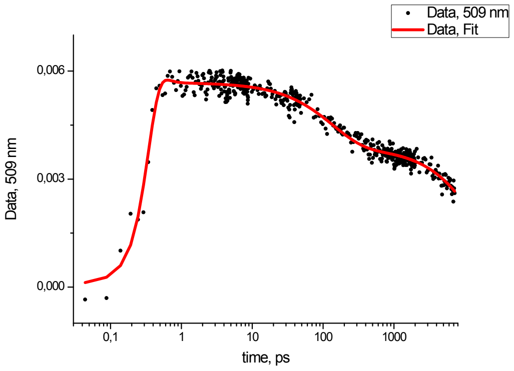 </td><td colspan="2">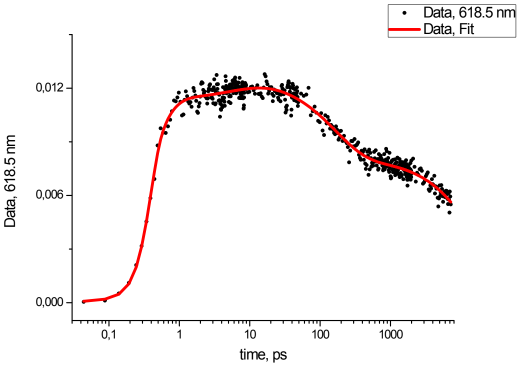 </td></tr>
<tr><th colspan="5">Pump 355 nm</th></tr>
<tr><th></th><th colspan="2">Fit of kinetic (509 nm)</th><th colspan="2">Fit of Kinetic (618nm)</th></tr>
<tr><th></th><th>t, ps</th><th>Normalized amplitude</th><th>t, ps</th><th>Normalized amplitude</th></tr>
<tr><td>t_1</td><td>0.173 (fixed)</td><td>0.268</td><td>0.248 (fixed)</td><td>-0.264</td></tr>
<tr><td>t_2</td><td>93.5 ± 14.8</td><td>0.246</td><td>7.1(fixed)</td><td>-0.041</td></tr>
<tr><td>t_3</td><td>17400 ± 2710</td><td>0.486</td><td>161 ± 26.3</td><td>0.222</td></tr>
<tr><td>t_4</td><td></td><td></td><td>18600 ± 2440</td><td>0.472</td></tr>
<tr><td colspan="3">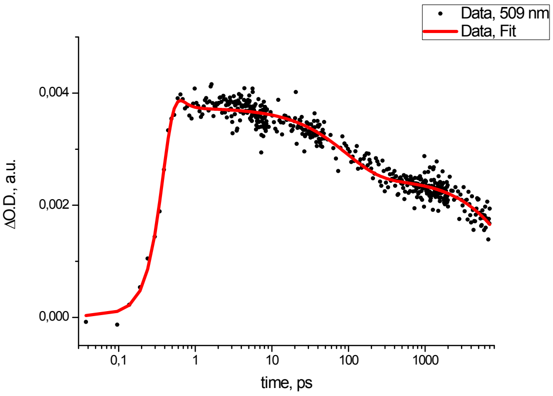 </td><td colspan="2">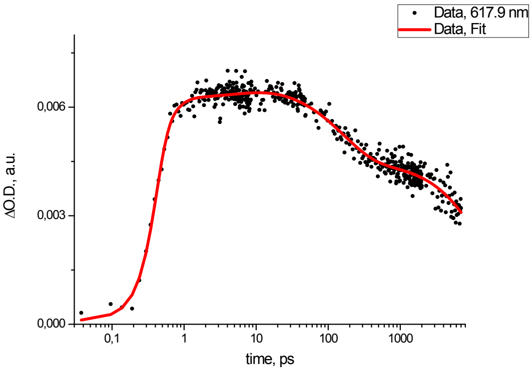 </td></tr>
</table>

Table S14. Fit of kinetic of selected wavelengths of ligand $\mathbf{L^{1B}}$.

The decay kinetic at 509 nm band for $\mathbf{L^{1B}}$ presents the different profile and time constants than complex **1B**. The much more similarity is visible in case of fit of kinetic at 618 nm. However, the t_2 component within few ps in case of complex **1B** represent the growing of ESA band, while in case of ligand $\mathbf{L^{1B}}$ decaying.

<table>
<tr><th colspan="5">Ligand L^{1B}</th></tr>
<tr><th rowspan="2"></th><th colspan="2">Fit of kinetic (509 nm)</th><th colspan="2">Fit of Kinetic (618nm)</th></tr>
<tr><th>t, ps</th><th>Normalized amplitude</th><th>t, ps</th><th>Normalized amplitude</th></tr>
<tr><td>t_1</td><td>0.163 ± 0.244</td><td>-0.332</td><td>0.304 (fixed)</td><td>-0.16</td></tr>
<tr><td>t_2</td><td>1.77 ± 0.576</td><td>0.195</td><td>8.45 ± 3.1</td><td>0.157</td></tr>
<tr><td>t_3</td><td>17.6 ± 8.44</td><td>0.105</td><td>98.5 ± 27</td><td>0.311</td></tr>
<tr><td>t_4</td><td>253 ± 49.3</td><td>0.137</td><td>1180 ± 306</td><td>0.199</td></tr>
<tr><td>t_5</td><td>Inf</td><td>0.231</td><td>Inf</td><td>0.173</td></tr>
<tr><td colspan="3">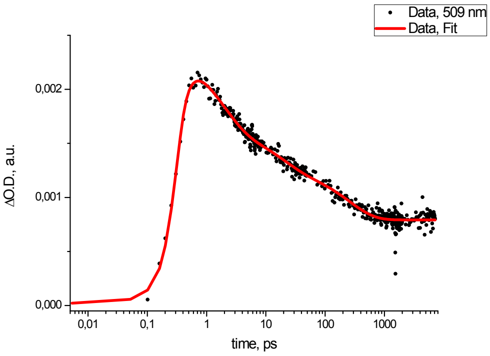 </td><td colspan="2">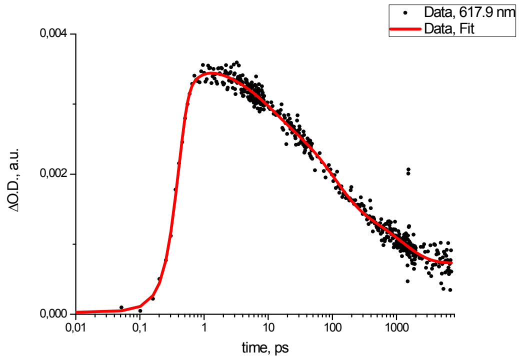 </td></tr>
</table>

Figure S28. Decay Associated Spectra of complexes **1, 1A, 1B** and ligand **L**^{1B}.

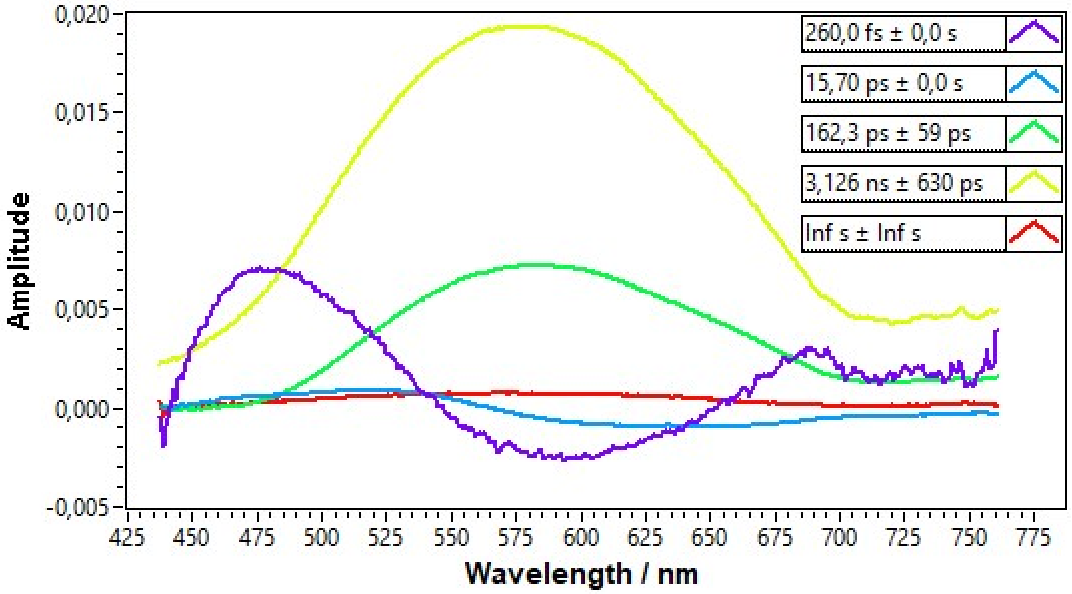

	1	
	Time constants/ps	Wavelength/nm (Sign)
DAS 1	0.26	480 nm (+), 595 (-)
DAS 2	15.70	515 (+), 635 (-)
DAS 3	162	580 (+)
DAS 4	3126	580 (+)
DAS 5	Inf	600 (+)

DAS 1 spectra shows decaying of ESA band 472 nm accompanied by growing of ESA band at 580 nm. Transition of DAS 1 to DAS 2 induce red shift accompanied by broadening of spectra. DAS 2 shows growing of the ESA band at 635. DAS 3 is blue-shifted compared to DAS 2 and represents decaying of ESA at 580nm. DAS 4 and DAS 5 correspond to ground state recovery .

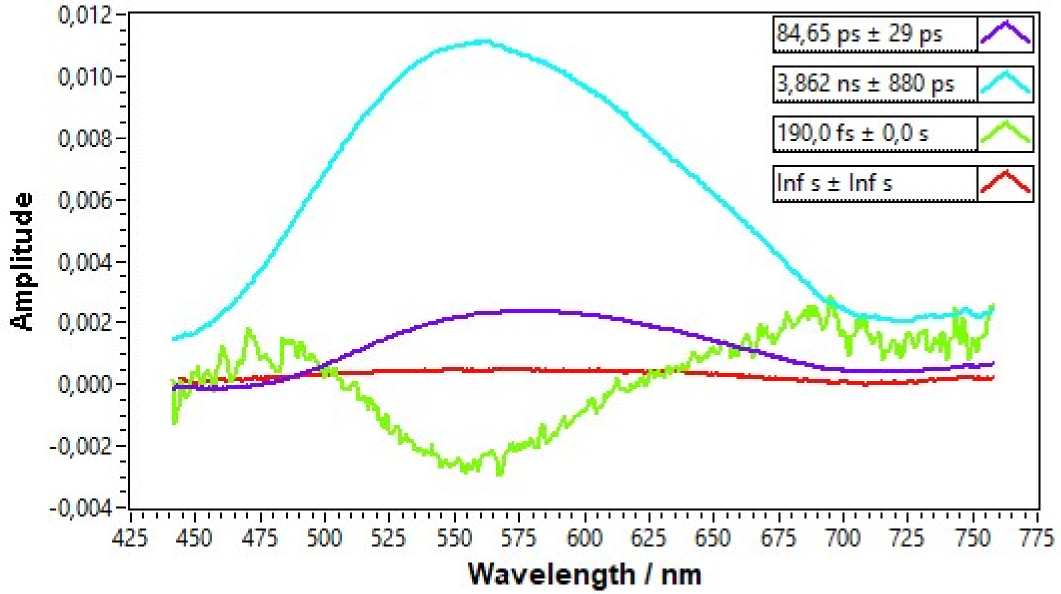

1A

	Time constants/ps	Wavelength/nm (Sign)
DAS 1	0.19	555 (-)
DAS 2	84.65	580 (+)
DAS 3	3862	565 (+)
DAS 4	Inf	580 (+)

DAS 1 corresponds to the growing of ESA band, while DAS 2 to the decaying. Transition from DAS 1 to DAS 2 is accompanied by red shift and broadening. DAS 3 and DAS 4 represent the ground state recovery.

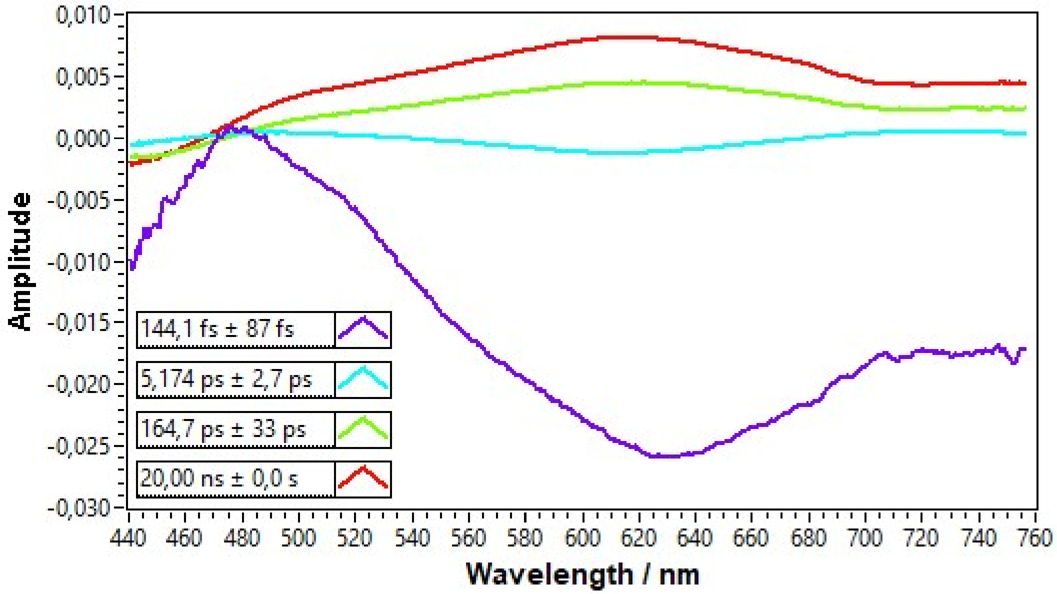

1B

	Time constants/ps	Wavelength/nm (Sign)
DAS 1	0.15	<440(-), 630 (-)
DAS 2	5.54	615 (-)
DAS 3	164.1	445 (-), 625 (+)
DAS 4	20000	445 (-), 615 (+)

DAS 1 shows growing of both ESA bands. DAS 2 represents however only growing of ESA at 618nm. Minimum at DAS 2 is blue shifted compared to DAS 1. DAS 3 corresponds to the decaying of ESA bands, while DAS 4 corresponds to the relaxation of the LEES to the GS.

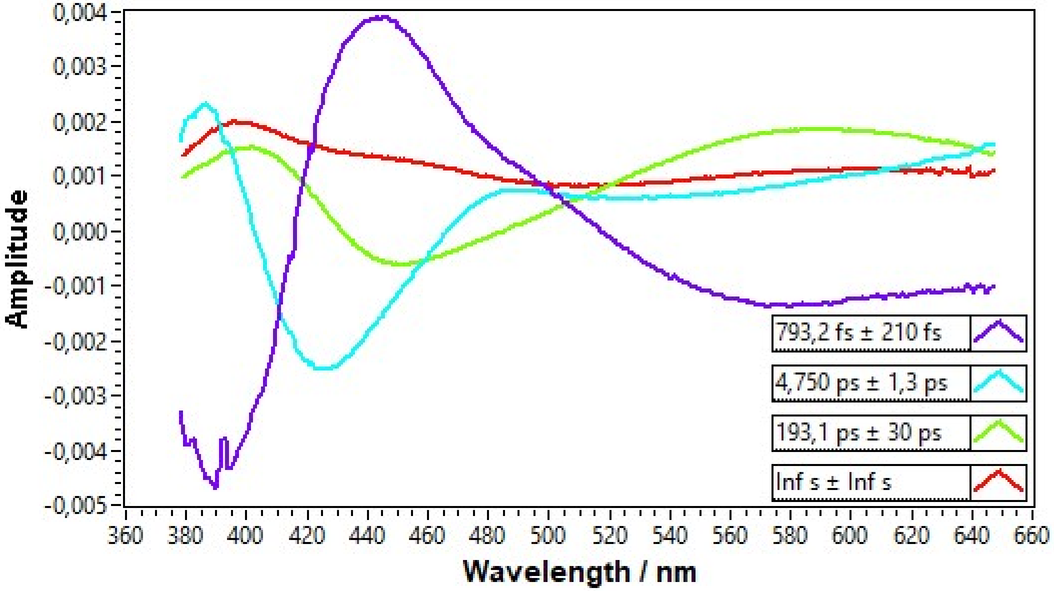

Ligand L^{1B}

	Time constants/ps	Wavelength/nm (Sign)
DAS 1	0.79	390 (-),450 (+), 575 (-)
DAS 2	4.75	393 (+), 427 (-), 485 (+), 650 (+)
DAS 3	193.1	400 (+), 450 (-), 590 (+)
DAS 4	Inf	395 (+), 450 (+)

DAS 1 represents decaying of S_1–S_n ESA band accompanied by growing of ESAs characteristic for polypiridine anionradical and pirollidine cationradical and SE band, while DAS 2 shows the decaying of ESA polypyridine anionradical and SE bands. DAS 3 with red shifted minimum compared to DAS 2 corresponds to the convolution of decaying of SE with triplet formation.

Energy diagrams

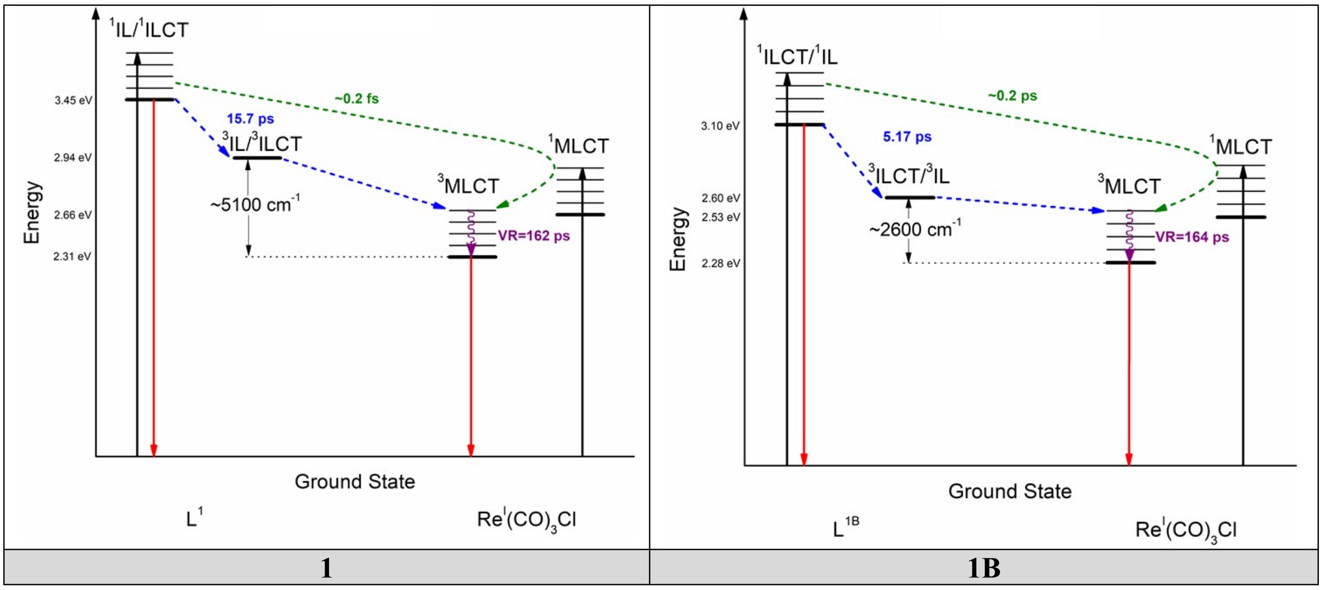

1	**1B**

Figure S29. Proposed energy level diagrams of the photophysical processes occurring in complexes **1** and **1B**.

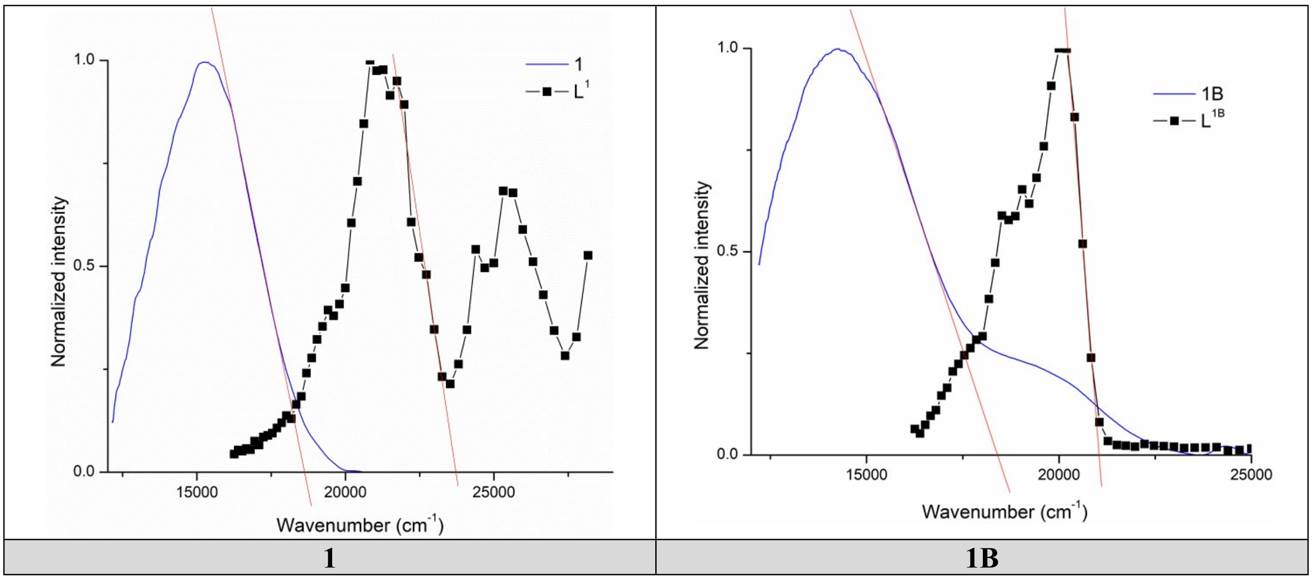

1	**1B**

Figure S30. Estimation of ^{3}MLCT and ^{3}IL/^{3}ILCT energies on the basis of r.t. emission spectra of complexes **1** and **1B** and 77 K phosphorescence of the appropriate ligands obtained with TRES measurements (delay 180 ns).

References

[1] T. Klemens, A. Świtlicka, A. Szlapa-Kula, S. Krompiec, P. Lodowski, A. Chrobok, M. Godlewska, S. Kotowicz, M. Siwy, K. Bednarczyk, M. Libera, S. Maćkowski, T. Pędziński, E. Schab-Balcerzak and B. Machura, Applied Organometallic Chemistry, 2018, 32, e4611.